BNL-NCS-51346
ENDF-294

Ni ELEMENTAL NEUTRON INDUCED REACTION CROSS-SECTION EVALUATION

M. Divadeenam

March 1979

INFORMATION ANALYSIS CENTER REPORT

NATIONAL NUCLEAR DATA CENTER
BROOKHAVEN NATIONAL LABORATORY
UPTON, NEW YORK 11973

national nuclear data center

BNL-NCS-51346
(ENDF-294)
UC-34c
(Physics-Nuclear-TIC-4500)

Ni ELEMENTAL NEUTRON INDUCED REACTION CROSS-SECTION EVALUATION

M. Divadeenam

March 1979

NATIONAL NUCLEAR DATA CENTER

BROOKHAVEN NATIONAL LABORATORY

ASSOCIATED UNIVERSITIES, INC.

Under Contract No. DE-AC02-76CH00016 With The

UNITED STATES DEPARTMENT OF ENERGY

This work was supported by the US Department of Energy.

Printed in the United States of America
Available from
National Technical Information Service
U.S. Department of Commerce
5285 Port Royal Road
Springfield, VA 22161

NTIS price codes:
Printed Copy: A06; Microfiche Copy: A01

ABSTRACT

A completely new evaluation of the nickel neutron induced reaction cross sections was undertaken as a part of the ENDF/B-V effort. (n,xy) reactions and capture reaction from threshold to 20 MeV were considered for $^{58,60,61,62,64}Ni$ isotopes to construct the corresponding reaction cross section for natural nickel. Both experimental and theoretical calculated results were used in evaluating different partial cross sections. Precompound effects were included in calculating (n,xy) reaction cross sections. Experimentally measured total section data extending from 0.7 MeV to 20 MeV were used to generate smooth cross section. Below 0.7 MeV elastic and capture cross sections are represented by resonance parameters.

Inelastic angular distributions to the discrete isotopic levels and elemental elastic angular distributions are included in the evaluated data file.

Gamma production cross sections and energy distribution due to capture and the (n,xγ) reactions were evaluated from experimental data.

Finally, error files are constructed for all partial cross sections.

CONTENTS

LIST OF TABLES

LIST OF ILLUSTRATIONS

I. INTRODUCTION

The Ni evaluation for ENDF/B-IV was done by Bhat.[1] When the present evaluation was about to be completed, Guenther et al.,[2] reported the results of Argonne-Livermore evaluation effort on the fast neutron cross section of elemental Nickel.

This is almost a completely new evaluation, in particular, the secondary neutron cross sections and angular distributions as well as the secondary neutron energy distributions for the inelastically scattered continuum neutrons have been updated. In addition, isotopic cross sections for the various (n,particle) cross sections were evaluated to construct the corresponding natural Ni files. Precompound effects were included in (n,particle) reaction cross sections.

From 1.0×10^{-5} eV to 690.0 keV, the resolved resonance region and the resonance parameters along with the smooth background cross sections have been taken from the ENDF/B-IV Ni evaluation (MAT=1190), which, in turn, were adopted from ENDF/B-III Ni (MAT=1123) evaluation.

The Ni total cross section data of Perey, Love and Kinney extending up to 20 MeV were used to construct smooth cross section file.

The following neutron and gamma production data are given for Ni in the energy range 1.0×10^{-5} to 20 MeV. (MAT No. 1328).

File 1: General description of the evaluation and relevant references.

File 2: Resonance parameters for ^{58,60,62,64}Ni from 1.0×10^{-5} eV to 690.0 keV.

File 3: Smooth cross sections for total, elastic, total inelastic, inelastic cross sections to 26 discrete levels, the inelastic continuum, (n,2n), (n,αn')+(n,n'α), (n,pn')+(n,n'p), (n,p), (n,d), (n,α), (n,2p) and capture cross sections. Extracted data for μ,ξ, and γ are also included. In addition, Hydrogen, Deuterium and Helium production cross sections are generated.

File 4: Angular distributions for elastic and inelastic scattering are given in terms of Legendre Polynomial coefficients in the c.m. system. In particular, the direct interaction effects (channel coupling) are considered for the inelastic angular distributions for the two lowest excited states of the even Ni isotopes.

File 5: Secondary neutron energy distribution for the inelastic continuum with precompound effects, (n,2n), (n,n'α) and (n,n'p) reactions are given.

File 12: Multiplicity for gamma-ray production due to capture from 1.0×10^{-5} eV to 1.0 MeV.

File 13: (n,xγ) production cross sections from 1.0 MeV to 20 MeV.

File 14: Angular distributions for photons assumed to be isotropic.

File 15: Normalized energy distribution of photons up to 1.0 MeV and due to non-elastic processes at higher energies.

II. NI ISOTOPES. Q-VALUES MASSES AND LEVEL SCHEMES

Ni isotopic abundances,[3] masses in ^{12}C scale[4] and the Q-values for the neutron induced reactions are given in Table 1. Capture γ-ray threshold and energies are taken from Refs. (5) and (6). Reactions like (n,h), (n,t) and (n,3n) were not considered for the evaluation because the expected magnitude for such reactions are negligibly small: in the microbarn range for the first two reactions and the Q-value is very high for the last reaction. Ni isotope level schemes are shown in Figure 1. Levels with known J^{π} below 3.5 MeV are shown for ^{58}Ni and ^{60}Ni. In addition, four excited levels for each of the remaining minor isotopes are shown. The continuum of levels beyond the descrete spectrum is described by a statistical level density formula.

TABLE 1

Abundances, Masses and Reaction Q-Values,
for the Nickel Isotopes

Reaction \ Mass			(Q Value (MEV)		
	^{58}Ni(.683)	^{60}Ni(.241)	^{61}Ni(.011)	^{62}Ni(.036)	^{64}Ni(.009)
	57.9353358	59.9307795	60.9310502	61.9283396	63.9279562
(n,γ)	8.9993	7.8195	10.5962	6.8376	6.0976
(n,p)	0.3947	-2.0411	-0.5252	-4.4343	-6.2168
(n,d)	-5.9526	-7.3081	-7.6360	-8.8964	-10.3114
(n,t)	-11.0724	-11.5107	-8.8700	-11.9750	-12.4600
(n,^{3}He)	-6.4856	-9.184	-10.4171	-12.1776	--
(n,α)	2.8902	1.3514	3.5749	-0.4352	-2.4315
(n,n'p)	-8.1772	-9.5327	-9.8606	-11.121	-12.536
(n,n'α)	-6.4083	-6.2948	-6.4681	-7.0217	-8.100
(n,2n)	-12.203	-11.3883	-7.8195	-10.5966	-9.6596
(n,2p)	-6.5579	-10.316	-9.299	-14.230	--

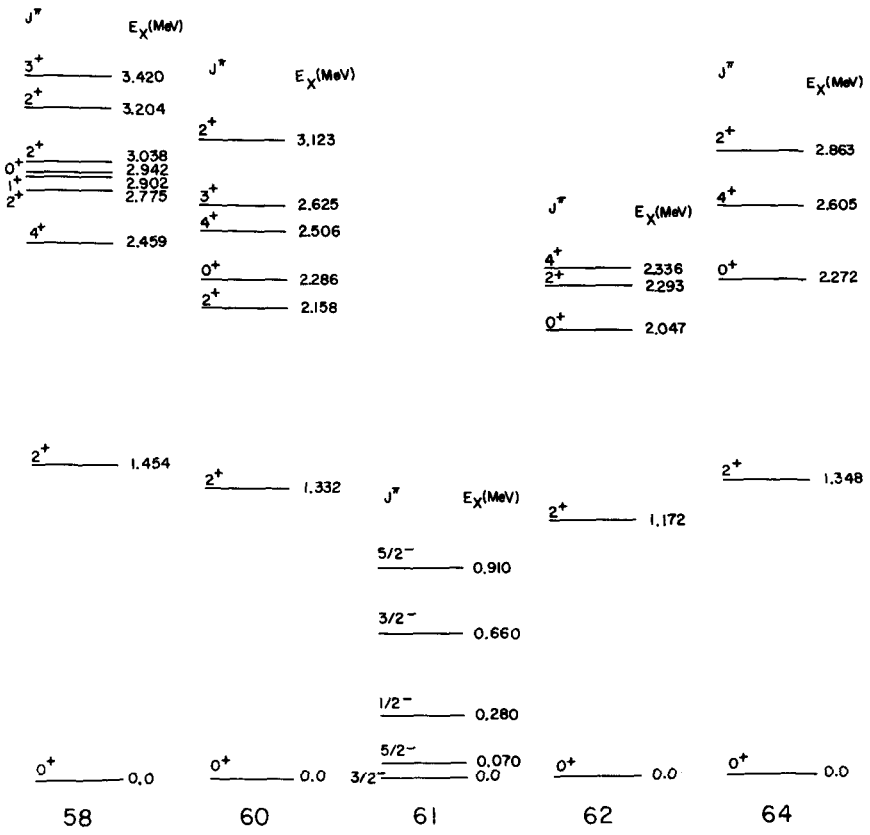

Figure 1. Ni Isotopic level schemes used for calculating inelastic level excitation functions.

Evaluated neutron induced cross sections for Ni isotopes were constructed from experimental and calculated results from threshold to 20 MeV neutron energy. Energy variation of a particular reaction channel cross section was determined from:

a. Available experimental data if extended over a wide energy range. This is the case only in a few situations.

b. Calculated cross sections when they agree with spotty measurements at one or more energy points.

c. Average of different measurements at one energy value were used to normalize the calculated cross sections. When there was no experimental data the calculated quantities were normalized to the predictions of systematic based cross sections.

d. Calculated cross sections if no experimental results were available.

The above procedure was adopted because of the uncertainty of some of the parameters that enter into statistical model calculations.

III. STATISTICAL MODEL CALCULATIONS

The (n,particle) cross sections form a major and important part of the ENDF/B data file. Most of the evaluations for the ENDF/B-IV version made use of the available (sometimes scanty) experimental data and supplemented either with simple model predictions or with one stage Hauser-Feshbach (HF) calculations.

To improve the situation, calculation of the reaction cross sections were performed within the framework of Hauser-Feshbach (compound) and pre-equilibrium (Griffin-Blann) statistical nuclear reaction theories. Uhl's code MODNEW[7] adapted and modified at BNL was used for the entire calculation. In addition COMNUC[8] was used to calculate inelastic level excitation functions. MODNEW incorporates the following simplifying assumptions:

1. Compound nuclear formation and decay is treated within the framework of Hauser-Feshbach formalism without width fluctuation.

2. Four exit channels, n, p, α and d in addition to the competing γ-channel.

3. Decay of the particles is assumed to be sequential.

4. Maximum of six compound nuclei can be considered in a reaction sequence.

5. Pre-equilibrium emission accounts for the fast interaction process. DWBA type of processes are not considered. In addition, the pre-equilibrium emission from the first compound nucleus is assumed to be adequate for mass ($A \leq 60$) and energy region ($E_n \leq 20$ MeV) under consideration.

6. The pre-equilibrium fraction PF is taken to be the same for all emitting particles. In addition, it is taken to be constant up to 20 MeV. However, calculations are presented in two instances for three different values of PF.

7. Weisskopf/Brink-Axel prescription for the Γ_γ (ε) calculation is employed. The maximum value for the γ-multipolarity is taken to be $3.\langle\Gamma_\gamma\rangle$ $\sim$ 1.5 eV was taken at neutron binding energy.

8. Global type of optical model parameters for n, p, d and α are used.

9. Nuclear level density is approximated with a fermi-gas model. Further comments will be made on the last two items later in this section.

COMNUC is a similar code except that it is limited to secondary reactions only.

Two examples of neutron induced reaction sequence are shown in Fig. 2. The upper part of the Fig. displays the (n,pn') reaction sequence. CN1 etc., refer to the first compound nucleus and so on... The thick arrows indicate the reaction path and cross section calculations were performed for the reaction stage terminating at the end of the thick arrows. In this example $\sigma_{n,p}$ and $\sigma_{n,pn'}$ were calculated. The third phase of the reaction sequence is required by the code for calculating the tertiary reaction cross section. The lower part of the figure displays the reaction sequence for (n,2n) reaction.

As mentioned earlier, Global type of parameters for n, p, d and were used in generating transmission coefficients with the help of ABACUS[9] code. The corresponding parameters are given in Table 2.

The parameters for neutrons correspond to those of Wilmore-Hodgson equivalent to Perey-Buck non-local,[10] and for proton, Perey's parameters[11] were used. For neutron and proton $T_{\ell-1/2}$ and $T_{\ell+1/2}$ were combined to give T_ℓ as required by the code

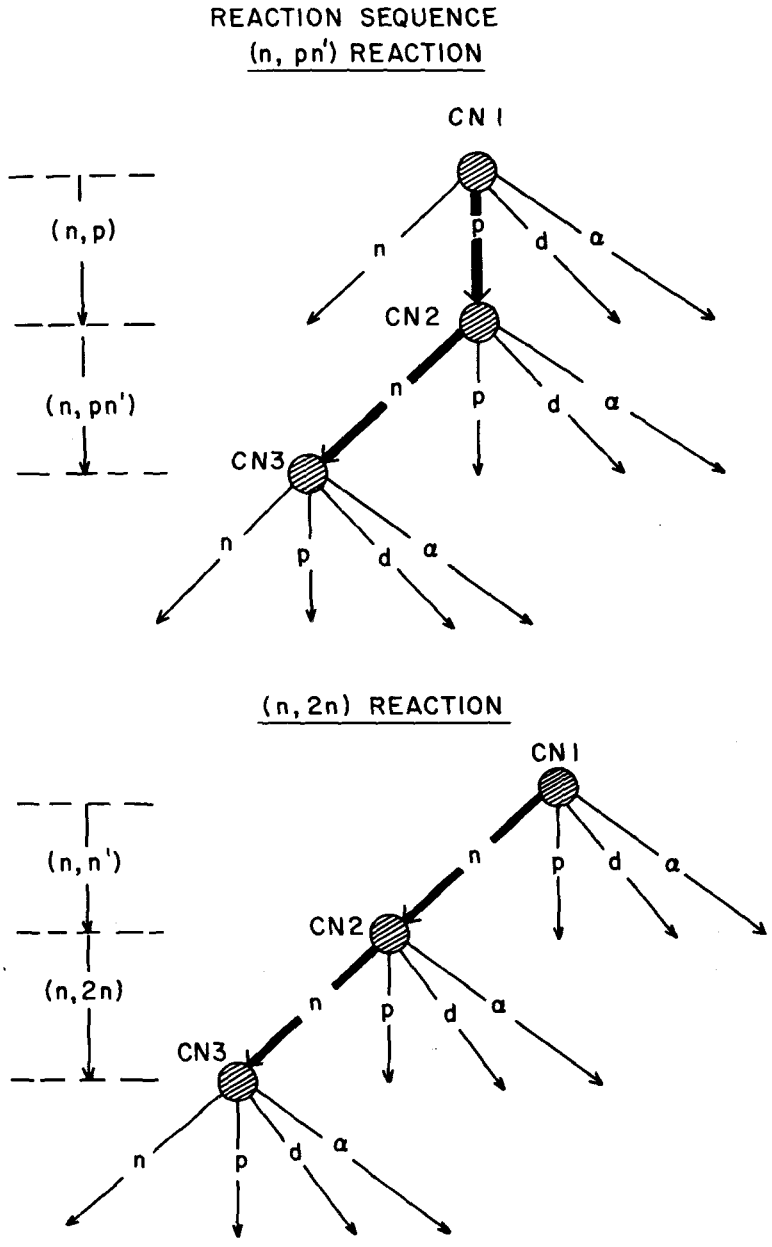

Figure 2. Example of a reaction sequence for model calculations.

TABLE 2

OPTICAL MODEL PARAMETERS

NEUTRON

$V_R = 47.01 - 0.267E - 0.0018\,E^2$ MeV

$r_R = r_{so} = 1.29$ fm

$a_R = a_{so} = 0.66$ fm

$W_D = 9.52 - 0.053E$ Mev

$r_D = 1.25$ fm

$a_D = 0.48$ fm

$V_{so} = 7$ MeV

$$T_\ell = \frac{\ell T_{\ell-\frac{1}{2}} + (\ell+1)T_{\ell+\frac{1}{2}}}{(2\ell+1)}$$

PROTON

$V_R = 52.2 - 0.3E$ MeV

$r_R = r_{so} = 1.25$ fm

$a_R = 0.65$ fm

$W_D = 11.5$ MeV

$r_D = 1.25$ fm

$a_D = a_{so} = 0.47$ fm

$V_{so} = 7.5$ MeV

DEUTERON

$V_R = 81.0 - .22E$ MeV

$r_R = 1.15$ fm

$a_R = 0.81$ fm

$W_D = 14.4 + .24E$ MeV

$r_D = 1.34$ fm

$a_D = 0.68$ fm

$V_{so} = 0$

$r_C = 1.15$ fm

ALPHA

$V_R = 193.3$ MeV

$r_R = 1.483$ fm

$a_R = 0.513$ fm

$W = 20.4$ MeV

$r_I = 1.483$ fm

$a_I = 0.304$ fm

$r_C = 1.4$ fm

MODNEW. Deuteron parameters quoted by Perey in his report,[10] were used while for α-particle, Satchler et al's,[12] parameters were employed.

A. Level Density Description

The Fermi-Gas model of Vonach and Hill,[13] was employed. Equivalence or compatibility of this description with that of Gilbert and Cameron was not investigated. Dilg, et al.,[14] have extracted level density parameters for various nuclei. They have also given a prescription for average type of parameters for nuclei around A=60. Their tabulated level density parameters were used and when there were none for a given nucleus, the average parameter prescription was used. For each nucleus two parameters, a and Δ, are involved for a given I/I_{rigid} ratio. $I/I_{rigid} = 1$ was used.

The level density formulae and the average parameter description are given below.

$$\rho(U,J) = \frac{1}{24\sqrt{2}} \frac{2J+1}{\sigma^3 a^{1/4}} \frac{\exp\left(2\sqrt{a(U-\Delta)} - J(J+1)/2\sigma^2\right)}{(U-\Delta+t)^{5/4}}$$

$$\rho(U) = \frac{1}{12\sqrt{2}} \frac{1}{\sigma a^{1/4}} \frac{\exp\left(2\sqrt{a(U-\Delta)}\right)}{(U-\Delta+t)^{5/4}}$$

$$U - \Delta = at^2 - t$$

$$\sigma^2_{rigid} = \frac{I_{rigid}\, t}{\hbar^2}; \quad \sigma^2 = \frac{I\, t}{\hbar^2}; \quad \eta = \frac{I}{I_{rigid}}$$

AVERAGE PARAMETERS ($40 < A < 63$)

$$\left.\begin{aligned} A &= 2.40 + 0.067A \\ \Delta &= -130/A + P \end{aligned}\right\} \eta = 1$$

$$P = \begin{cases} 2\,\delta\,A^{-1/2} & \delta = 12.8 \text{ MEV} \\ \delta\,A^{-1/2} & \\ \mu\,A^{-1} & \mu = 29.4 \text{ Mev} \end{cases}$$

When the experimental data were available and/or extended over a wide energy range, the level density parameters were varied. In the case of ^{58}Ni cross sections for three different channels, (n,p), (n,2n) and (n,pn') were simultaneously fit by varying the appropriate level density parameters. The level density parameters used in the calculations are shown in Table 3. The parameters shown are for the same two reaction sequences presented in Fig. 2.

B. (n,Particle) Reactions

Hauser-Feshbach calculations with pre-compound effects were performed for

(n,p), (n,α), (n,d), (n,n'),

(n,pn') (n,n'p), (n,αn'), (n,n'α), and (n,2n) reactions for all Ni isotopes. In addition, ^{58}Ni(n,2p) reaction cross sections were calculated.

Calculated results were compared to experiment in the case of:

^{58}Ni(n,p), ^{58}Ni(n,2n), ^{58}Ni(n,pn'+n'p+d), ^{58}Ni $\sigma^{m}_{np}/\sigma^{m+g}_{np}$, and ^{60}NI(n,p).

In the case of ^{60}Ni(n,p), the intermediate structure observed is interpreted in terms of the Giant dipole excitation (cf. section VIIC).

1. <u>^{58}Ni(n,p) Reaction.</u> As pointed out earlier, level density parameters were adjusted to fit simultaneously the (n,p), (n,2n) and (n,pn'+n'p+d) cross sections. In other words, the ^{58}Ni, ^{58}Co, ^{57}Ni and ^{57}Co level density parameters were varied to improve the fits.

TABLE 3

Level Density Parameters

Reaction	(n,2n)				(n,pn)			
Compound Nucleus	a	Δ	BE	Nucleus	a	Δ	BE	Nucleus
	5.77	-0.76		^{59}Ni	5.77	-0.76		^{59}Ni
A = 59	5.40	2.55	9.00	^{58}Ni + n	5.40	2.55	9.00	^{58}Ni + n
	6.52	0.00	8.61	^{58}Co + p	6.52	0.00	8.61	^{58}Co + p
	5.70	-0.40	6.11	^{55}Fe + α	5.70	-0.40	6.11	^{55}Fe + α
	6.12	-0.20	14.95	^{57}Co + d	6.12	-0.20	14.95	^{57}Co + d
A = 58	5.32	0.30	12.21	^{57}Ni + n	6.12	-0.02	8.57	^{57}Co + n
	6.12	-0.02	8.48	^{57}Co + p	6.22	-0.48	6.95	^{57}Fe + p
	6.35	0.89	6.41	^{54}Fe + α	6.35	-1.95	6.72	^{54}Mn + α
	6.75	-1.80	17.33	^{56}Co + d	6.35	-0.89	12.38	^{56}Fe + d
A = 57	6.75	0.70	10.26	^{56}Ni + n	6.75	-1.80	11.38	^{56}Co + n
	6.75	-1.80	7.35	^{56}Co + p	6.35	-0.89	6.03	^{55}Fe + p
	5.70	-0.06	7.58	^{53}Fe + α	5.46	-0.71	7.08	^{54}Mn + α
	5.81	0.93	15.22	^{55}Co + d	5.70	-0.40	15.00	^{56}Fe + d

The underlined nucleus corresponds to the compound nucleus for the next stage of reaction.

Calculated curves for precompound fraction PF = 0.0, 0.2 and 0.4 are shown for (n,p) in Figs. 3a and 3b. The threshold region of the (n,p) reaction (PF=0) is shown in Fig. 3a. The fit is good except at the peak position (cf Fig. 3b). A reduction of "a" (^{58}Co) the level density parameter by 2% changes the peak value by 45 mb. At the high energy end (En>12 MeV) it was difficult to choose the appropriate PF value due to large uncertainties in the measured cross sections.

It should be pointed out that a model calculation to be discussed below predicted a PF value of $\sim$0.2 at 14 MeV and $\sim$0.3 at 20 MeV neutron energy.

In Fig. 4 the calculated results are compared with experimental data for the σ^m/σ^{m+g} ratio. This ratio is expected to be sensitive to the choice of the spin-cut-off parameter. No attempt was made to vary the spin-cut-off parameter to fit the experimental data well. The theoretical results shown here correspond to the same set of calculations that were shown in the previous two Figs.

2. ^{58}Ni(n,2n) Reaction. In Fig. 5 the calculated curves for PF=0.0 and 0.2 are compared to experimental data up to 20 MeV. Experimental data of Bayhurst, et al., and Prestwood et al., are too high compared to the rest. Similarly Paulsen's data beyond 18 MeV are also high. Details of the ^{58}Ni(n,2n) experimental data will be discussed in section VIIB.

3. ^{58}Ni(n,pn'+n'p+d) Reactions. In Fig. 6 the sum of $\sigma_{n,pn'}$, $\sigma_{n,n'p}$ and $\sigma_{n,d}$ cross sections is compared with the experimental data around 14 MeV neutron energy. The calculated cross section is slightly under-predicted.

4. ^{60}Ni(n,p) Reaction. Fig. 7 presents the comparison of calculated results with the available experimental data up to 20 MeV. In this case also the calculations were performed for PF=0.0, 0.2 and 0.4. Agreement between theory and experiment is good except below 8 MeV and around the peak value. The low energy part could be improved by varying the proton optical model parameters and a better fit around the peak may be difficult due to the strong intermediate structure exhibited by the experimental data between 8-16 MeV. This aspect of the ^{60}Ni(n,p) data is discussed in Section VIIC2.

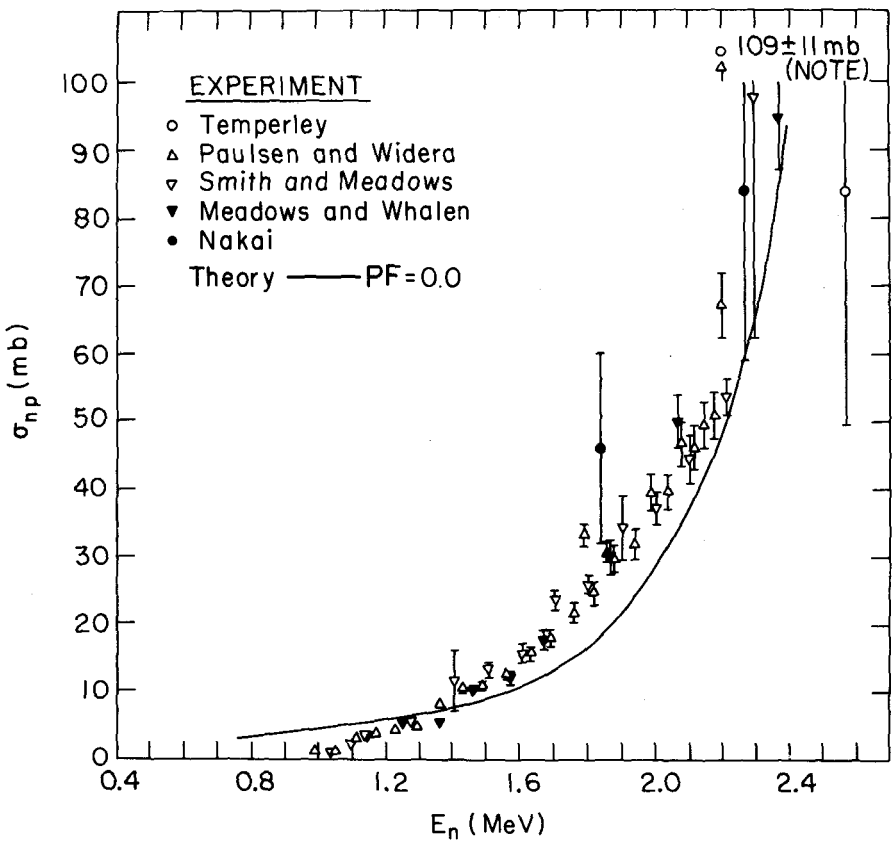

Figure 3a. Comparison of experimental $^{58}Ni(n,p)$ data with model calculated results; 0.8-2.5 MeV.

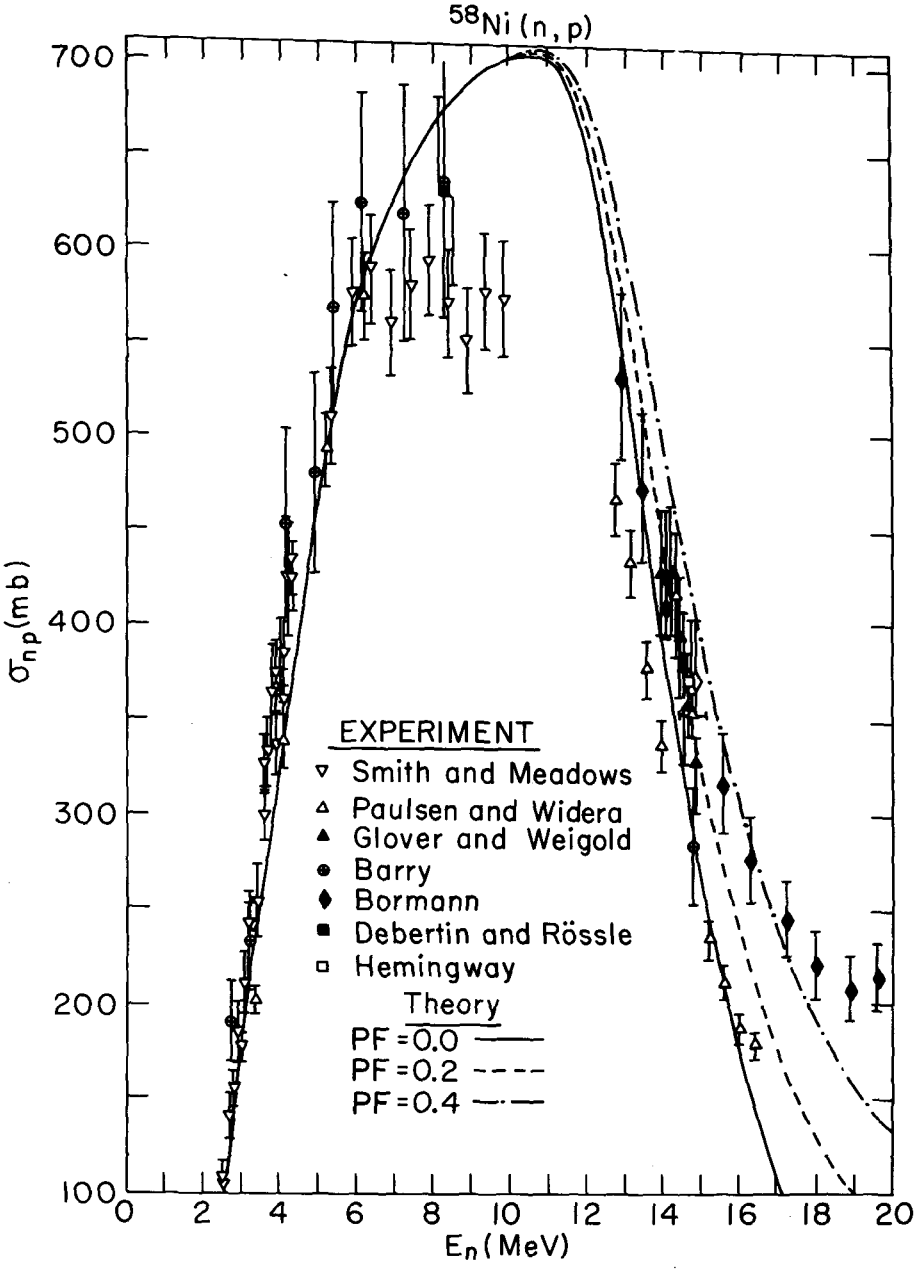

Figure 3b. Same as Fig. 3a; 2.5-20 MeV.

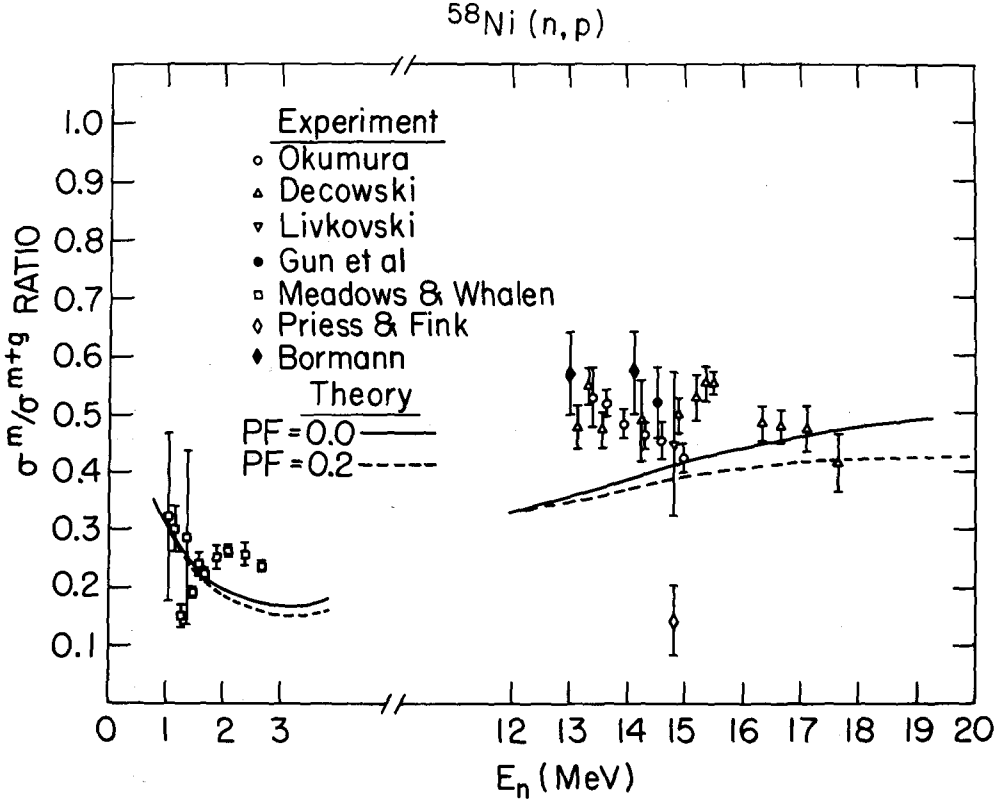

Figure 4. Comparison of measured σ^m/σ^{m+g} with model predictions for $\sigma(n,p)$ reaction.

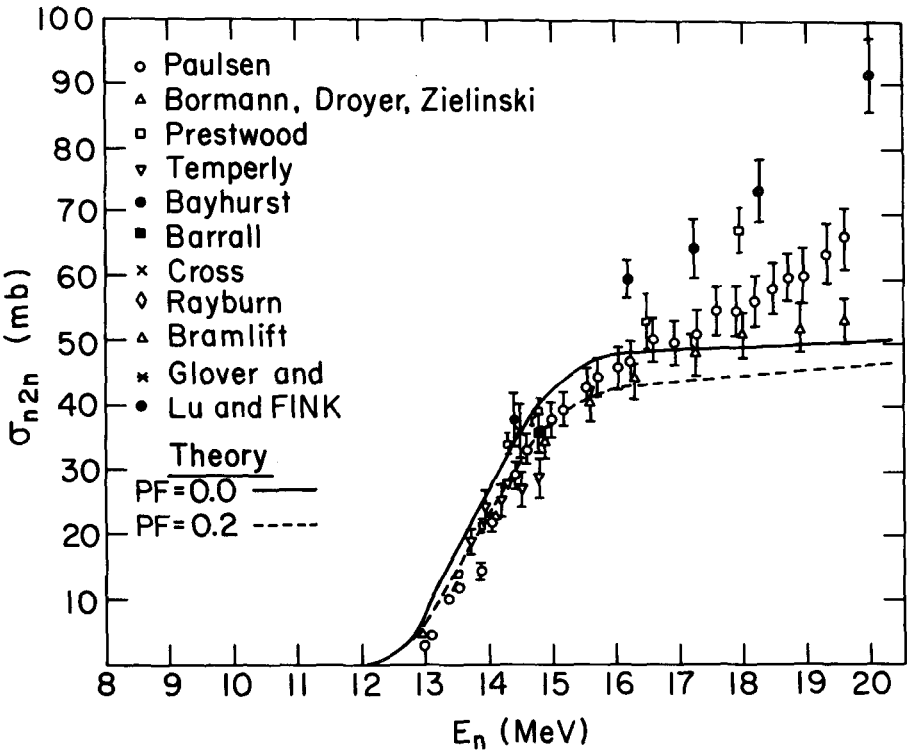

Figure 5. Comparison of experiment with theory for $^{58}Ni(n,2n)$ reaction.

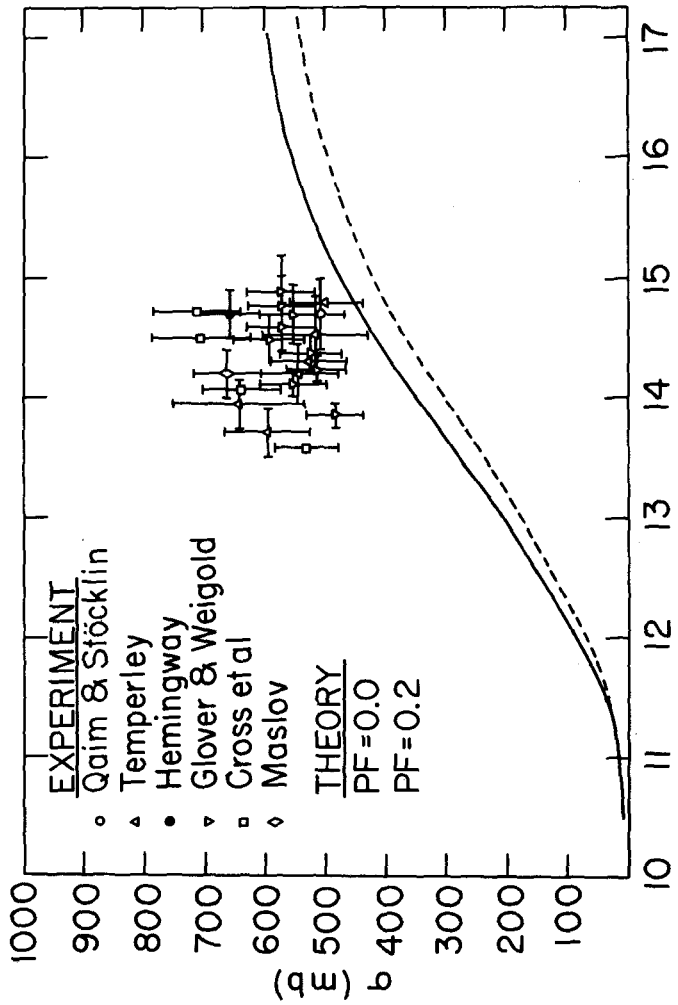

Figure 6. Comparison of experiment with theory for ^{58}Ni(n,n'p+pn'+d) reactions.

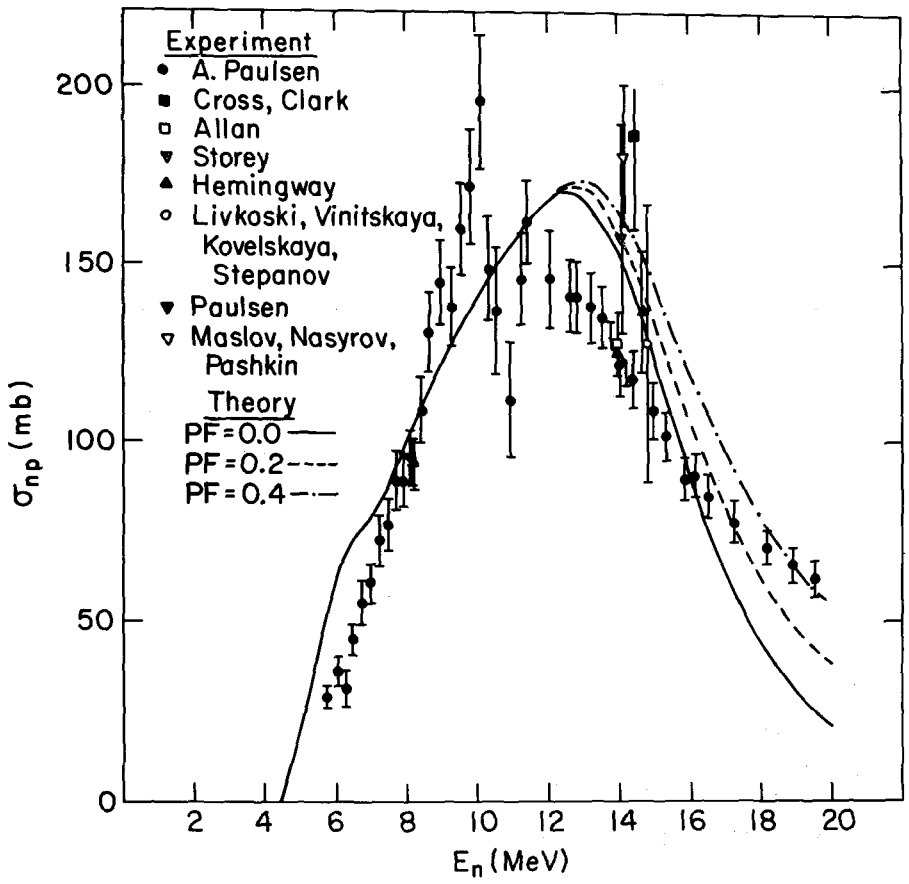

Figure 7. Comparison of experiment with theory for $^{60}Ni(n,p)$ reaction.

5. (n,n') Reaction. Inelastic excitation functions are known only for a few isotopic levels and extend only up to about 7 MeV neutron energy. To supplement these up to 20 MeV and construct excitation functions for the remaining Ni isotope levels, Hauser-Feshbach calculations were performed for the isotopic levels below 3.5 MeV excitation. Both COMNUC and MODNEW codes were used for this purpose. In addition JUPITOR[15], was used to account for the direct inelastic effects in calculating differential cross sections.

In Fig. 8 the excitation functions for the first 2^+ levels of ^{58,60,62}Ni are shown. Calculated results agree quite well with experiment for ^{58}Ni and ^{60}Ni levels. However, in the case of ^{62}Ni (natural abundance $\sim$1%) the experimental data appears to be in error: because the peak value of the $\sigma_{inel} >> 1.4$ barns, which is about the value of the measured non-elastic cross section for Ni.

C. Precompound Fraction (PF) Estimation

Blann's GDH model[16] was employed to calculate the precompound fraction PF defined below.

Both the precompound and the compound contributions were computed. Evaporation model was used for the latter one. The predicted results for precompound fraction were calculated as a function of neutron energy and mass number. In the bottom part of Fig. 9 results for ^{58}Ni PF are shown as a function of neutron energy. The three quantities shown are defined to be:

$$PFN = \sigma^{pre}_{nn'} / (\sigma^{pre}_{nn'} + \sigma^{comp}_{nn'})$$

$$PFN' = \sigma^{pre}_{nn'} / \sigma_{reaction}$$

$$PFT = (\sigma^{pre}_{nn'} + \sigma^{pre}_{np}) / \sigma_{reaction}$$

Experimentally the quantity PFN is measured in an inelastic neutron scattering measurement. The measured value of PFN is about 0.20 at 14 MeV which is in good agreement with the predicted result, and the calculated value of about .30 at 20 MeV is also in good agreement with the required value of PF to reproduce the ex-

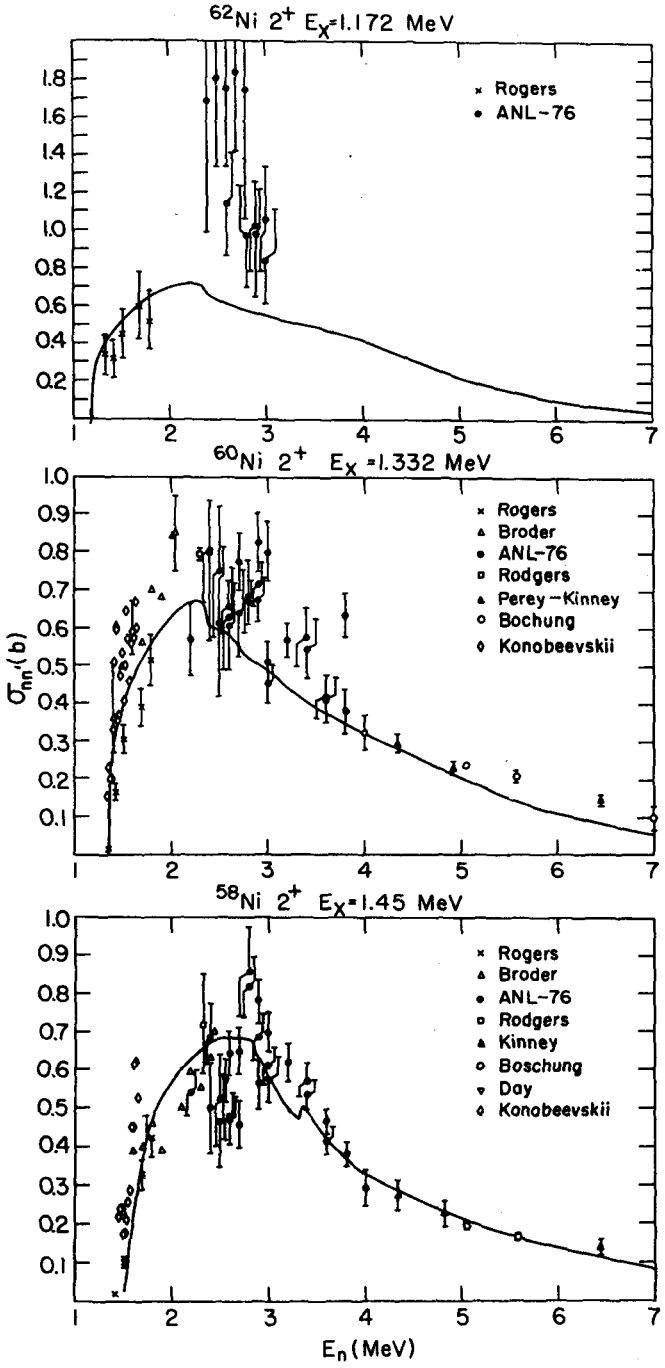

Figure 8. Comparison of HF predictions for the inelastic excitation to the first 2$^+$ levels of ^{58,60,62}Ni.

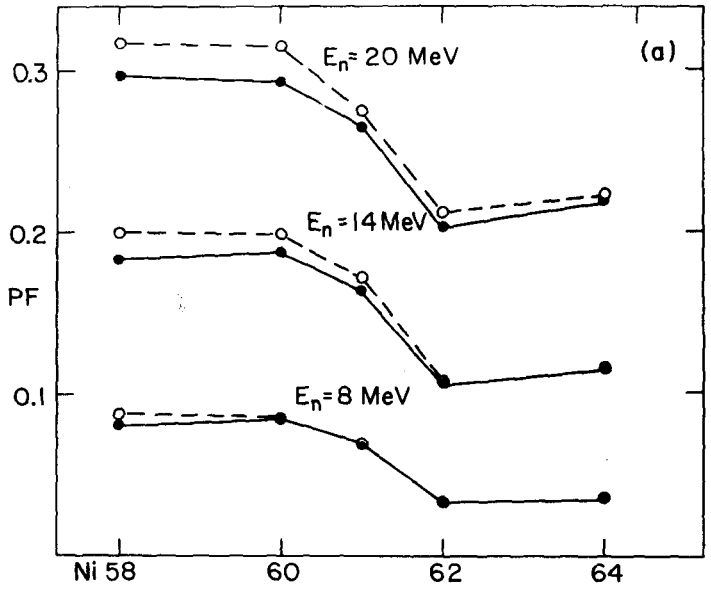

Figure 9a. Ni isotopic mass dependence of the precompound fraction PF at 8, 14 and 20 MeV.

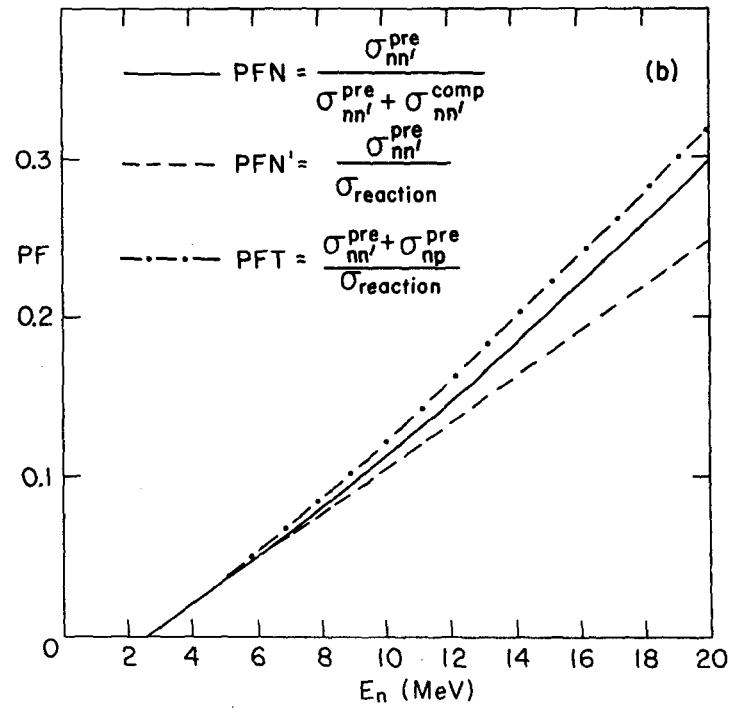

Figure 9b. Theoretical prediction of PFN, PFN' and PFT as a Function of neutron energy for ^{58}Ni.

perimental data at higher energy in the case of (n,p) cross section (see Fig. 3b). The quantity PFN will be referred to as PF.

At the top of Fig. 9 both PFN and PFT are shown for all Ni isotopes at 8, 14 and 20 MeV. Variation of the pre-equilibrium fraction with A is gradual. The predicted change is to a large extent attributed to the Q-values for the outgoing particles and to a lesser extent on the increasing mass number.

The pre-equilibrium fraction results presented here should be considered as qualitative in that the calculated results are based on the very simple-minded evaporation model for the equilibrium process.

In summary, the statistical model description for the neutron induced reactions can be suitably applied to generate neutron cross sections in the MeV range. Availability of the pertinent experimental data helps in determining the required parameters if they are not determined from a different kind of data. The intermediate structure observed in ^{60}Ni(n,p) cross section may be interpreted as due to doorway structure related to the Giant Dipole phenomenon (cf. VII C2). Inclusion of the pre-equilibrium contribution in the calculation is borne out by the experimental data. The energy variation of the precompound fraction suggested by the experimental data is reproduced by the Blann's GDH model calculations.

IV TOTAL CROSS SECTION

There are three data sets that extend up to 20 MeV neutron energy. These were measured at NBS,[17] Karlsruhe,[18] and ORNL.[19] The ORNL data set measured by Perey, Love and Kinney are the latest of the three sets. The ENDF/B-IV version incorporated the combined data sets of NBS and Karlsruhe. The two data sets were merged at 11 MeV neutron energy: Details of the merger procedure and reasons for adopting such a procedure are discussed in Ref. 1. For the present evaluation it was decided to use the ORNL data because they represented the most recent measurements with good resolution except at very low energy in the resonance region. Such a shortcoming is irrelevant for the purpose at hand because the resonance region extends up to 690 keV and is represented by the resonance parameters. Guenther, et al.,[2] recently reported total cross section measurement extending up to 5 MeV. Because of the energy range limitations, their data were not considered for the evaluation of the total cross section.

The ORNL energy resolution (burst 5 ns and 47.35 meter flight path) is comparable to the NBS. Perey, et al. used two sample thicknesses approximately 0.2 and 1.0 atoms per barn. At low energies ($\sim$200 keV), the two sample thickness cross sections

do not agree quite well when there is unresolved resonance structure. However, where the structure is resolved the two sets of transmission data are consistent. Compared to the Karlsruhe data the ORNL data are lower in the valleys, but agree in the high energy region. However, as pointed out earlier, these limitations are not of concern here as the lowest range of interest is 690 keV.

Even though no background corrections were made on the measured transmission data,[19] it appears that such corrections are negligible in comparison to the counting statistics (<1/3 of them) above 500 keV. This is due to the ORNL of acquiring the transmission data: thick uranium filler in the beam (5.5 in), high counting rates and a very large flight station.

The ORNL cross section data corresponding to two sample thicknesses referred to above were simultaneously displayed on the interactive CTR screen for a careful evaluation to arrive at a smooth cross section curve. Both the peaks and valleys in the cross section were looked at and the resonance structure displayed by the data was retained up to 5 MeV, beyond which a very smooth curve is drawn to represent the data up to 20 MeV. Experimental data and the evaluated total cross section curve is shown in Figs. 10a through 10f.

In general, the comparison (not shown) of the presently evaluated curve with that of Version IV curve is good (cf. figs 10a-f) except in the low energy region - the peaks and the minima are pronounced in the present evaluated cross section data set.

V NON-ELASTIC SCATTERING CROSS SECTION

Non-elastic cross section represents the sum of all reaction processes except the elastic scattering. Sphere transmission method of measuring the non-elastic cross section is more reliable than measuring the angular distribution of elastic scattering and subtracting the integral $\int\sigma_{nn}(\Theta)d\Omega$ from the total cross section. Two factors make the second method unreliable:

1. Angular range of the measurement.

2. Any presence of intermediate (or resonance) structure in the elastic and total cross section, if the beam resolution and the target thickness are not broad enough to average out the resonance structure.

Non-elastic scattering cross section represents the upper bound for the sum of all the possible reaction cross sections at a given energy. A knowledge of the magnitude of the cross sec-

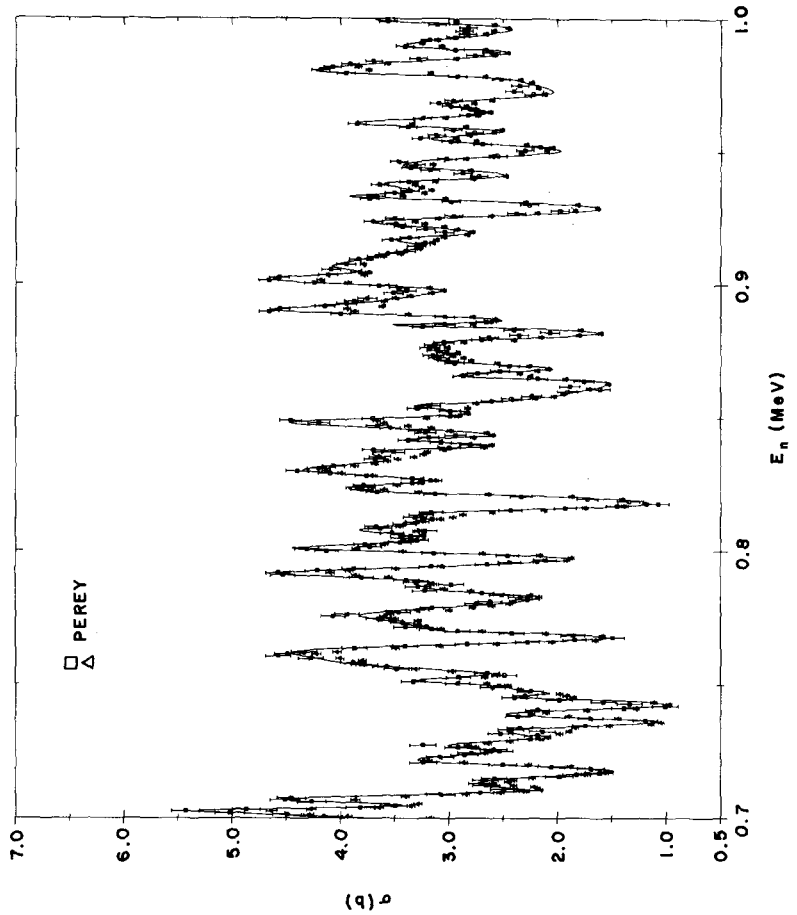

Figure 10a. Ni total neutron cross section data of Perey, Love and Kinney. Triangles and squares correspond to thick and thin sample transmission. Ni total cross section 0.7-1.0 MeV.

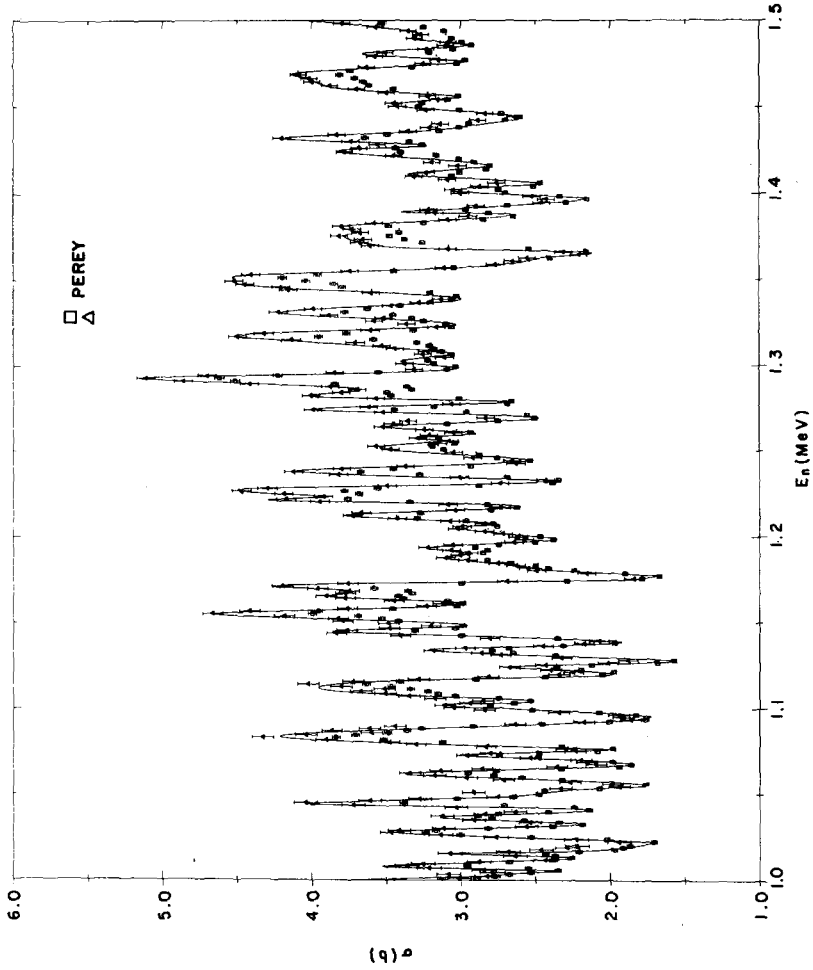

Figure 10b. Ni total cross section 1.0-1.5 MeV.

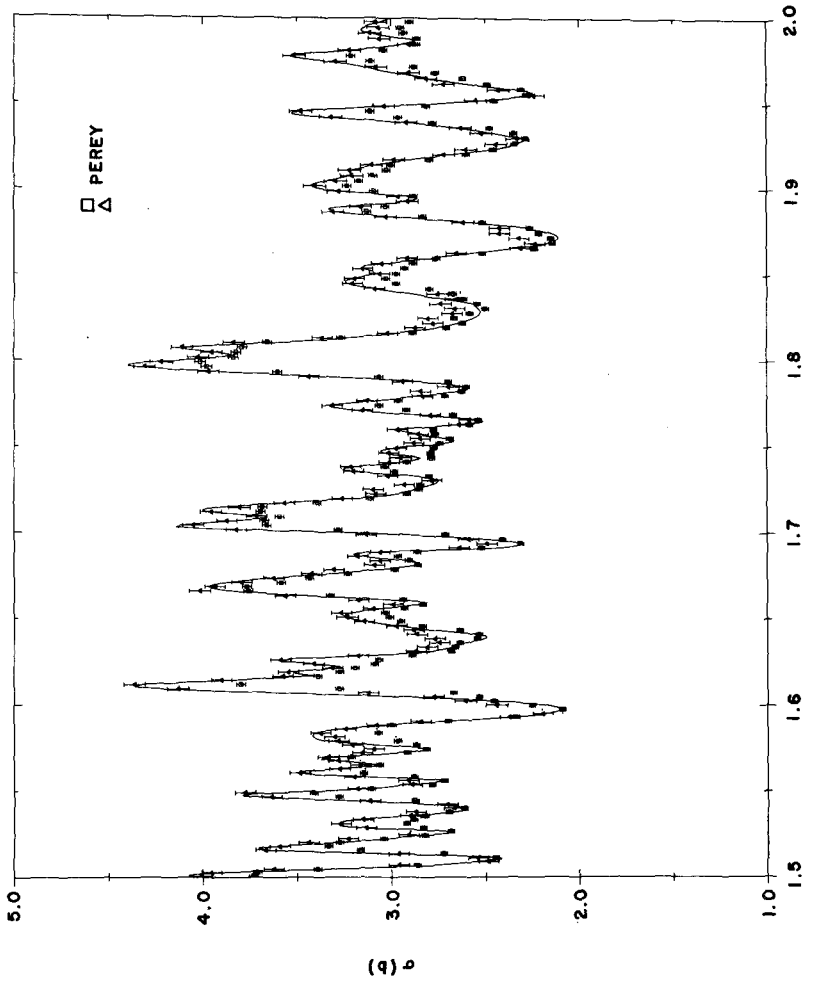

Figure 10c. Ni Total cross section 1.5-2.0 MeV.

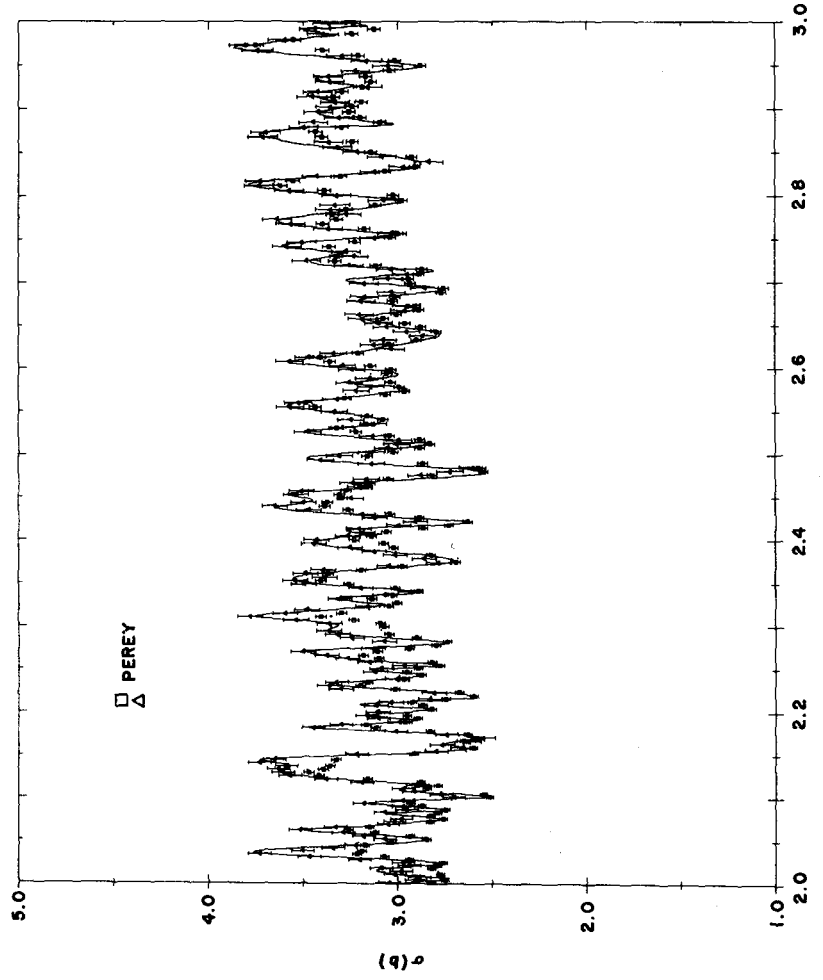

Figure 10d. Ni Total cross section 2.0-3.0 MeV.

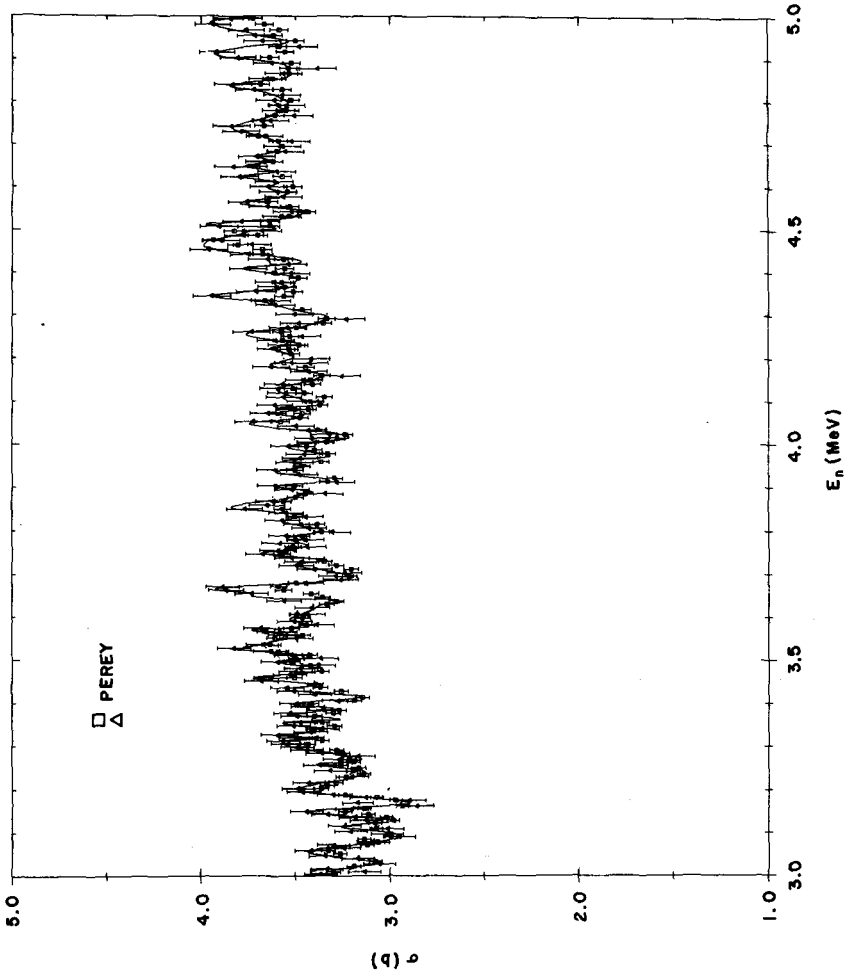

Figure 10e. Ni Total cross section 3.0-5.0 MeV.

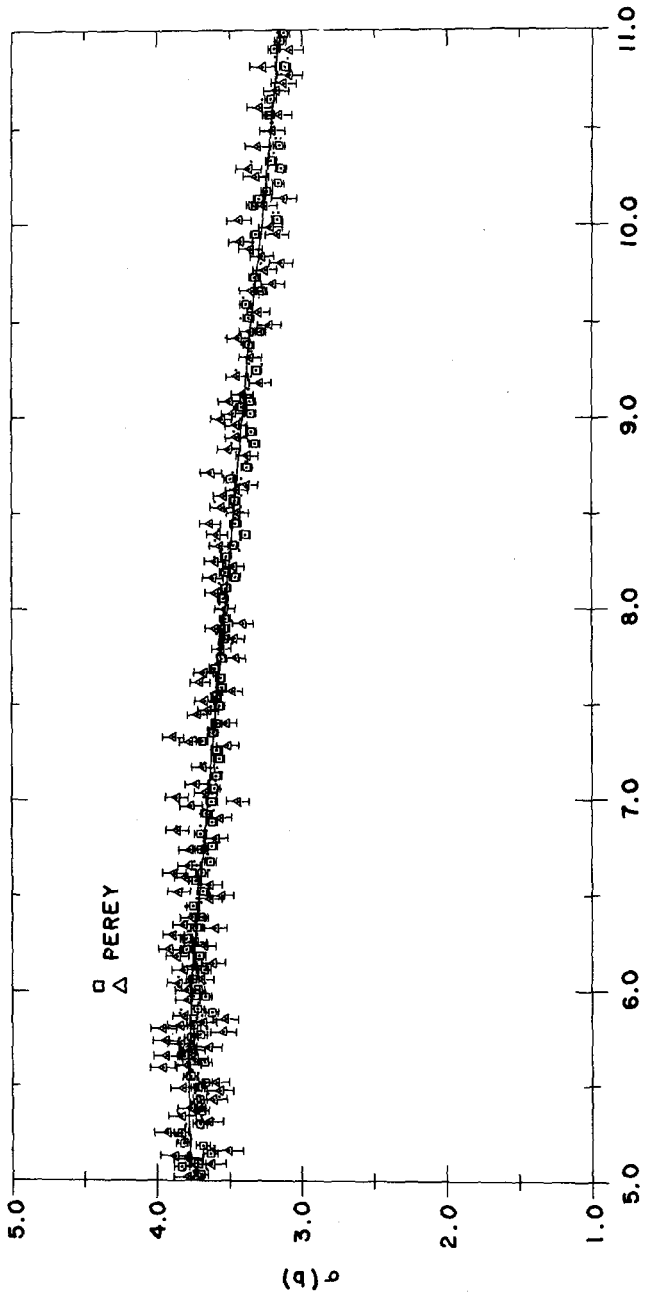

Figure 10f. Ni Total cross section 5.0-11.0 MeV.

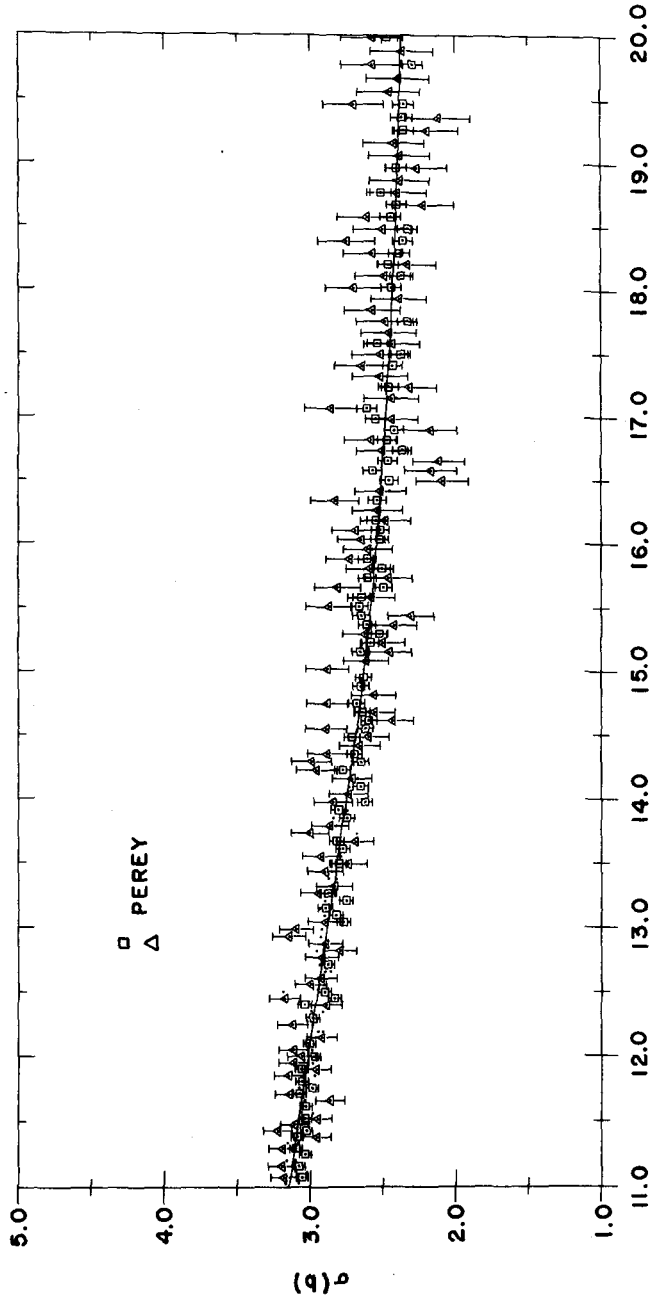

Figure 10g. Ni Total cross section 11.0-20.0 MeV.

tion may be useful in estimating the contribution due to some partial cross section for which no experimental data is available.

The available experimental data,[20-30] on the non-elastic scattering cross section have been discussed extensively and summarized in Ref. 1. The evaluated ENDF/IV and V curves, and the data are shown in Fig. 11. A few experimental points[28] are high compared to the evaluated curve between 2 and 8 MeV neutron energy.

VI ELASTIC SCATTERING CROSS SECTION

Below 690 keV the elastic scattering is described by the resonance parameters. Beyond 690 keV the elastic cross section curve up to 20 MeV was constructed by subtracting the non-elastic cross section from the total cross section. The available experimental data,[31-43] summarized in Ref. 1, are plotted (cf. Figs. 12a through 12f) along with ENDF/B-IV and V evaluated curves. For any meaningful comparison of the evaluated curve with the data, suitable averaging of the data has to be performed. In general, the average trend of the curve agrees fairly well with the data up to 6 MeV. However, beyond 6 MeV the data are slightly lower than the curve. This could be due to extrapolation of the differential elastic data to 0° and 180° as well as some other problems connected with the detection technique, etc.

VII (N, PARTICLE) CROSS SECTIONS

A. Inelastic Scattering Cross Section

1. Total Inelastic Scattering Cross Section. A table summarizing the total inelastic cross section data is given in Bhat's Ni evaluation report.[1] Broder's data,[44,45] obtained by looking at the inelastic gamma-rays extends from 1.40 to 5.42 MeV. In addition Fujita, et al.,[46] and Salnikov, et al.,[47] detected the outgoing neutrons at 14 MeV. Apparently these investigators underestimated the contributing (n, particle) reaction cross sections to obtain an unreasonably large total inelastic cross section of 0.76 barn (cf. Fig. 13), which is about more than 50% of the total non-elastic cross section. An improved estimation of the (n, particle) cross section results in a much more reasonable value for the total inelastic cross section ($\sim$.3 barn) at 14 MeV. The evaluated total inelastic cross section curve is compared both with the available data and the Version IV evaluated curve. Notice the 14 MeV points (cf. Fig. 13) which were used in arriving at the Version IV avaluated curve are too high compared to the presently evaluated curve.

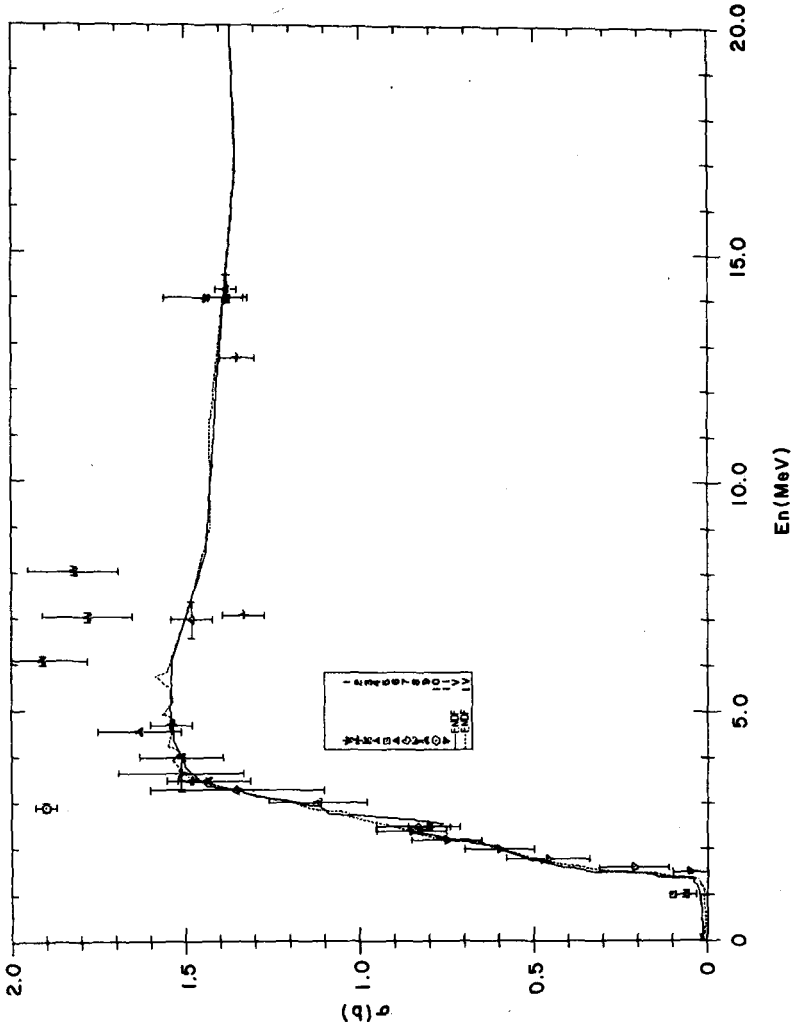

Figure 11. Ni Non-elastic experimental data and the evaluated curve. Numbers 1 to 11 given against the symbols refer to Refs. 20-30 respectively.

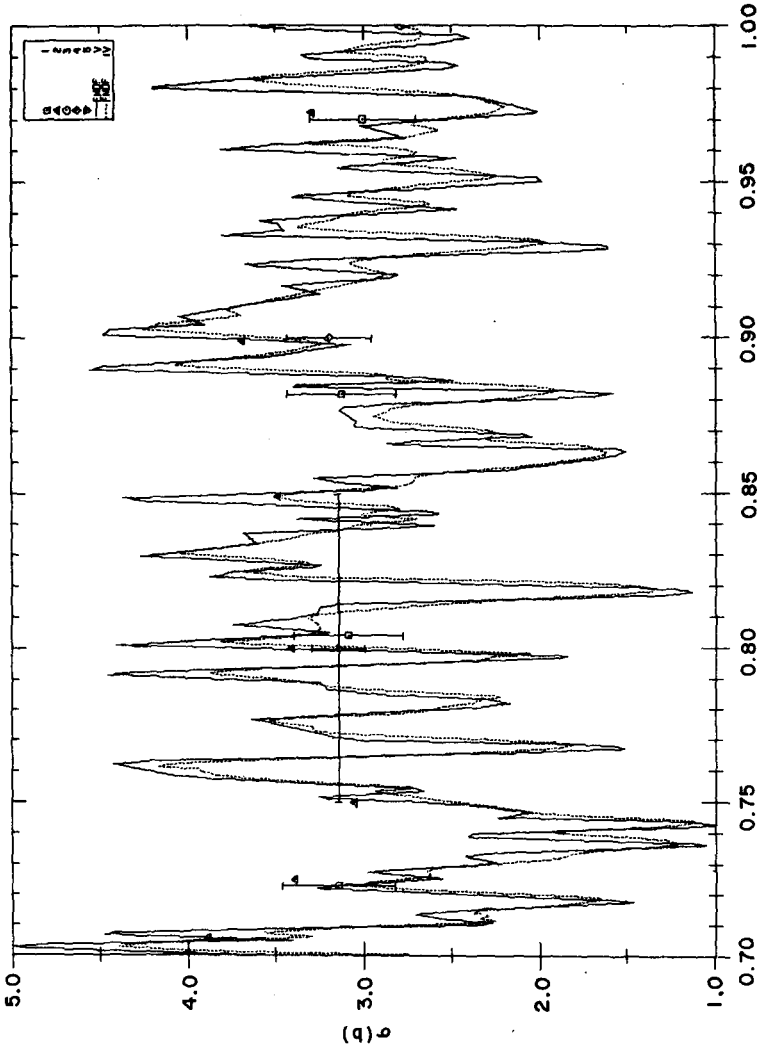

Figure 12a. Ni Elastic Scattering cross sections 0.7-1.0 MeV. Numbers 1 to 5 correspond to references 31, 32, 24, 37 and 38 respectively.

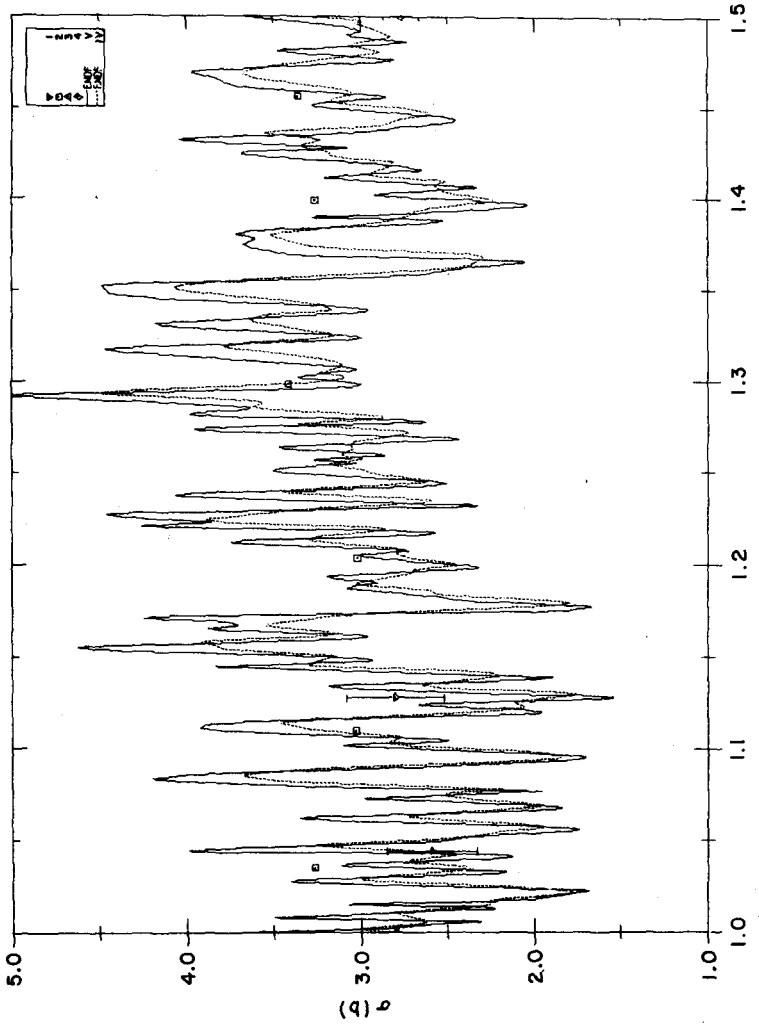

Figure 12b. Ni Elastic scattering cross section 1-1.5 MeV. Numbers 1 to 5 correspond to references 31, 32, 29 and 38 respectively.

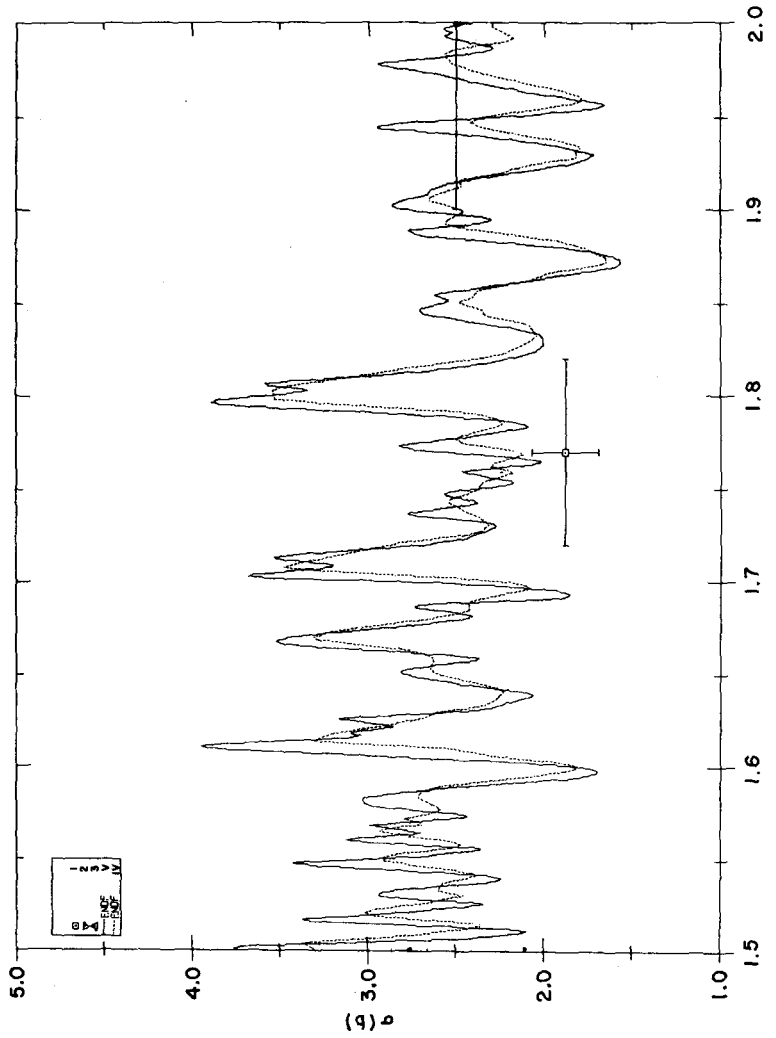

Figure 12c. Ni elastic scattering cross section 1.5-2.0 MeV. Numbers 1, 2 and 3 correspond to Refs. 36, 39 and 40 respectively.

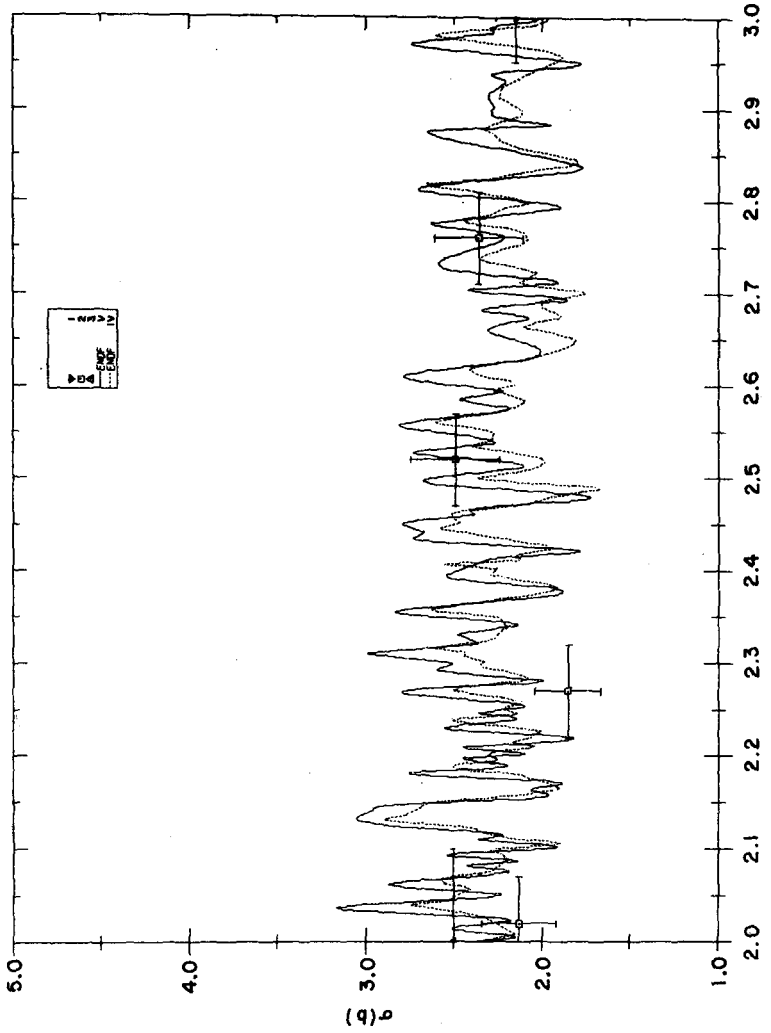

Figure 12d. Ni elastic scattering cross section 2.0-3.0 MeV. Numbers 1, 2 and 3 correspond to Refs. 35, 36 and 39 respectively.

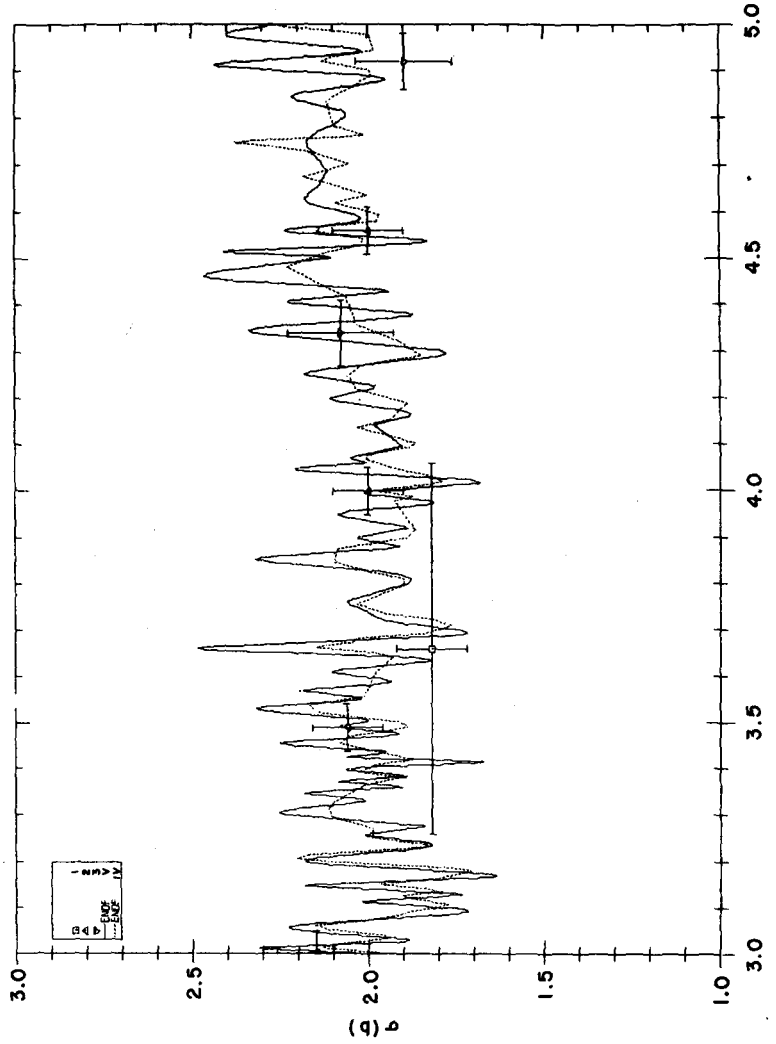

Figure 12e. Ni elastic scattering cross section 3.0-5.0 MeV. Numbers 1, 2 and 3 correspond to Refs. 27, 35 and 41 respectively.

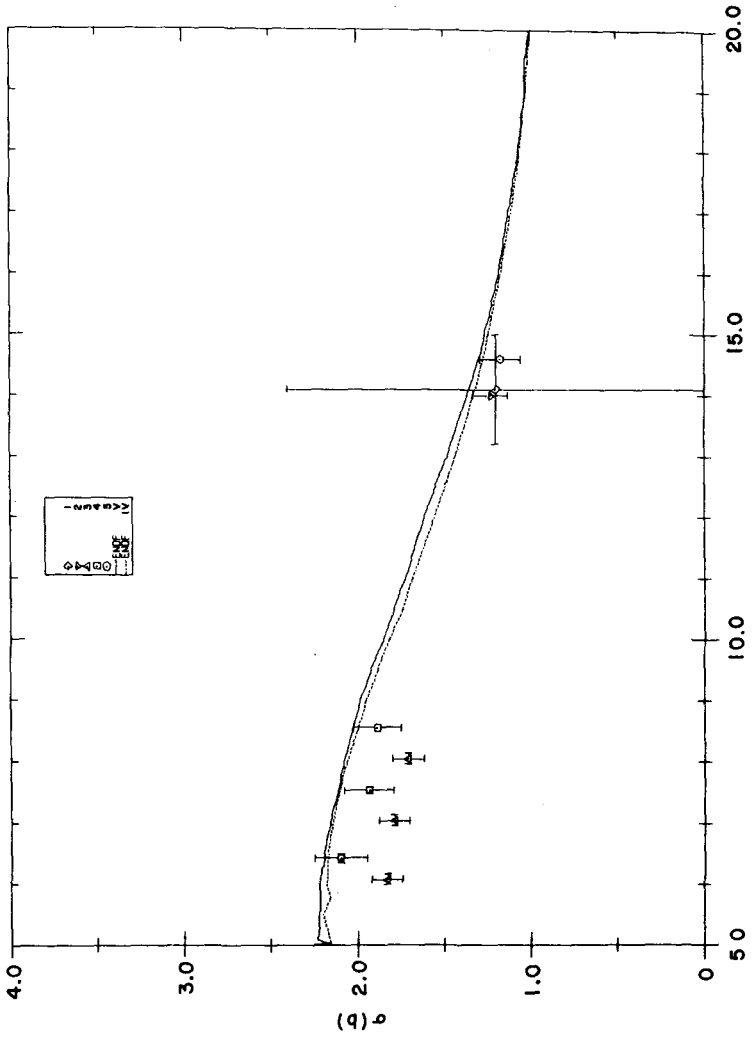

Figure 12f. Ni elastic scattering cross section 5.0-20. MeV. Numbers 1-5 correspond to Refs. 33, 34, 35, 42 and 43 respectively.

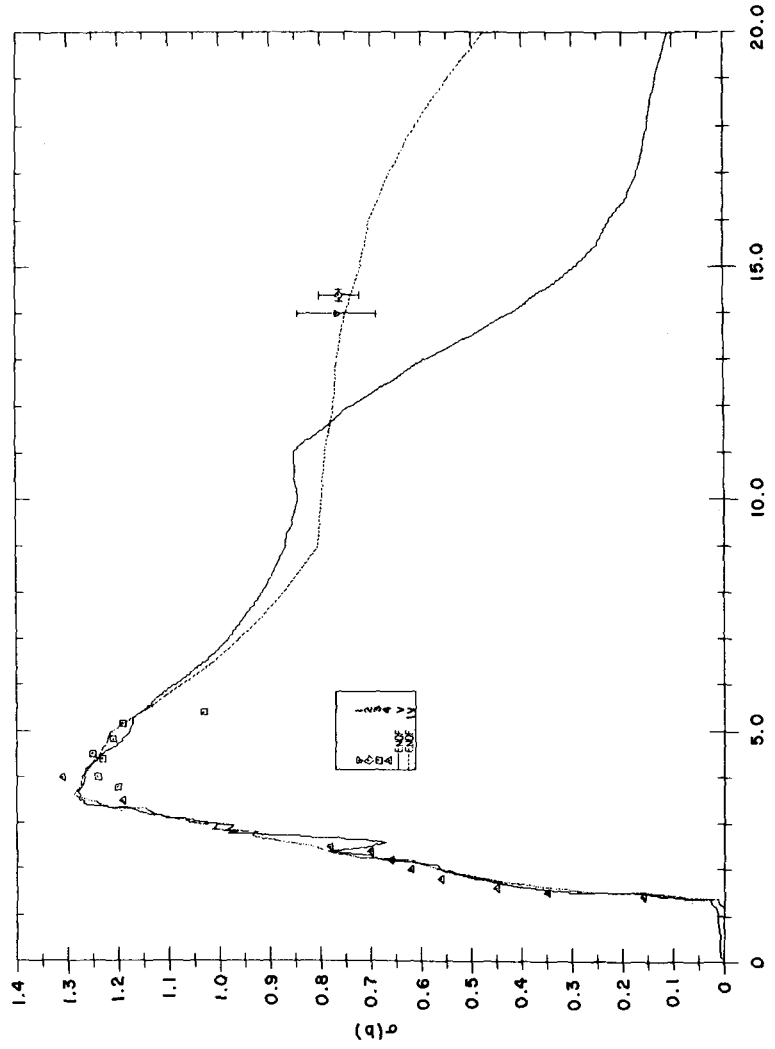

Figure 13. Total inelastic cross section: Experimental data, ENDF/B-IV and V version evaluated curves. Numbers 1-4 correspond to Refs. 44-47 respectively.

2. (n,n') Continuum Cross Section. The difference of $\sigma_{nn'}$ (total) $-\Sigma\sigma_{nn}^{1}$, is the (n,n') continum cross section. A comparison of the ENDF/IV and V cross section for the inelastic continuum is shown in Fig. 14.

3. Inelastic Discrete Level Excitation Cross Sections. Inelastic cross section to a discrete level is measured either by measuring gamma-rays produced by inelastic scattering or by measuring directly the inelastically scattered neutrons at different angles. In the former case, corrections have to be made for the contributions due to higher lying states.

Reasonably extensive data are available for the first excited states of ^{58}Ni, ^{60}Ni and ^{62}Ni isotopes. The maximum energy range of measurements is about 7 MeV. Furthermore, the measured experimental data extends up to about 4 MeV for six additional levels. In particular experimental data only at a few energies are available for some high-lying levels. No experimental data are available for ^{61}Ni and ^{64}Ni excited levels.

Experimental inelastic excitation functions to individual levels are used to normalize the Hauser-Feshbach (COMNUC/MODNEW) calculations. Direct inelastic effects are included for the first two excited states of even-even isotopes by joining the HF calculated results with JUPITOR calculations, which consider the coupling of inelastic channels. HF calculated results are used for the levels for which there is no experimental data available.

COMNUC and JUPITOR calculations were performed by Bhat for the even Ni isotopes. COMNUC (and MODNEW) calculations were performed for the odd isotope ^{61}Ni.

a. E_x = 1.172 MeV ($62:2^+$). Rogers',[48] and Smith's,[49] data are considered for the evaluation. In addition, Tsukada, et al.,[56] measured the 1.172 MeV level excitation cross section at E_n = 2.6 MeV energy. The experimental data of Roger's agree well with COMNUC calculations, whereas Smith's data with large error bars are in disagreement with theory (cf Fig. 15a). Furthermore, as pointed out in Section III B5 some of the data points between 2.4-2.8 MeV are even higher than the total nonelastic cross section, which is about 1.5 barn at these energies. Such unreasonable values for the inelastic cross section to the 1.172 MeV levels might be due to the small isotopic abundance, impurities in the sample, and also due to weak excitation of the level in question. Under these circumstances the calculated cross section is adopted for the evaluated excitation function for the ^{62}Ni 2^+ level at 1.172 MeV.

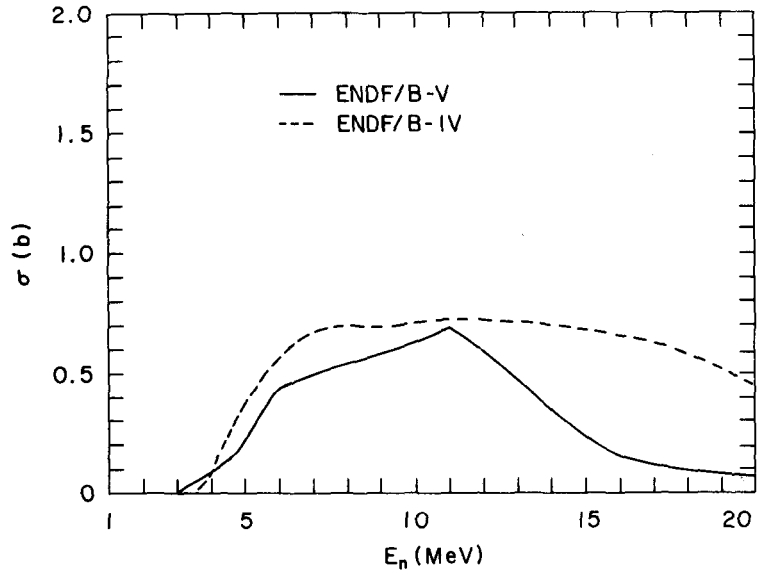

Figure 14. Ni(n,n') continuum cross section.

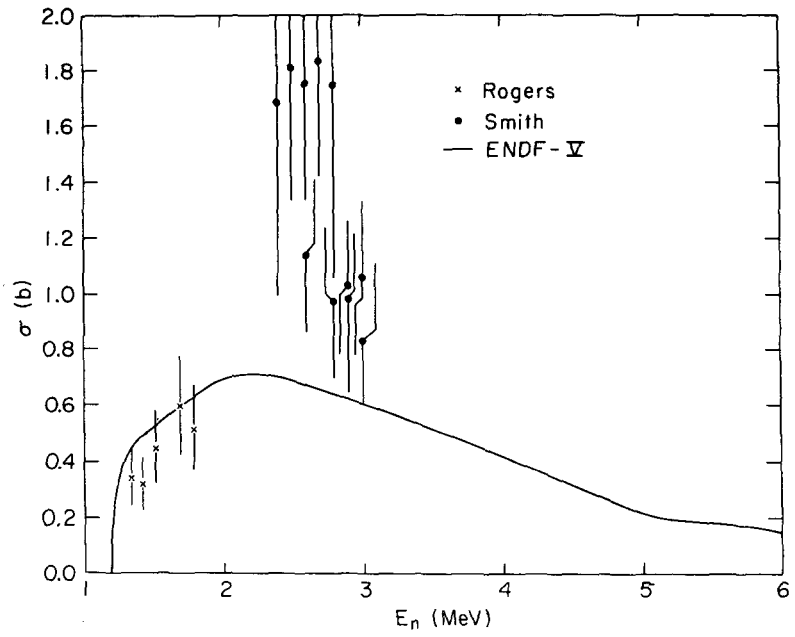

Figure 15a. Inelastic scattering cross section E_x=1.172 MeV.

b. E_x = 1.332 MeV (^{60}Ni 2$^+$). Experimental data for the ^{60}Ni 2$^+$ (1.332 MeV) level extends from threshold to 7 MeV (cf Fig. 15b). Konobeevskii's data,[54] fluctuate rapidly below 1.7 MeV neutron energy. In addition, Smith's data,[49] indicates strong fluctuations up to 3.6 MeV. The evaluated curve retains some broad structure suggested by the Argonne data.[49] It should be pointed out that the ^{60}Ni and NiO total cross section data,[18,19] have rapid fluctuations up to a few MeV neutron energy. The HF calculated results are used to extrapolate the evaluated curve and at 10 MeV the JUPITOR coupled channel calculated results were joined to the low energy curve.

c. E_x = 1.452 MeV (^{58}Ni 2$^+$). Energy variation of the experimental cross for the 1.452 MeV ^{58}Ni 2$^+$ level is similar to the ^{60}Ni 2$^+$ level at 1.332 MeV, in that there are violent fluctuations in the data below 1.7 MeV and also between 2.0 and 3.4 MeV (cf Fig. 15c). The strong broader structure exhibited by Smith's data,[49] is retained in the evaluated curve. Both in the case of 1.332 and 1.452 MeV levels, it is not possible to correlate the apparent structure with doorway state intermediate structure until detailed angular distribution are measured or appropriate doorway state calculations are performed. As pointed out earlier, the natural Ni total cross section data,[19] exhibit structure extending up to 5.0 MeV neutron energy.

d. E_x = 2.158 MeV (^{60}Ni 2$^+$). Experimental data (Smith,[49] Perey, et al.,[55] and Boschung,[53]) extend up to 5.5 MeV. Tsukade's data,[56] (not shown) is in general agreement with Smith's data. The Hauser-Feshbach calculated cross sections agree well with these experimental data. The coupled channel calculated results were merged with the Hauser-Feshbach results to extend the evaluated curve (cf. Fig. 15d) to 20 MeV.

e. E_x = 2.286 MeV (^{60}Ni 0$^+$). There are two other levels (2.293 [^{62}Ni 2$^+$] MeV and 2.272 [^{64}Ni 0$^+$] MeV) in the vicinity of the 2.286 MeV level. Proximity of additional levels makes it difficult to isolate the 2.286 level excitation in an inelastic scattering experiment. This is obvious from Fig. 15e in the sense that agreement between theory and experiment[49] is off by at least a factor of 2 at 4 MeV. Incidentally, Tsukade's data,[59] (not shown) is in general agreement with theory. The Hauser-Feshbach calculated results were adopted for the evaluated curve.

f. E_x = 2.482 (^{58}Ni 2.459 + ^{60}Ni 2.506). Smith, et al.,[49] measured cross section for the combined excitation of ^{58}Ni 2.459 MeV and ^{60}Ni 2.506 MeV 4$^+$ states around 3.7 MeV neutron energy. In the absence of separate experimental data for each of the levels mentioned, the Hauser-Feshbach calculated cross sections to the two levels were added and normalized to Smith's data. The renormalized theoretical results were adopted for the evaluated

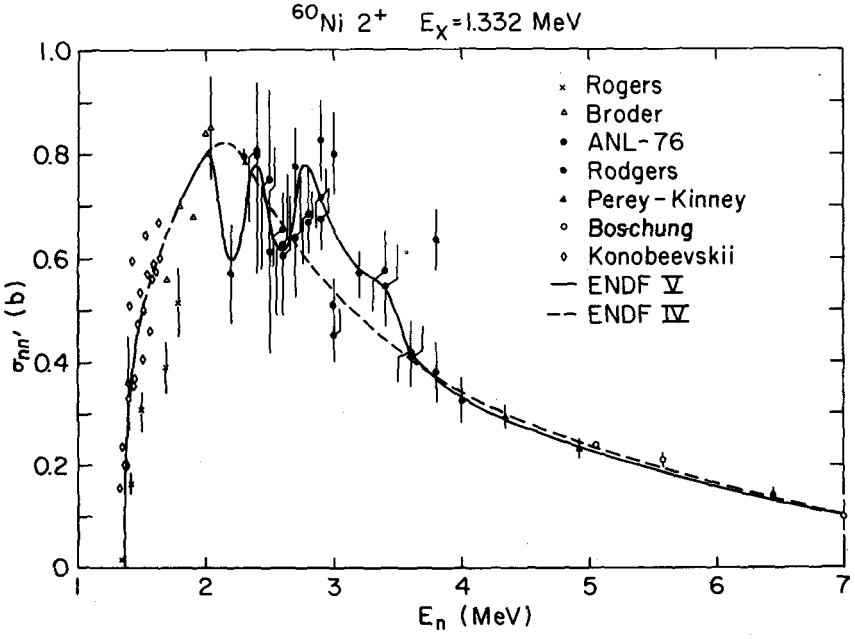

Figure 15b. Inelastic scattering cross section E_x=1.332 MeV.

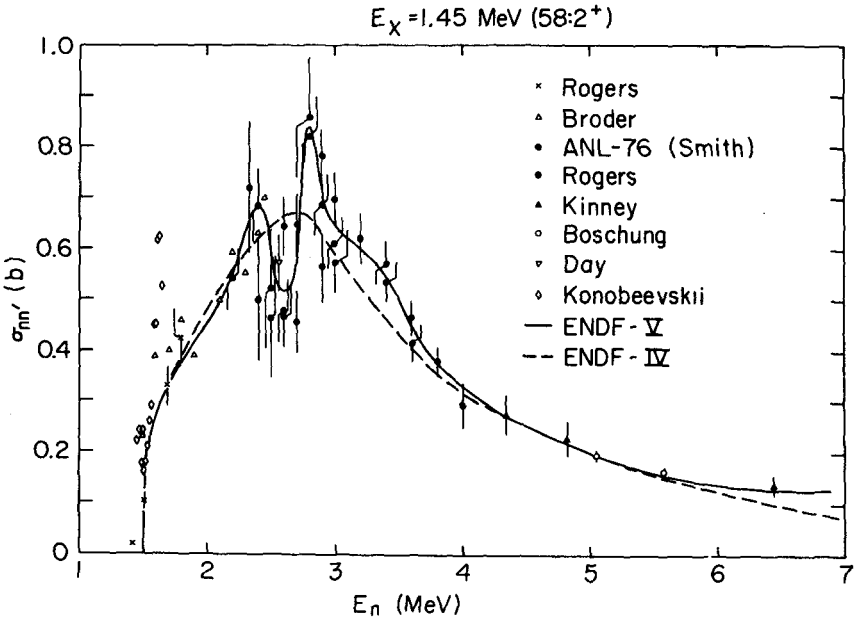

Figure 15c. Inelastic scattering cross section E_x=1.454 MeV.

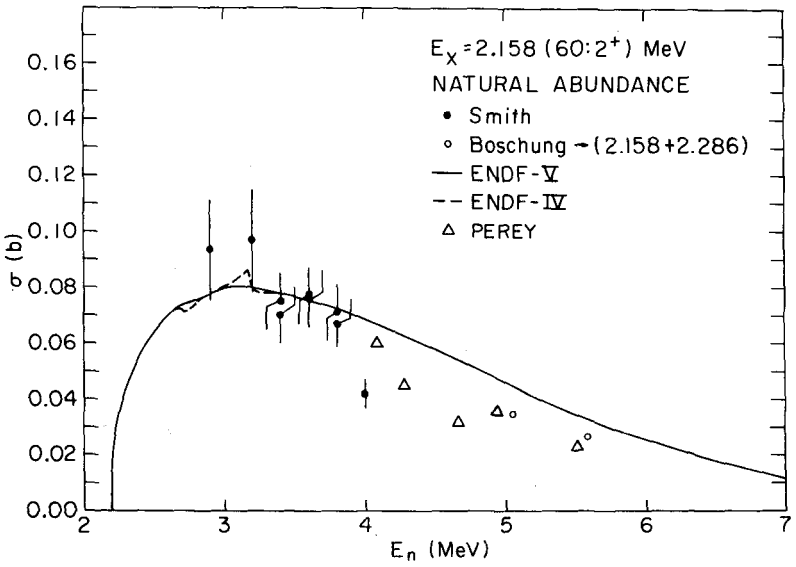

Figure 15d. Inelastic scattering cross section E_x=2.158 MeV.

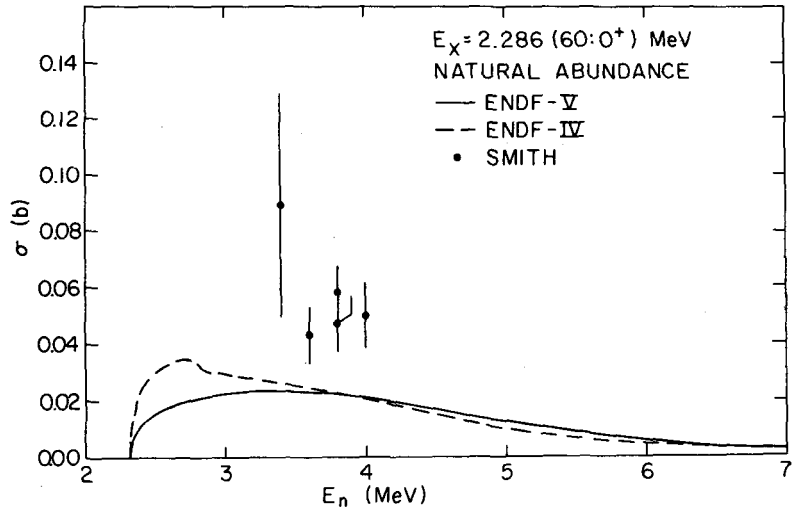

Figure 15e. Inelastic scattering cross section E_x=2.286 MeV.

excitation functions for both the levels mentioned above. Boschung's points at 5 and 5.5 MeV are shown for comparison in Fig. 15f.

g. E_x = 2.625 MeV ($60{:}3^+$). In the case of the 2.625 MeV level excitation only the Argonne data (Smith[49]) are adequately resolved, whereas the inelastic cross sections both measured by Kinney and Perey,[55] and Boschung,[53] correspond to the sum of the ^{60}Ni 2.506 MeV and the 2.625 MeV level excitation. To construct the ^{60}Ni 2.625 MeV level cross section from the latter data set, the evaluated 2.506 MeV level cross sections were subtracted from the measured (2.506 + 2.625) MeV cross sections at different energies up to 5.5 MeV. The actual measured cross sections (2.506 + 2.625 MeV) and the 2.625 MeV level derived cross sections (symbols with dots) are plotted (cf. Fig. 15g) at each energy and they are connected by vertical bars. The evaluated curve based on Hauser-Feshbach results is shown as a smooth curve. Considering all the uncertainties involved in the experimental data, the evaluated curve is a reasonably good approximation to represent the 2.625 MeV level excitation cross section.

h. E_x = 2.775 MeV ($58{:}2^+$). There are only two data points corresponding to the 2.775 MeV level and the Hauser-Feshbach calculated curve goes through one of the experimental points. The calculated curve was adopted for the evaluation purposes (cf. Fig. 15h).

i. E_x = 2.902 - 3.42 MeV. The Hauser-Feshbach calculated results were adopted for the remaining 17 levels for which no experimental data exist.

A. Secondary Continuum Neutron Distribution.

Parameters extracted by Hermsdorf, et al.[60], around 14 MeV for the emitted neutron distribution were used. In particular, the cross section for the inelastic process is represented by:

$$\sigma_{nn'}(E) = \sigma^{cn}_{nn'}(E) + \sigma^{pre}_{nn'}(E)$$

$$\sigma^{cn}_{nn'}(E) = a_{cn}(E)e^{-E/T}$$

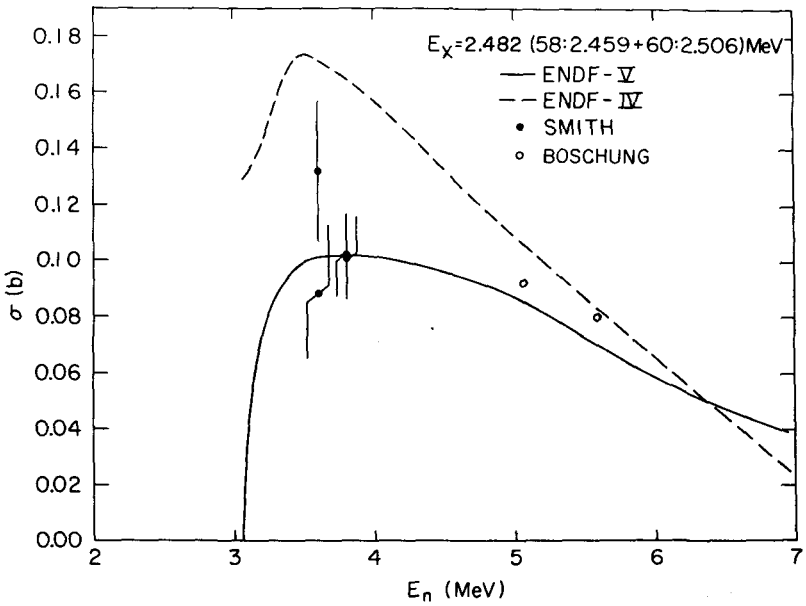

Figure 15f. Inelastic scattering cross section E_x=(2.49+2.506) MeV.

The upper triangles and circles correspond to the sum of the inelastic excitation to two nearby Levels at 2.506 MeV and 2.625 MeV, while the lower set of points with dots were obtained by subtracting the evaluated curve for the 2.506 level from the experimental (top) points. The two sets of points are connected by vertical bars. Smith's data are shown as black circles.

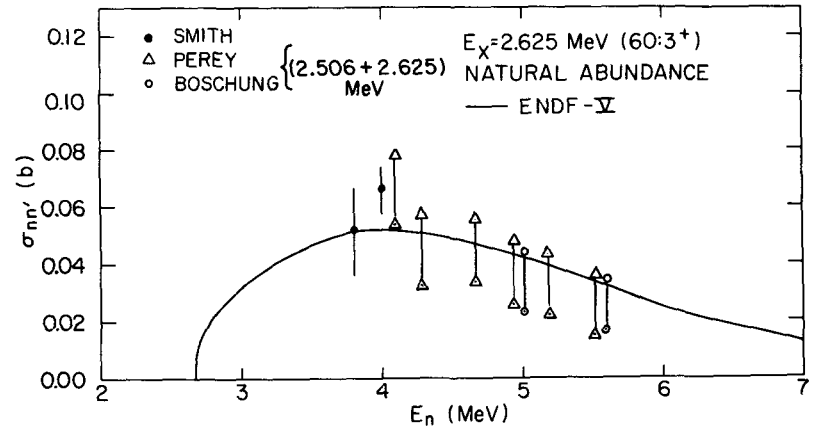

Figure 15g. Inelastic scattering cross section E_x=2.625 MeV.

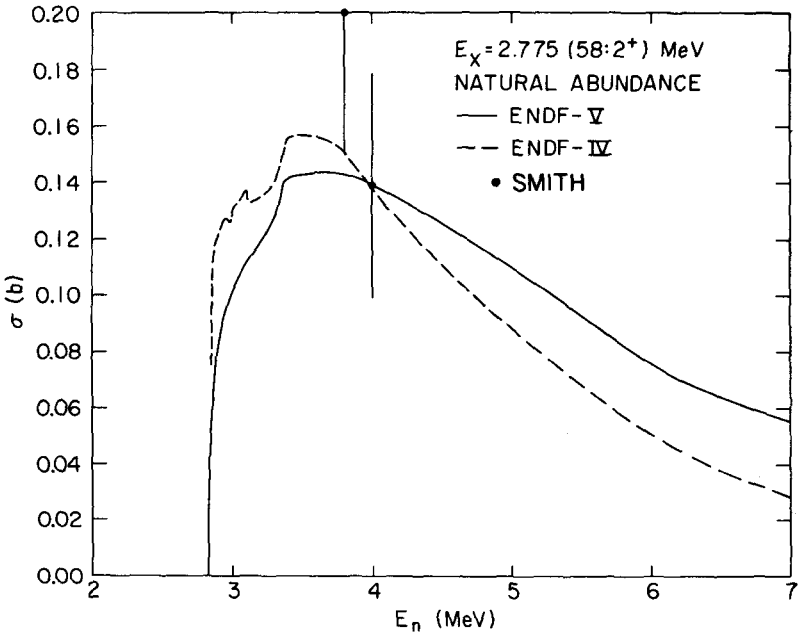

Figure 15h. Inelastic scattering cross section E_x=2.775 MeV.

$$\sigma_{nn'}^{pre}(E) = a_{pre}(E)e^{-E/T}$$

$$T = 1.3 \text{ MeV}$$

The coefficients $a_{cn}(E)$ and $a_{pre}(E)$ were adjusted at each incident neutron energy so that

$$PF(E) = \frac{\sigma_{nn'}^{pre}(E)}{\sigma_{nn'}^{cn}(E) + \sigma_{nn'}^{pre}(E)} = \frac{a_{pre}(E)}{a_{cn}(E) + a_{pre}(E)}$$

where PF is an energy dependent precompound fraction calculated from Balnn's formulation. See Section IIIC for details regarding the PF calculation. Energy distribution of the secondary neutrons is calculated at different energies from 3.0-20.0 MeV. Even though the procedure adopted is a simple one but the precompound fraction used is in excellent agreement with that determined by Kammerdiener[43], at 14 MeV and also as suggested by the (n,p) cross section calculations based on HF and precompound formation.

B. (n,2n) Reaction

1. ^{58}Ni(n,2n) Cross Section. Since the last evaluation of ^{58}Ni(n,2n) reaction only one set of new measurements were done by Bayhurst, et al.[76] They used radio chemical methods for measuring the cross section. The ^{27}Al(n,α) reaction cross section was measured to determine the neutron fluence. The ^{58}Ni(n,2n) measured cross sections were renormalized to the ENDF/IV ^{27}Al(n,α) cross section.

There are extensive measurements[61-75] (in addition to the one referred to above) on the ^{58}Ni(n,2n) cross section (cf Fig. 16). Paulsen and Liskien and Bormann, et al., measured the (n,2n) cross section over a wide energy range. Details of their data and other data have been discussed by Bhat,[1,77] in his evaluation.

It should be pointed out that some of the cross sections which re-quired renormalization have been corrected for the ENDF-IV cross sections. The exception being that of

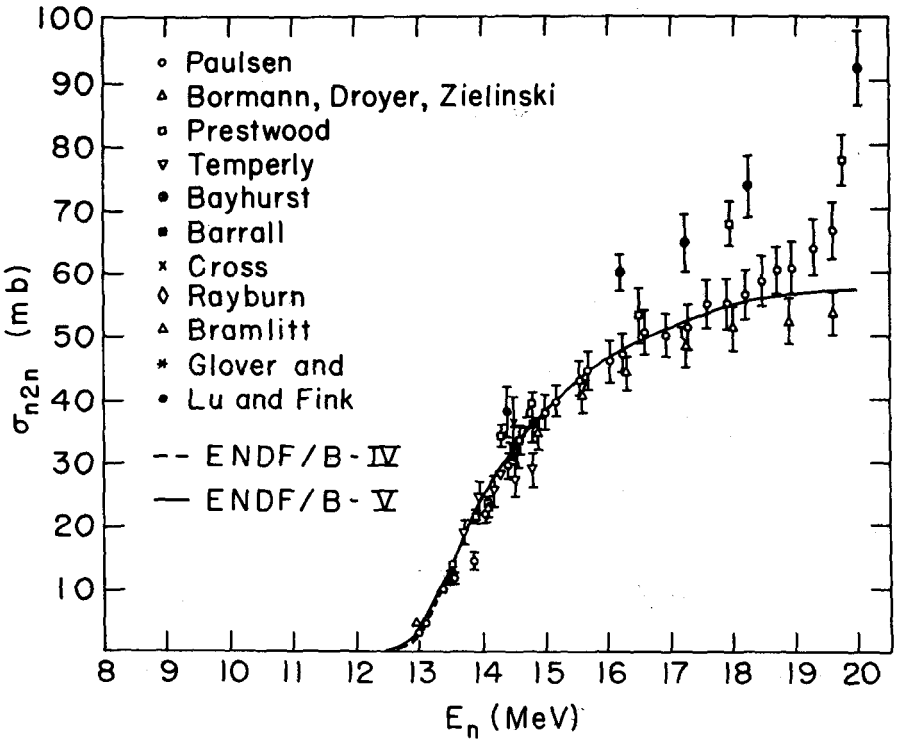

Figure 16. ^{58}Ni(n,2n) cross section.

Prestwood and Bayhurst who measured with respect to $^{238}U(n,f)$. The $^{238}U(n,f)$ cross sections are not listed in their paper for use in renormalization.

Paulsen and Liskien,[61] and Bormann's data,[62] are in good agreement with each other below 16 MeV, while they diverge above this energy with the Paulsen data being larger than the other set.

There are three other sets that extend up to 20 MeV: one by Prestwood and Bayhurst,[63] the second by Bayhurst, et al.,[76] and the third one by Jeronymo et al.[64] These data agree with the general trend up to 14 MeV; above this energy they are very high. Particularly that of Bayhurst, et al., which are recent measurements. From their paper, it is not clear whether they had done any multiple scattering corrections, etc.

The Jeronymo data (not shown in the Figure) are too low to be considered for evaluation. Similarly Lu and Fink,[65] Cross et al.,[66] measured around 14 MeV. All of these three measured cross sections are higher than the rest. They were not given any weight in the evaluation.

Glover and Weigold's measurements,[75] (not shown) follow the general trend of the other data.

The evaluated curve (cf, Fig. 16) was drawn following the general trend of the Bormann data and at higher energies lying in between Paulsen-Liskien[61] and Bormann data. Near the threshold HF calculated values were used to draw the curve. Essentially, the present evaluation is the same as that done by Bhat,[1,77] except near the threshold.

Incidently, Qaim,[79] reported the 14.7 MeV $^{58}Ni(n,2n)$ cross section to be 35 ± 3 mb, which is in good agreement with the evaluated curve shown in Fig. 16. Marcinkowski and collaborators,[78] evaluated the $^{58}Ni(n,2n)$ reaction. Their evaluation puts the (n,2n) cross section slightly higher than the present evaluation beyond 14 MeV. In particular, their evaluated cross section at 20 MeV is about 20% higher than that given here. Details of the measured $^{58}Ni(n,2n)$ cross section data used in the evaluation are given below:

E_n range (MeV)	Method	Renormalized	Standard	Reference
16.2-20	Radiochemical	yes	Al(n,α)	Bayhurst, et al.
12.9-19.6	Activation	-	Absolute	Paulsen-Liskien
12.9-19.6	Activation	not required	Hydrogen	Bormann

E_n range (MeV)	Method	Renormalized	Standard	Reference
13.7-14.8	Activation	-	Absolute	Temperley
13.5-19.8	Radiochemical	-	$^{238}U(n,f)$	Prestwood
13.8-14.9	Activation	-	Absolute	Glover-Weigold

2. $^{60,61,62,64}Ni(n,2n)$ Cross Sections. There are no experimental data available for all but ^{58}Ni of the Ni isotopes. The code MODNEW was used to predict (n,2n) cross sections for all the four remaining isotopes. Due to uncertainties in the statistical model parameters, the predicted cross section for each isotope at 14 MeV was normalized to the results of THRESH,[80] which are based on systematics. The resulting normalization factor was used to renormalize the MODNEW calculated results for that isotope. The final $^{60,61,62,64}Ni$ (n,2n) excitation functions are shown in Fig. 17, along with the $^{58}Ni(n,2n)$ evaluated curve.

3. Ni(n,2n) Cross Section. The Ni(n,2n) excitation function constructed from the individual isotopes is shown in Fig. 18. ENDF IV evaluation puts the curve low at 14 MeV and high at 20 MeV neutron energy.

C. (n,p) Cross Section

1. $^{58}Ni(n,p)$ Cross Section. The data on $^{58}Ni(n,p)$ cross section are extensive,[82-102] and of reliable quality. This reaction is used in dosimetry applications, and also treated as a secondary standard for measuring other neutron induced reactions.

The previous $^{58}Ni(n,p)$ evaluation was done by Schenter.[81] In the low energy region, his evaluation closely follows the experimentally measured values of Smith and Meadows,[82] in that local fluctuations of the cross section were retained in the evaluated curve. In addition, the 6-13 MeV range had only four measured points. However, for the present evaluation, extended measurements by Smith and Meadows,[83] are available.

The most extensive sets of data on $^{58}Ni(n,p)$ reaction are:

1. Smith and Meadows[82] 0.44 - 10.0 MeV
2. Meadows and Whalen[84] 1.04 - 2.67 MeV
3. Barry, *et al*[88] 1.6 MeV - 15 MeV
4. Paulsen and Widera[86] 1.2 and 12.7 - 16.4 MeV
5. Okumura[97] 13.4 - 15 MeV
6. Bormann[91] 13.0 - 19.6 MeV

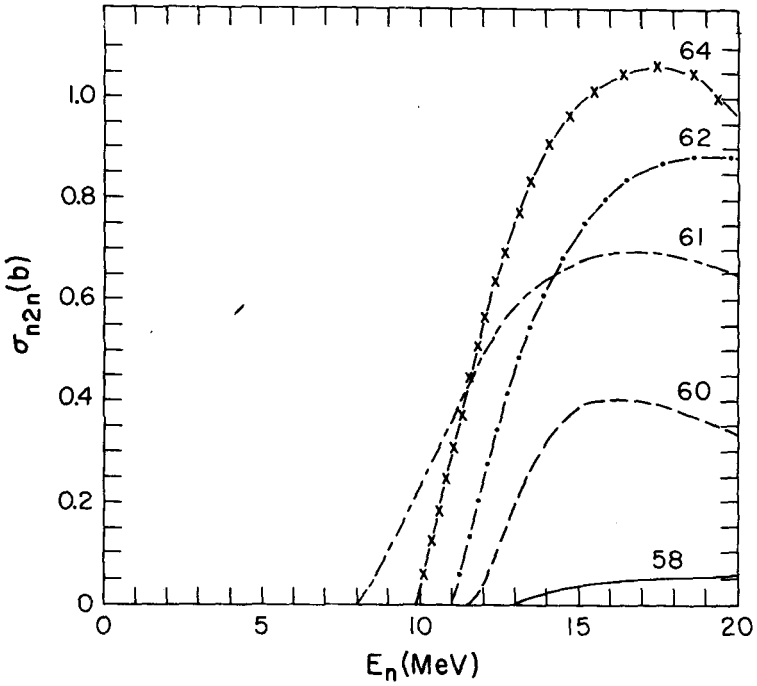

Figure 17. Ni isotope (n,2n) evaluated cross section.

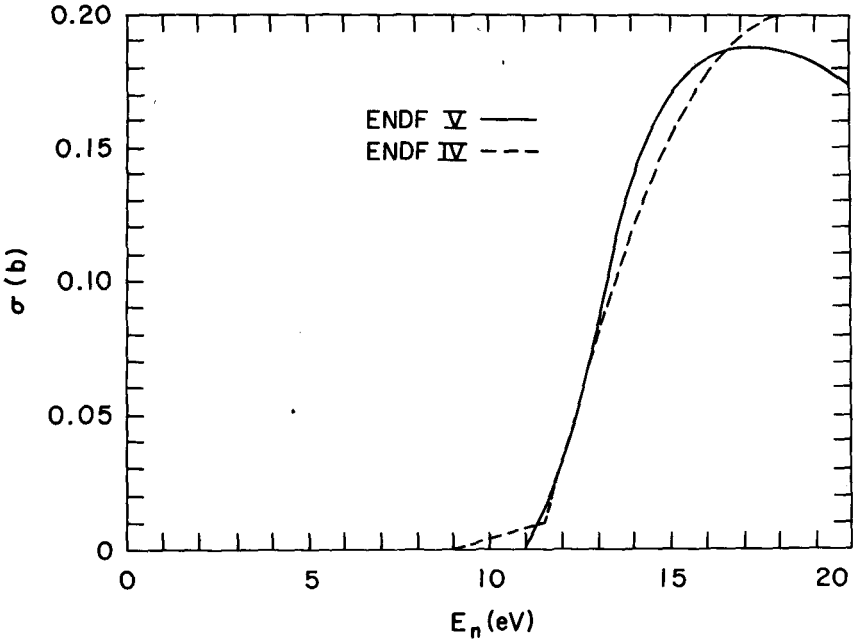

Figure 18. Natural Ni(n,2n) evaluated cross section.

In addition, there are other measured data sets at a few energy points ranging from 2-15 MeV.

For the purpose of evaluation, the entire experimental data was reviewed* in detail in the following energy ranges:

0.4 - 1.0 MeV
1.0 - 2.0 MeV
2.0 - 4.0 MeV
4.0 - 6.0 MeV
6.0 - 10.0 MeV
10.0 - 12.7 MeV-Gap - (no data)
12.7 - 15.0 MeV
15.0 - 20.0 MeV

a. 0.4 - 1.0 MeV Region. In this low energy region, only the data of Smith and Meadows,[82] is available. There are some deviations from the expected, smooth energy dependence of the low energy (n,p) cross section. The 0.5 MeV and 1 MeV cross section values were determined from the simple prescription (given in Fermi's book) for exothermic neutron-induced (and outgoing charge-particle) reactions. Most of the experimental points at these low energies follow this prescription. Comparison of the present evaluation vs. Schenter's evaluation is shown in Fig. 19a.

b. 1.0 - 2.0 MeV Region. In this energy range, Smith-Meadows,[82,83] Meadows-Whalen,[84] Paulsen-Widera,[86] Temperley,[85] and Nakai,[87] data are shown. Temperley points are too high compared to the general trend of the Smith-Meadows and Meadows-Whalen data. Furthermore, Nakai's points have very large errors. Temperley's and Nakai's data were not considered in the evaluation.

As in Fig. 19a, the evaluated curve is shown along with the ENDF/B-IV evaluation in Fig. 19b.

c. 2.0 - 4.0 MeV Region. There are several data sets in this energy range. Smith-Meadows data,[83] covers most of the range, Gonzalez's,[102] points, and some of the Konijn's,[89] points are high and a few of the latter ones are low beyond 3.5 MeV from the general trend of most of the data points, while Nakai's points are low. Some structure (fluctuation) is evident in the 2.5-4 MeV range, especially around 3.0 MeV, and 3.25 MeV in the Smith-Meadows data. For the purpose of evaluation, it was decided to draw a smooth curve to indicate the increasing trend of experimental points. Schenter's evaluation retained all of the

*Comments regarding experimental technique etc., are given under each reference quoted.

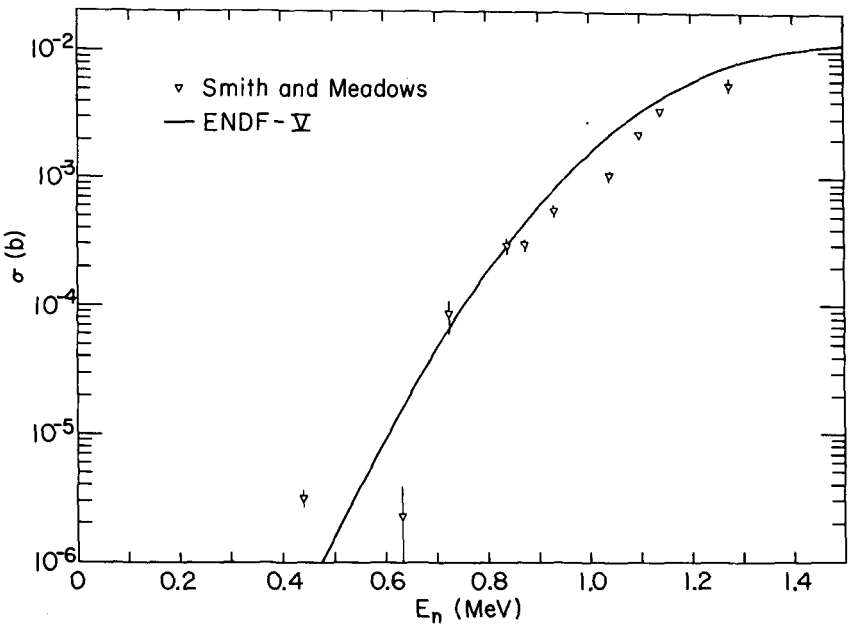

Figure 19a. $^{58}Ni(n,p)$ cross section 0.4-1.4 MeV.

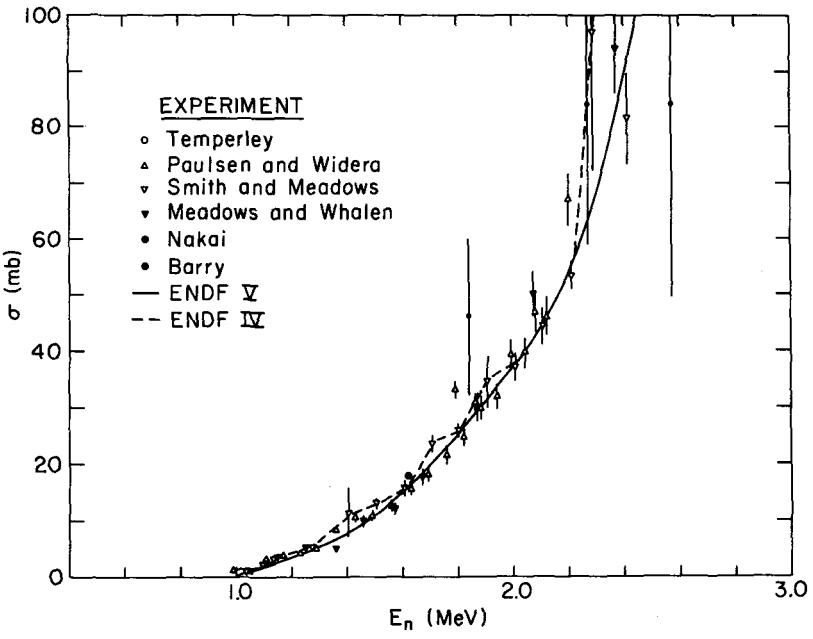

Figure 19b. $^{58}Ni(n,p)$ cross section 1.0-2.5 MeV.

details of local fluctuations. The evaluated curve and Schenter's curve are shown for comparison in Fig. 19c.

d. 4.0 - 4.0 MeV Region. Three data sets cover this energy range-there is some paucity of the data which suggest fluctuations, however, a smooth curve indicating the increasing trend of the data is drawn as an evaluated curve. As in the other energy regions considered, the ENDF/B-IV evaluation retains most of the observed structure in the evaluated curve (cf. Fig. 19d).

e. 6.0 - 10.0 MeV Region. Two data sets span this energy range. Barry's points are higher than that of Smith-Meadows, whereas Smith-Meadows data set has some point scatter. For the evaluation purpose a smooth curve (Fig. 19e) is drawn with a value of 600 mb at 8.5 MeV in the evaluated curve. Notice Schenter's curve is higher than the present evaluation.

f. 10.0 - 12.7 MeV Region. Unfortunately no experimental data exists in this energy region. The evaluated curves below 10 MeV and above 12.7 MeV were smoothly joined (cf. Fig. 19e).

g. 12.7 - 15.0 MeV Region. From Fig. 19f it is noted that there are several experimentally measured cross sections in the 14-15 MeV range. Point scatter is very large in the measured cross sections. Decowski's,[94] points are very high - above the general trend of the other points in this energy region. A curve through most of the points in the 13-15 MeV range is drawn in this region. The choice to draw an evaluated curve is not unique.

h. 15-20 MeV Region. Two data sets cover this energy range, that of Paulsen-Widera,[86] and Bormann,[91] extending only up to 18 MeV. A curve through mid-way between these two sets is drawn. This is justified on the ground that HF calculations with 0.3 precompound fraction predicts a similar trend.

Fig. 19e displays a comparison to ^{58}Ni(n,p) cross section evaluations (2-20 MeV) for ENDF/B-IV and V along with experimental data.

2. ^{60}Ni(n,p) Cross Section. Extensive data for this reaction are measured by Paulsen and Liskien,[103,104] spanning the energy range 6-19 MeV. In addition to this data set, there are some spotty measurements around 14 MeV. Except Allan's[108] data, the rest of the 14 MeV data are high compared to the general trend indicated by the Paulsen and Liskien data.

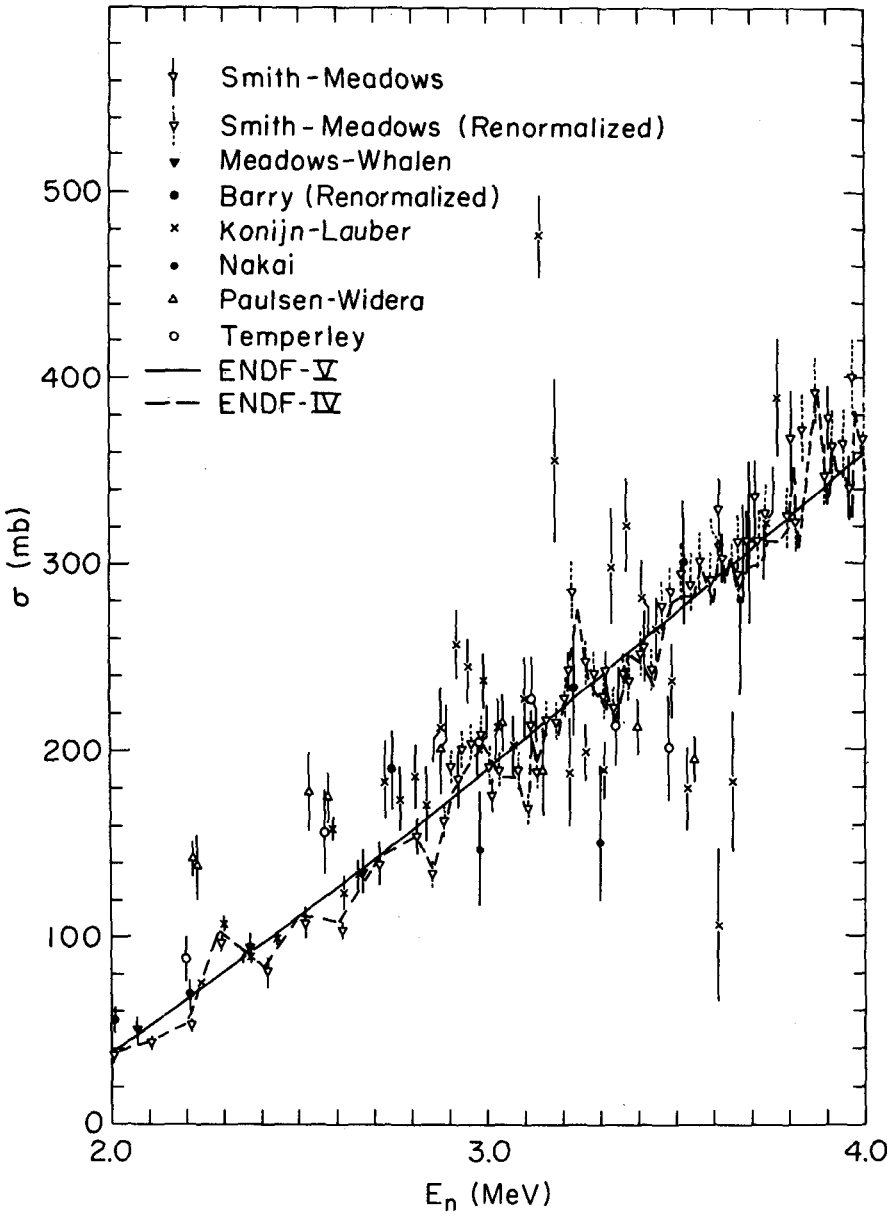

Figure 19c. $^{58}Ni(n,p)$ cross section 2.0-4.0 MeV.

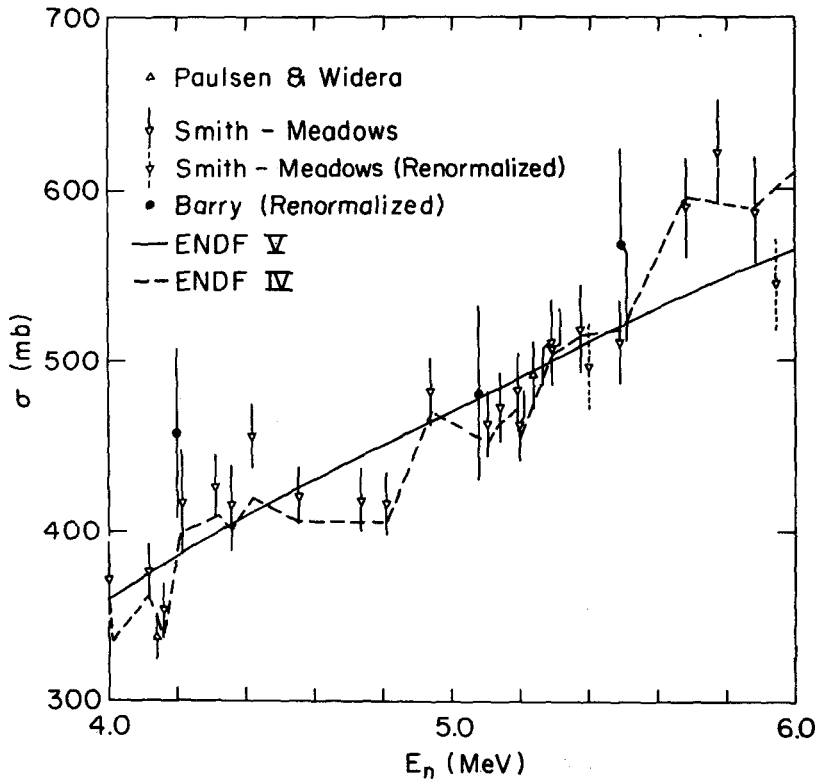

Figure 19d. $^{58}Ni(n,p)$ cross section 4.0-6.0 MeV.

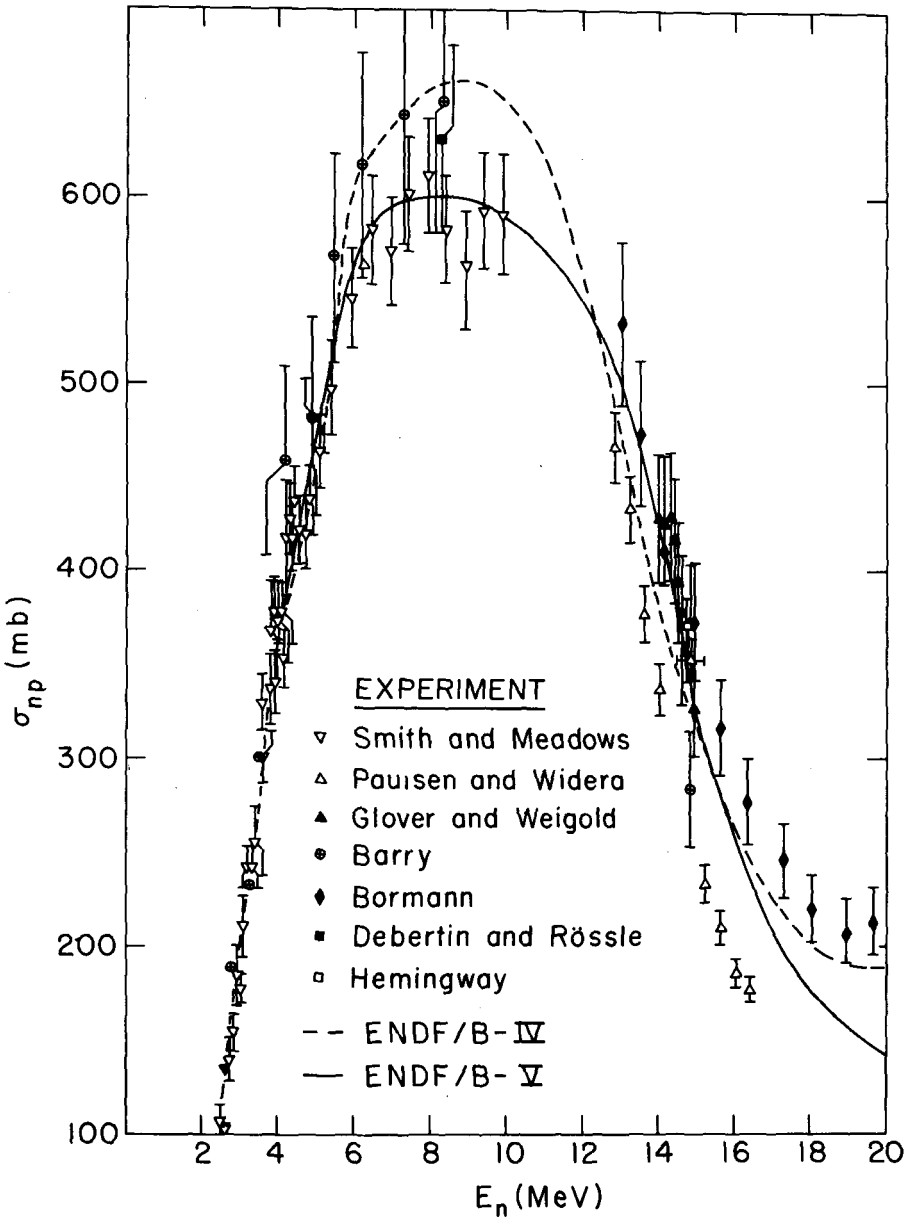

Figure 19e. ^{58}Ni(n,p) cross section 2.0-20.0 MeV.

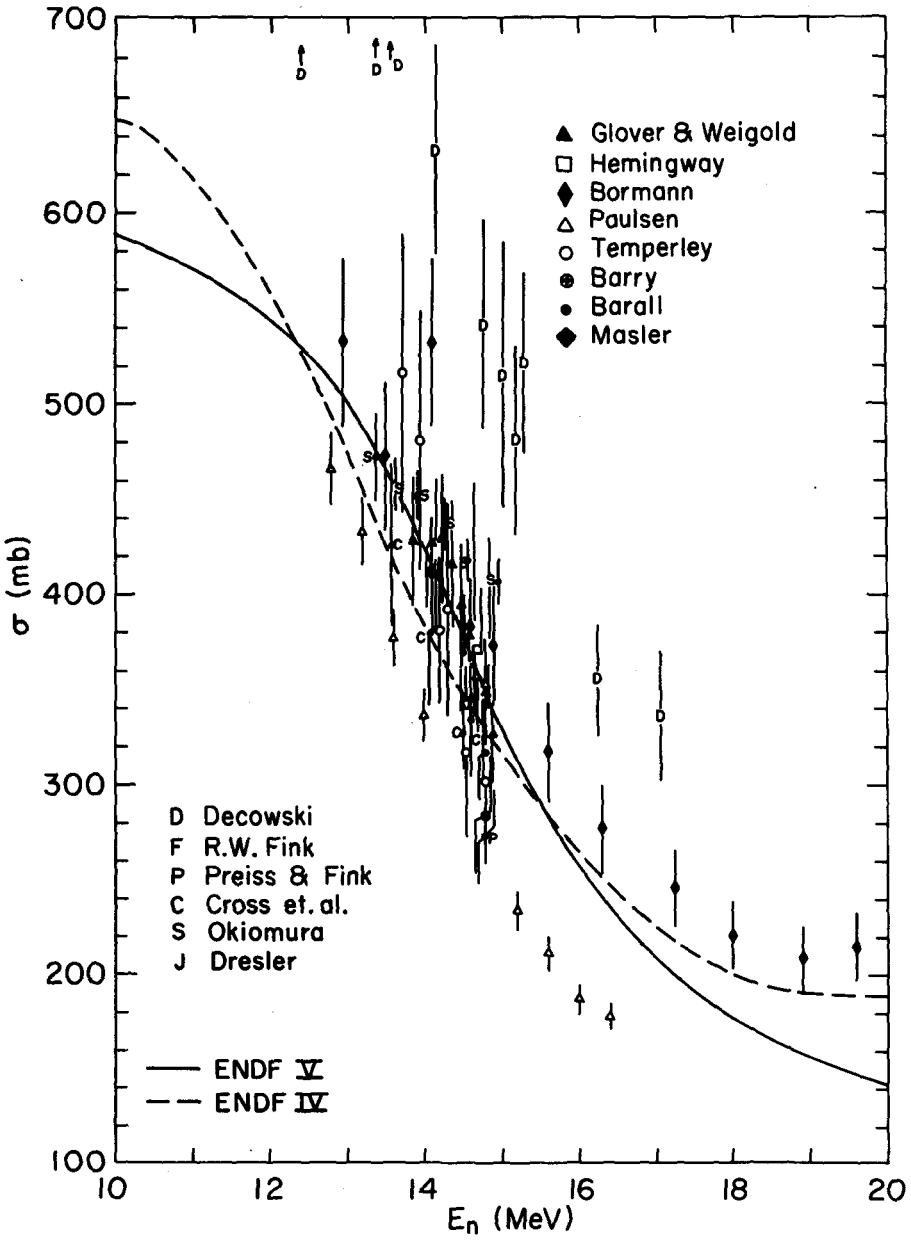

Figure 19f. $^{58}Ni(n,p)$ cross section 10.0-20.0 MeV.

Bhat,[106] has done the previous (ENDF/B-IV version) $^{60}Ni(n,p)$ evaluation. The present evaluation differs from that of Bhat's in two respects.

a. The low energy ($\leq$6 MeV) part of the $^{60}Ni(n,p)$ cross section was extrapolated with the help of the HF predicted (n,p) cross section from threshold to 6 MeV neutron energy.

b. The dominant structure suggested by Paulsen-Liskien data set is retained in the evaluated curve (Fig. 20a). Justification for such a procedure is given below.

To explain the Giant resonance phenomenon in ^{60}Ni compound nucleus ($^{60}Ni + \gamma \rightarrow X+a$) Ligensa and Greiner,[113] have performed lp-lh calculations for $J = 1^-$, T=1 states in ^{60}Ni. They predict five 1^- states between 16-22 MeV excitation in ^{60}Ni. In addition, they also calculated neutron and proton escape widths for these 1^- states to the corresponding ground and excited states. Giant dipole energy position is a slowly varying function of A. The ^{61}Ni "2p-1h" states could be constructed by coupling the ^{60}Ni ground state to the predicted ^{60}Ni 1^- states. The excitation energies in ^{61}Ni would be the same as those in ^{60}Ni. Now if we subtract the neutron binding energy from the ^{60}Ni "1p-1h" state energies, we get the "2p-1h" state energies with respect to neutron threshold. The "2p-1h" state energies ($J^{\pi} = 1/2^+ \text{ --- } 5/2^+$) and their neutron, proton escape widths and the corresponding resonance strengths are shown in Table 4. Resonance Strengths are shown both for spreading width $\Gamma^{\downarrow} = 0$ and $\Gamma^{\downarrow} = .5$ MeV. We would like to point out that all the numbers quoted in this Table are taken from Ligensa and Greiner's paper.

A comparison of the resonance strengths shown in Table 4 with the $^{60}Ni(n,p)$ experimental cross section data is shown in Fig. 20b. The resonance strengths are shown as vertical bars, the cross hatched bar refer to the resonance strength when $\Gamma^{\downarrow} =$ 0.5 MeV and the full height of the bar corresponds to the situation when $\Gamma^{\downarrow} = 0$. The smooth curve through the experimental points is drawn merely to guide the eye. The sum of escape widths $\Gamma_n^{\uparrow}$ and $\Gamma_p^{\uparrow}$ are also shown in numbers adjacent to the resonance-strength bars. As can be seen, the agreement between theory and experiment is remarkable; both the relative strength and the energy position of the predicted 2p-1h doorways are in general agreement with experiment. Until the exact calculations for the ^{61}Ni 2p-1h doorways is performed, this type of comparison should be considered as semi-quantitative type. One might ask: Why the intermediate structure is observed in $^{60}Ni(n,p)$ and not in $^{58}Ni(n,p)$? Two possible explanations are:

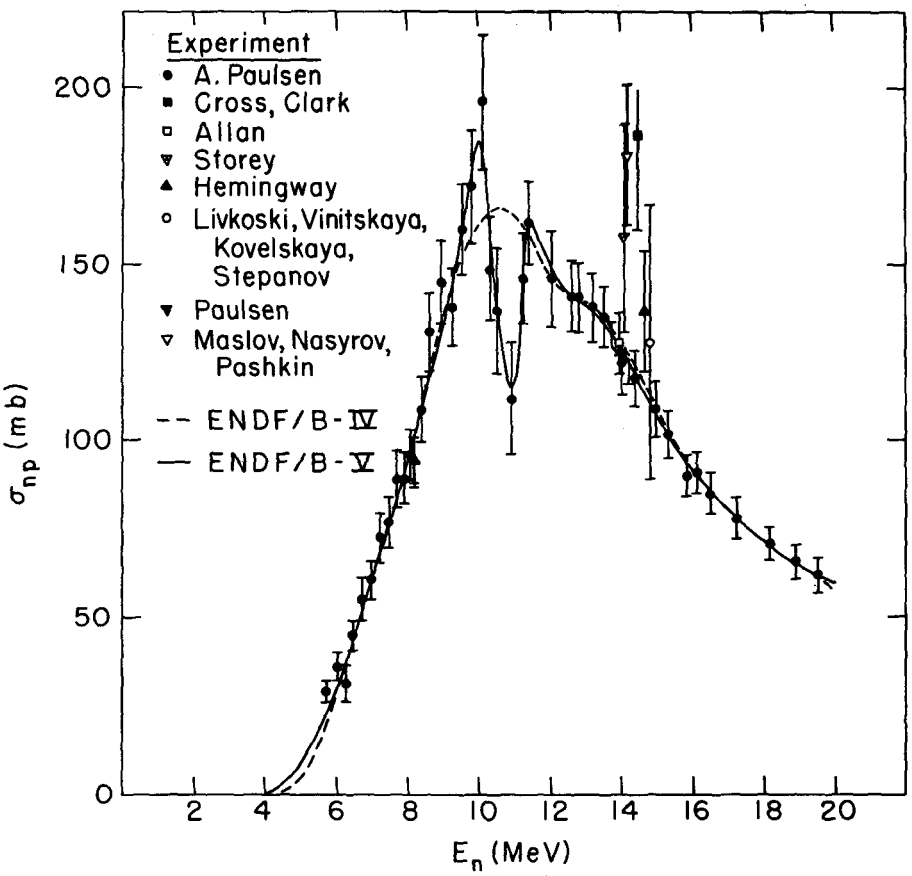

Figure 20a. $^{60}Ni(n,p)$ cross section.

Table 4

^{60}Ni Giant Dipole Resonances

^{60}Ni	^{60}Ni + n	WIDTHS			RESONANCE STRENGTH		Dipole Strength
(E_{p-h}) (MeV)	E_n (MeV)	$\Gamma_{no}^{\uparrow}$ (MeV)	$\Sigma\Gamma_{ni}^{\uparrow}$ (MeV)	$\Sigma\Gamma_{pi}^{\uparrow}$ (MeV)	$\Gamma^{\downarrow}$=o	$\Gamma^{\downarrow}$=.5MeV	
16.35	8.53	.29	.36	.07	.110	.023	428
18.17	10.33	.29	.46	.14	.113	.034	185
19.17	11.35	.04	.42	.13	.017	.005	21
19.68	11.86	.21	.50	.28	.097	.036	92
21.02	13.20	.10	.75	.38	.036	.023	35

$$\text{Resonance Strength (at Resonance)} = \frac{\Gamma_{no}^{\uparrow}\Gamma_{p}^{\uparrow}}{(\Gamma^{\uparrow}+\Gamma^{\downarrow})^2}$$

$$\Gamma^{\uparrow} = \Gamma_{n}^{\uparrow} + \Gamma_{p}^{\uparrow}$$

$$\Gamma_{n}^{\uparrow} = \sum_{i} \Gamma_{ni}^{\uparrow} \quad (i \rightarrow \text{ground and excited states})$$

$$\Gamma_{p}^{\uparrow} = \sum_{i} \Gamma_{pi}^{\uparrow}$$

$\Gamma_{no}^{\uparrow}$ = Ground State (or elastic escape width)

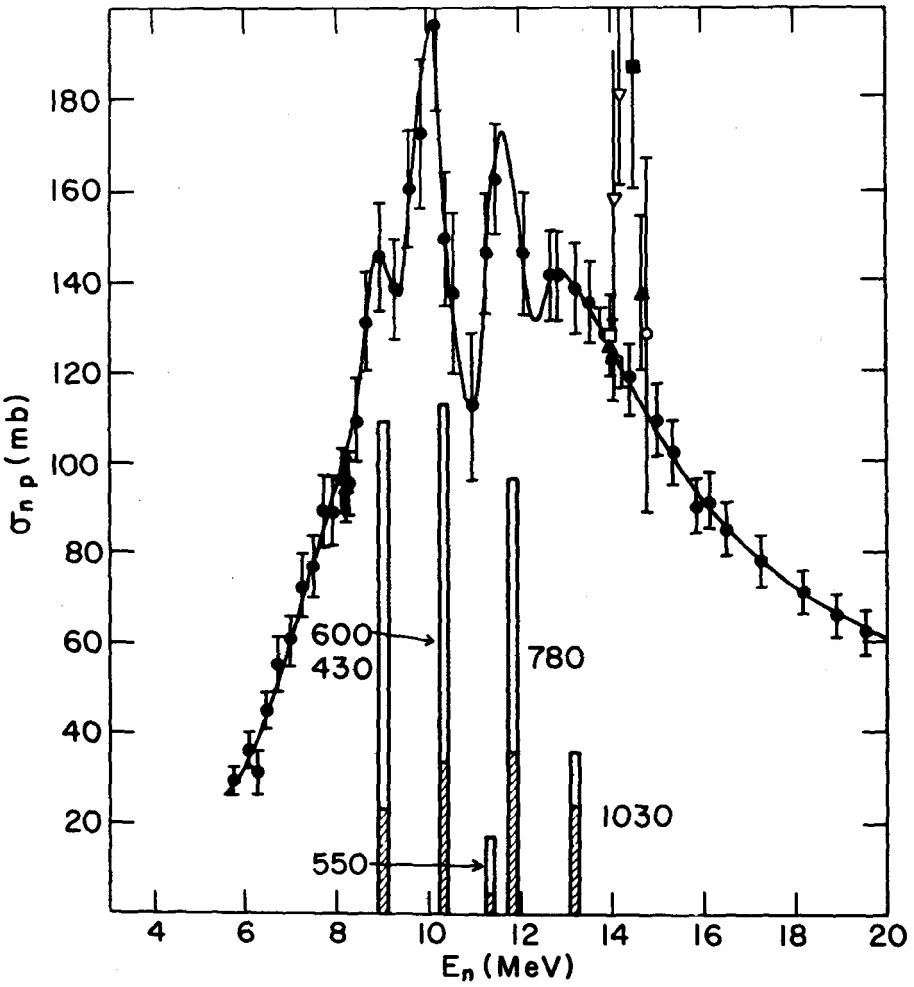

Figure 20b. Doorway intermediate structure interpretation of the $^{60}Ni(n,p)$ cross section.

i. The peak cross section for $^{60}Ni(n,p)$ is only 160 mb, whereas it is about 650 mb in the case of $^{58}Ni(n,p)$. It would be difficult to observe the intermediate structure in $^{58}Ni(n,p)$ with similar strength as observed in $^{60}Ni(n,p)$, because the background cross section is too large for the fluctuations to be discernible as resonances.

ii. ^{60}Ni ground state could be treated as the neutron sub-shell closed at $2p_{3/2}$. Whereas in the case of ^{58}Ni, there are two particles (holes) in $1f_{7/2}$ ($2p_{3/2}^{-1}$) sub-shell.

3. $^{61,62,64}Ni(n,p)$ Cross Sections. In the absence of extensive experimental measurements MODNEW calculations were performed for the minor Ni isotopes ^{61}Ni, ^{62}Ni, ^{64}Ni. There are only two or three (n,p) cross sections measured around 14 MeV neutron energy for each of the isotopes. The theoretical excitation function for each isotope was normalized to the average of experimental cross sections. The corresponding evaluated excitation functions with experimental points are shown in Figs. 21, 22 and 23.

4. Ni(n,p) Cross Section. The isotopic cross sections (cf. Fig. 24a) were combined to construct the natural Ni(n,p) cross sections up to 20 MeV neutron energy. The Ni(n,p) excitation function is shown in Fig. 24b.

D. (n,pn'), (n,n'p) and (n,d) Cross Sections.

Generally these reactions are studied with activation technique, which does not allow for the separation of the different reaction components. Only particle detection for example the counting of deuterons in (n,d) reaction leads to the measurement of the corresponding component for the production of the final nucleus. In the absence of the separate measurement for each of the (n,pn'), (n,n'p) and (n,d) cross sections, the measured activation cross section was treated as a sum of the three components for comparison with the corresponding sum based on Hauser-Feshbach calculations. For brevity the symbol (n,pn') will denote the sum $\sigma(n,pn') + \sigma(n,n'p) + \sigma(n,d)$.

1. $^{58}Ni(n,pn')$ Reaction. There are extensive measurements around 14 MeV neutron energy (cf. Fig. 6). Weighted average of all the measurements was determined to normalize the MODNEW calculated cross sections. The normalized curve and the experimental data are shown in Fig. 25a, while the excitation function extending up to 20 MeV is shown in Fig. 25b.

2. $^{60}Ni(n,pn')$ Reaction. As in the case of ^{58}Ni, the 14 MeV experimental average cross section was used to normalize the model calculated cross sections to generate the $^{60}Ni(n,pn')$ exci-

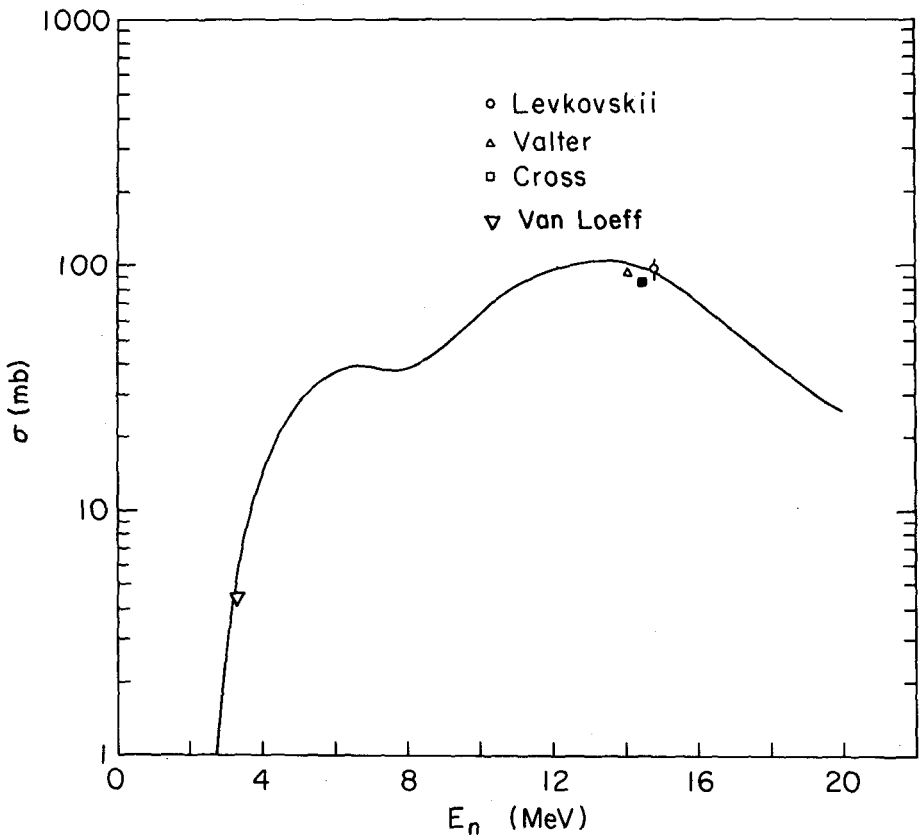

Figure 21. $^{61}Ni(n,p)$ cross section.

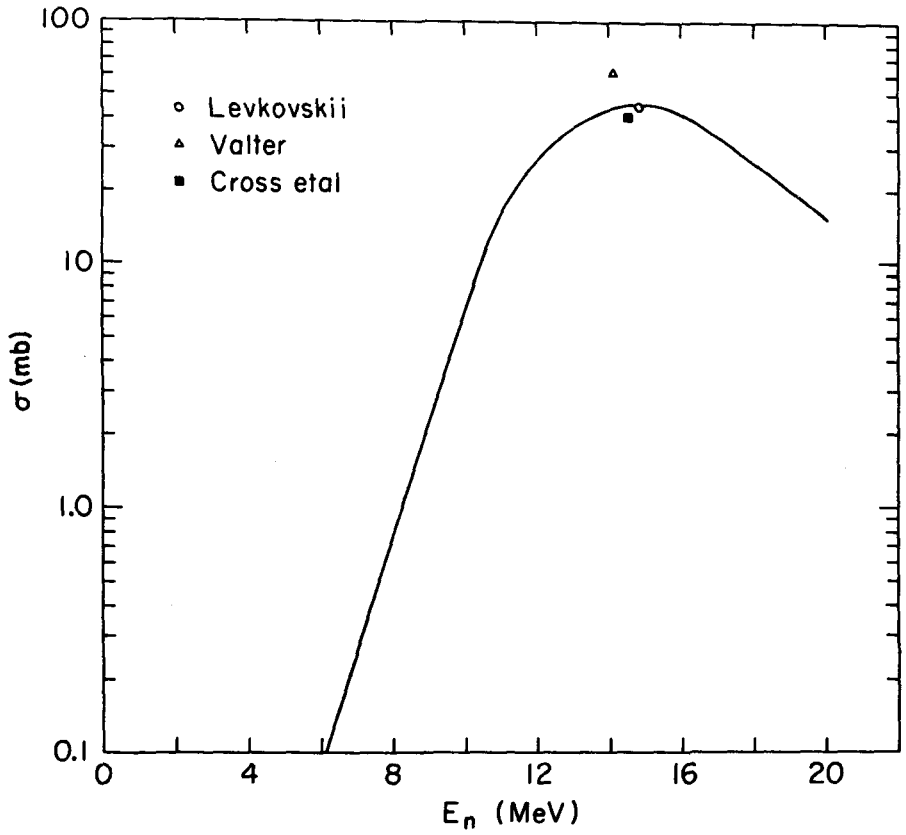

Figure 22. $^{62}Ni(n,p)$ cross section.

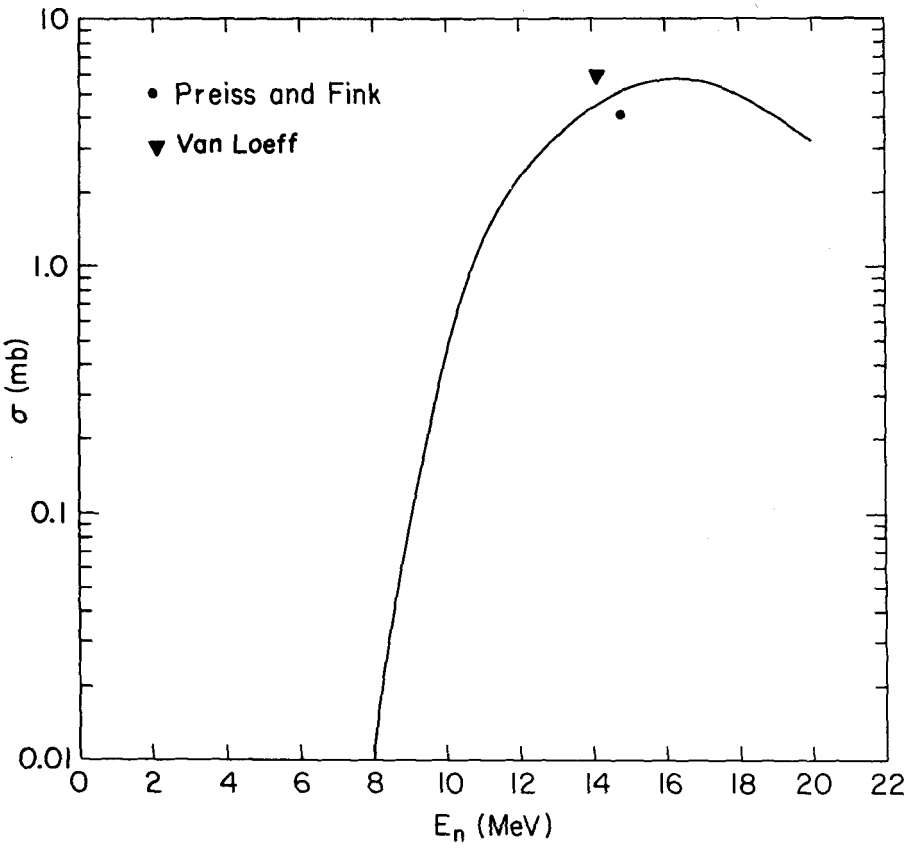

Figure 23. $^{64}Ni(n,p)$ cross section.

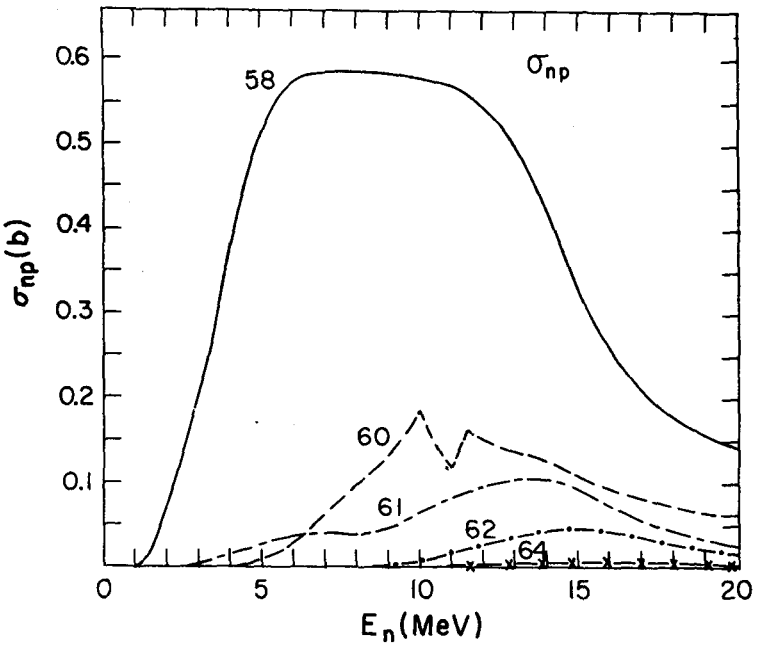

Figure 24a. ^{58,60,61,62,64}Ni(n,p) evaluated cross sections.

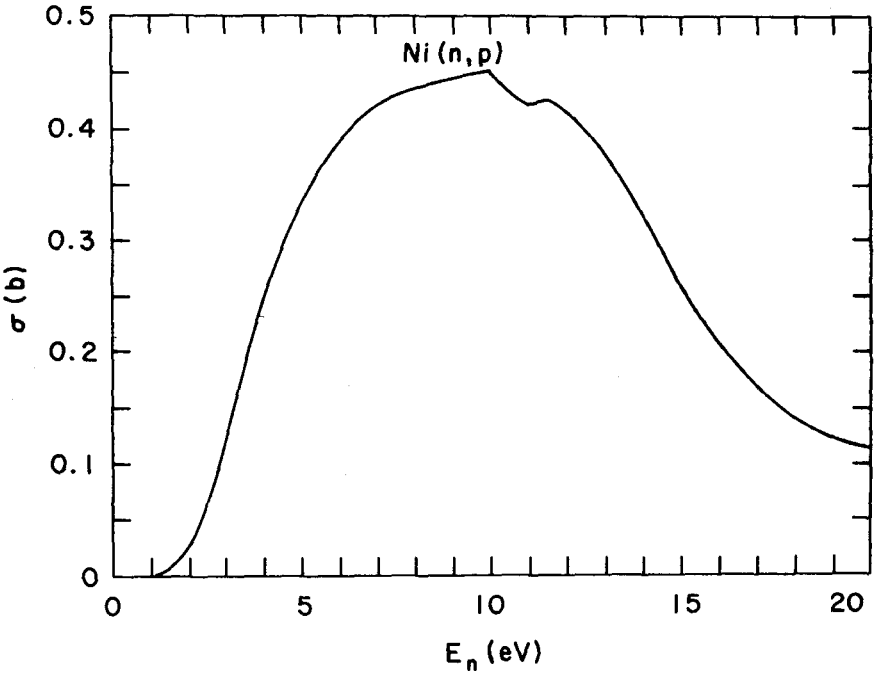

Figure 24b. Natural Ni(n,p) evaluated cross section.

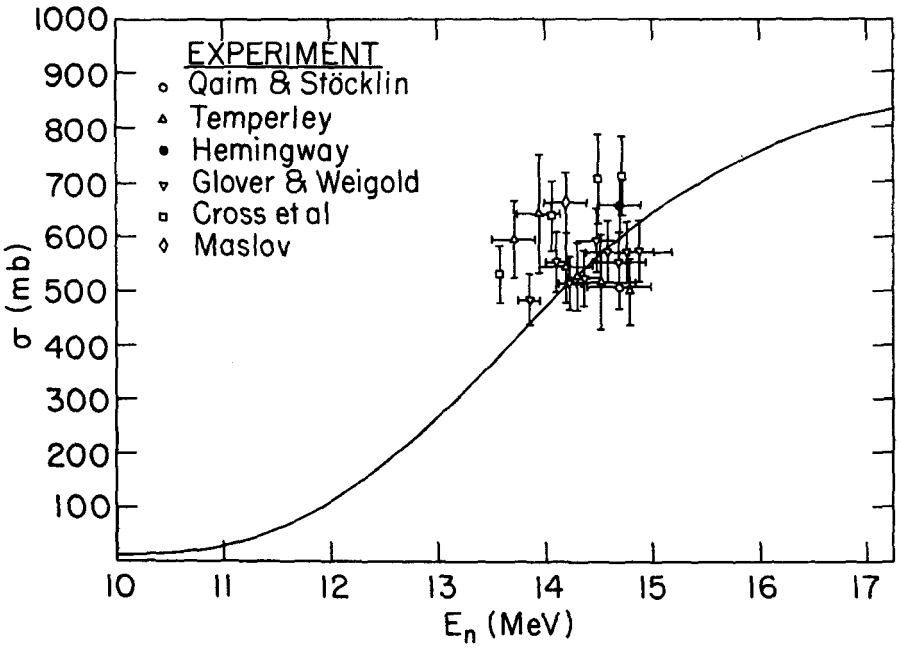

Figure 25a. ^{58}Ni(n,pn'+n'p+d) cross section 10-17 MeV.

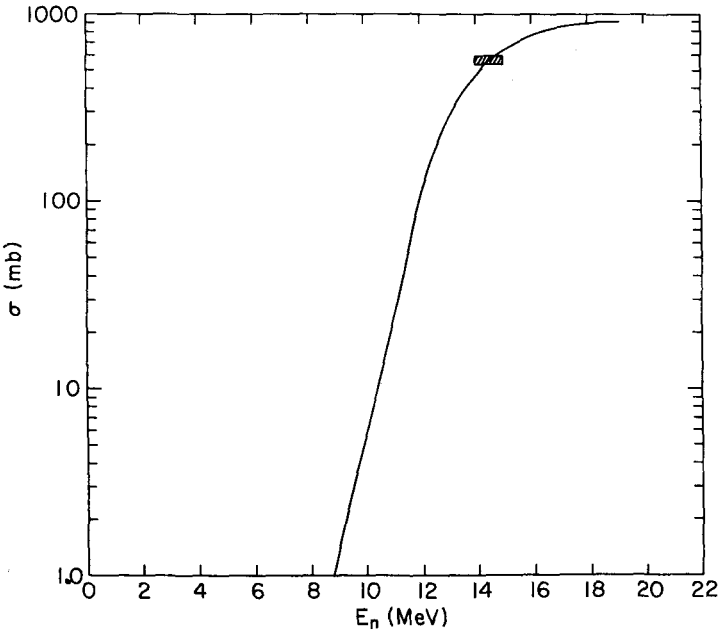

Figure 25b. ^{58}Ni(n,pn'+n'p+d) cross section 9-20 MeV.

tation function. The evaluated curve and the experimental points are displayed in Fig. 26.

3. ^{61}Ni(n,pn') Reaction. There are no experimental data for the odd isotope. The difference of σ_{non} and the sum of the partial cross sections

$$(\sigma_{n,p} + \sigma_{n,2n} + \sigma_{n,\alpha} + \sigma_{n,\alpha n'} + \sigma_{n,n'\alpha} + \sigma_{n,n'})$$

was taken to represent the $\sigma_{n,pn'}$ for this isotope. σ_{non} for ^{61}Ni was taken to be the same as for natural nickel. The evaluated excitation function is shown in Fig. 27.

4. ^{62,64}Ni(n,pn') Reactions. For each of the heavier nickel isotopes there is only one experimental point, making it rather difficult to test the reliability of the measurement. The model calculated excitation functions were adopted as the evaluated curves, which are shown with the corresponding measured points in Figs. 28 and 29.

The sum of (n,pn') and (n,n'p) cross sections evaluated for natural Ni is displayed in Fig. 30, and the Ni(n,d) cross section is shown in Fig. 31.

E. (n,2p) Cross Section

The isotopic Q-value for this reaction is high except for ^{58}Ni, the most abundant isotope. ^{58}Ni was considered for evaluating the (n,2p) reaction. In the absence of any experimental data for this reaction MODNEW calculated cross sections were adopted for the evaluation purposes. The Ni(n,2p) excitation function is shown in Fig. 32.

F. Hydrogen Production Cross Section

Fig. 33 displays the total hydrogen production cross section (n,p) + (n,n'p) + (n,pn') + 2(n,2p) which was constructed from the individual components for natural nickel. The sudden jump around 12 MeV in the excitation function is due to the onset of the tertially reactions like (n,n'p) and (n,2p).

G. (n,α), (n,αn') and (n,n'α) Cross Sections

No differential measurements on these reactions were available* for evaluation. Only the integral measurements for the separated Ni isotopes due to Farrar,[120] were available.

*Dolya et al's,[122] measurements on (n,α) reaction on some of the Ni isotopes became available only recently. They were too late for inclusion in the evaluation.

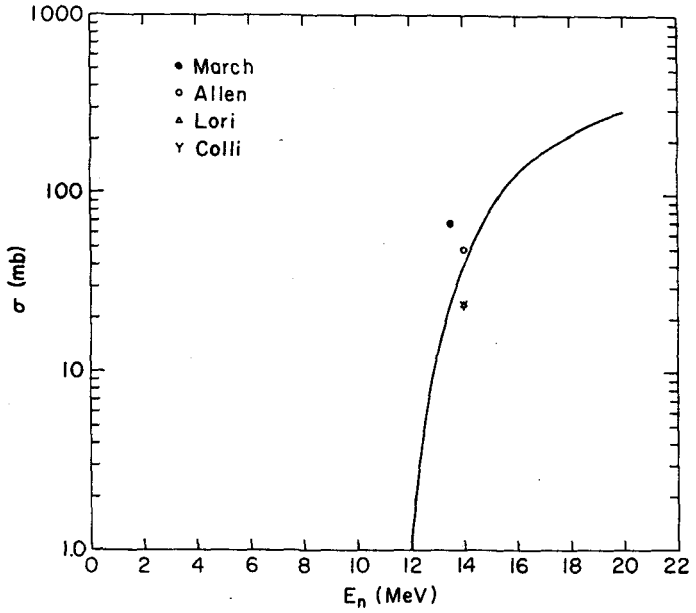

Figure 26. ^{60}Ni(n,pn'+n'p+d) cross section.

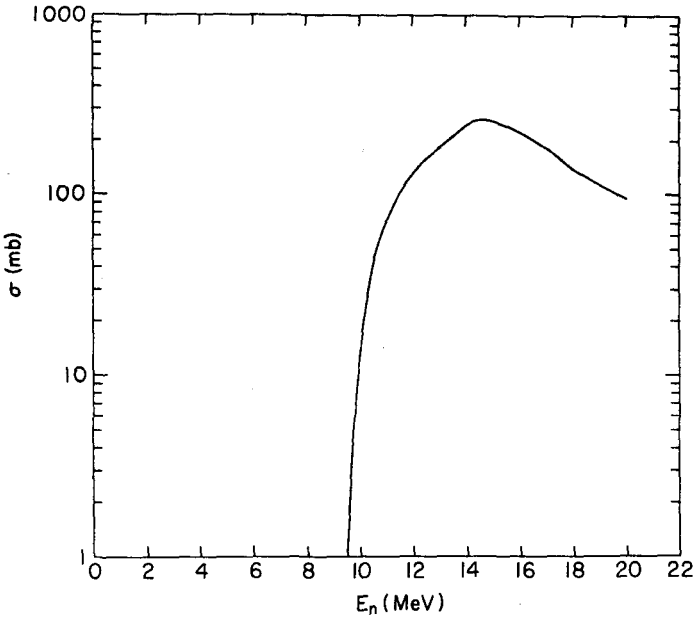

Figure 27. ^{61}Ni(n,pn'+n'p+d) cross section.

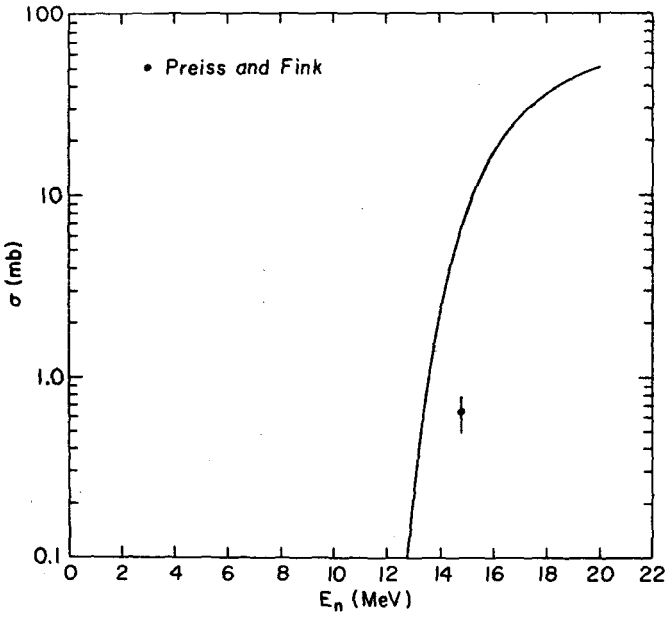

Figure 28. ^{62}Ni(n,pn'+n'p+d) cross section.

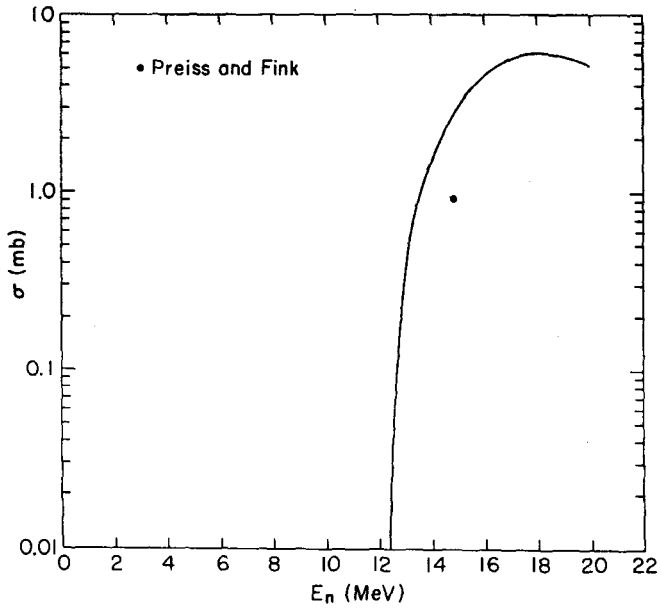

Figure 29. ^{64}Ni(n,pn'+n'p+d) cross section.

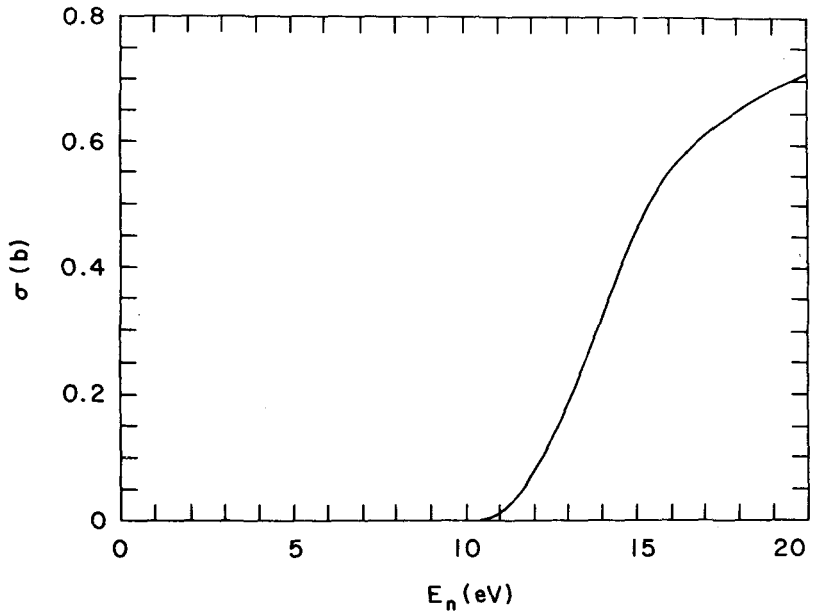

Figure 30. Ni(n,n'p) cross section.

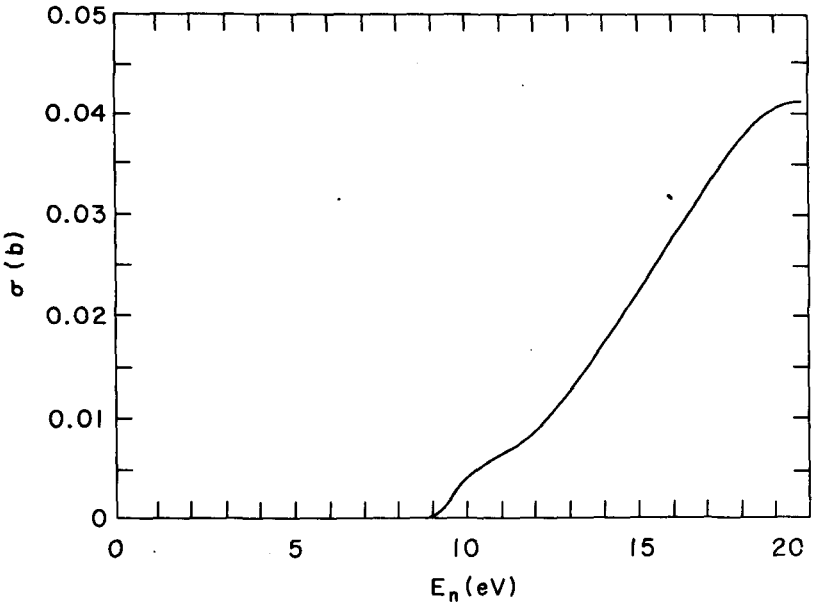

Figure 31. Ni(n,d) cross section.

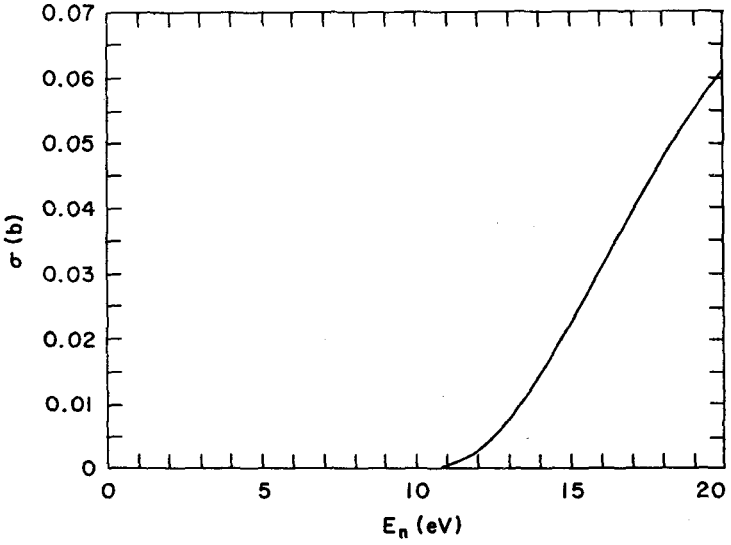

Figure 32. Ni(n,2p) cross section.

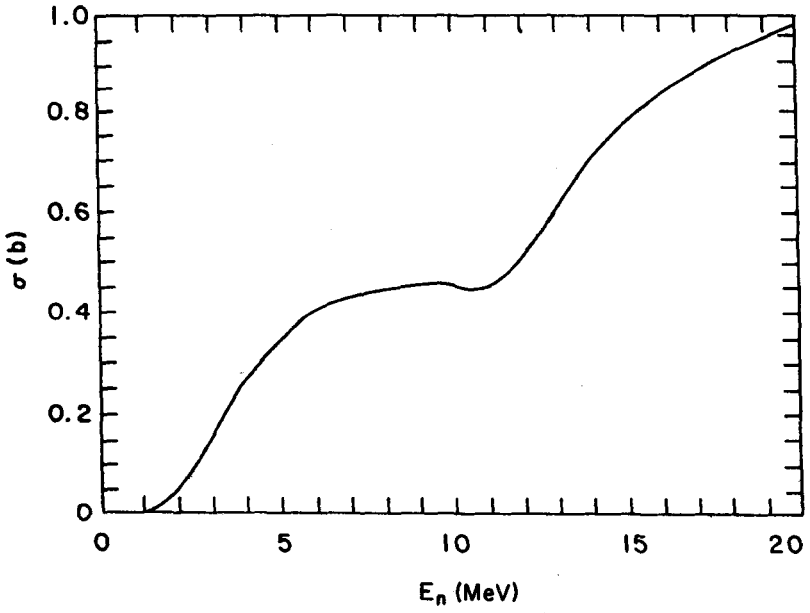

Figure 33. Ni total hydrogen production cross section.

These were corrected for fluency changes suggested by the author. The sum $(n,\alpha) + (n,\alpha n') + (n,n'\alpha)$ was constructed for each isotope to evaluate the fission spectrum average (T = 1.29 MeV). The calculated fission spectrum average was normalized to the experimental value. The resulting normalization factor was used to renormalize the component reactions (n,α), $(n,\alpha n')$ and $(n,n'\alpha)$ for each isotope to construct the evaluated excitation functions.

The (n,α), $(n,n'\alpha) + (n,\alpha n')$ and the helium production cross sections for natural nickel are displayed in Figs. 34, 35 and 36 respectively.

VIII ANGULAR DISTRIBUTIONS

A. Elastic Angular Distribution

Recent elastic angular distributions measured at Argonne (Smith et al),[49] were used to update the angular distribution file in Version IV. Smith's data extends from 0.345 MeV to 4 MeV. The energy resolution was 30 keV and the measurements were made at 30 energies in 10° - 160° angular range. Optical model predicted (ABACUS) angular distributions were used to extapolate the angular distributions to 0° and 180°. Elastic angular distributions at few neutron energies with the corresponding Wick's limits are shown in Fig. 37.

B. Inelastic Angular Distributions

In previous Ni evaluations inelastic angular distributions were assumed to be isotropic, which is a very poor representation of the inelastic process. It was decided to represent angular distribution on a more realistic basis. Both Compound Nuclear (COMNUC) and Direct Interaction (JUPITOR) angular distributions generated by Bhat (in connection with his evaluation for Version IV, but not used) were combined to construct the angular distribution file. In particular, contribution due to higher of the components is depleted to the extent of the minor component. This procedure is adopted due to the lack of the knowledge of the relative contribution of the compound nuclear and direct interaction components to the inelastic cross section. The desired effect of forward peaking angular distribution at higher energy due to direct interaction process is achieved.

IX CAPTURE REACTIONS

A. Capture Cross Section

No new measurements have been reported since the last Ni evaluation.[1] An attempt was made to look at Beer and Spencer's data[58] in the resonance region. The ^{58}Ni experimental data

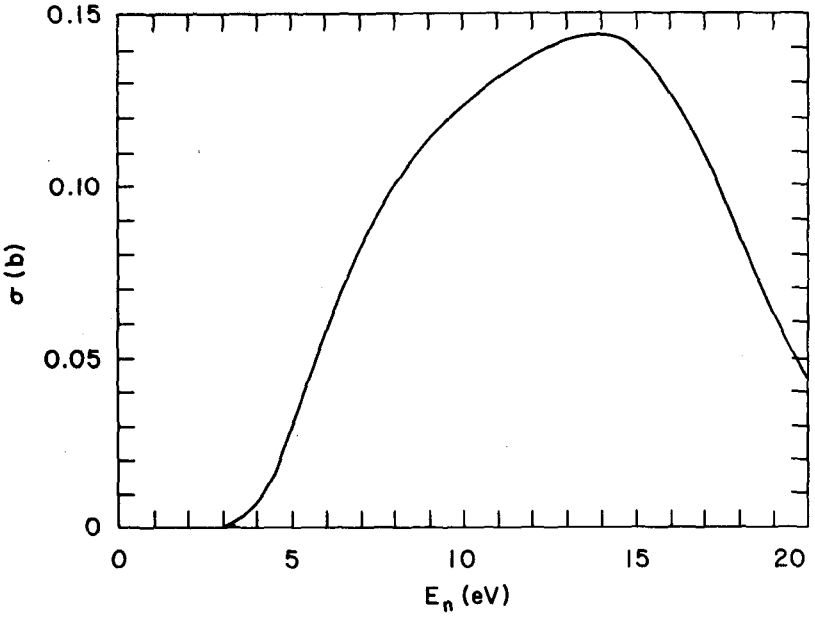

Figure 34. Ni(n,α) cross section.

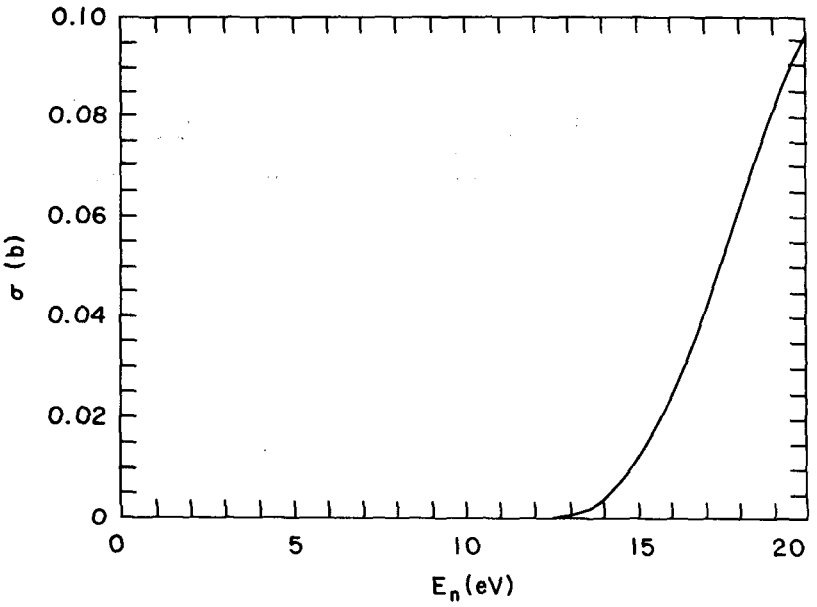

Figure 35. Ni(n,n'α) cross section.

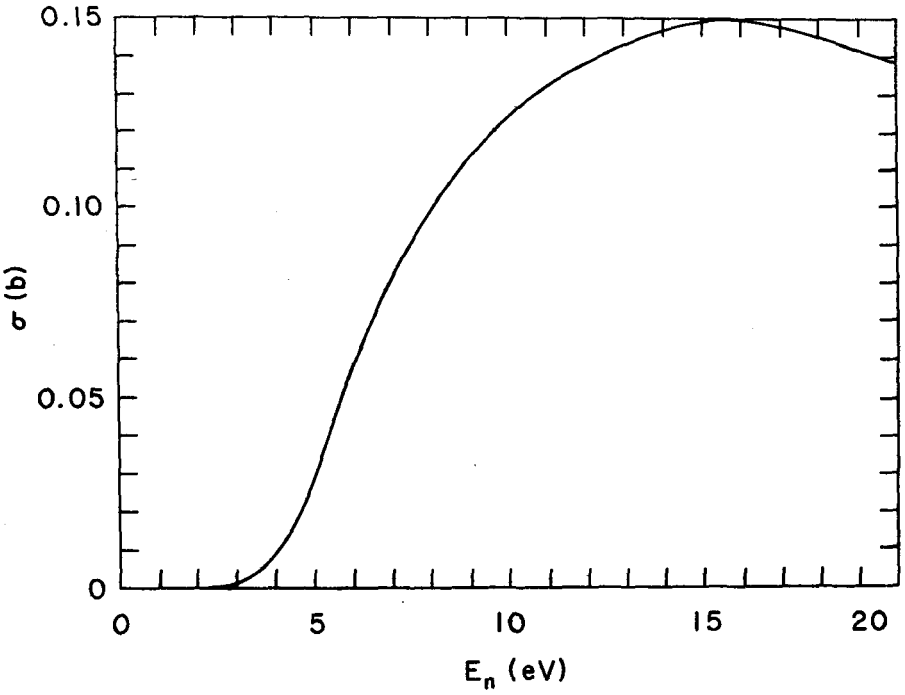

Figure 36. Ni total alpha production cross section.

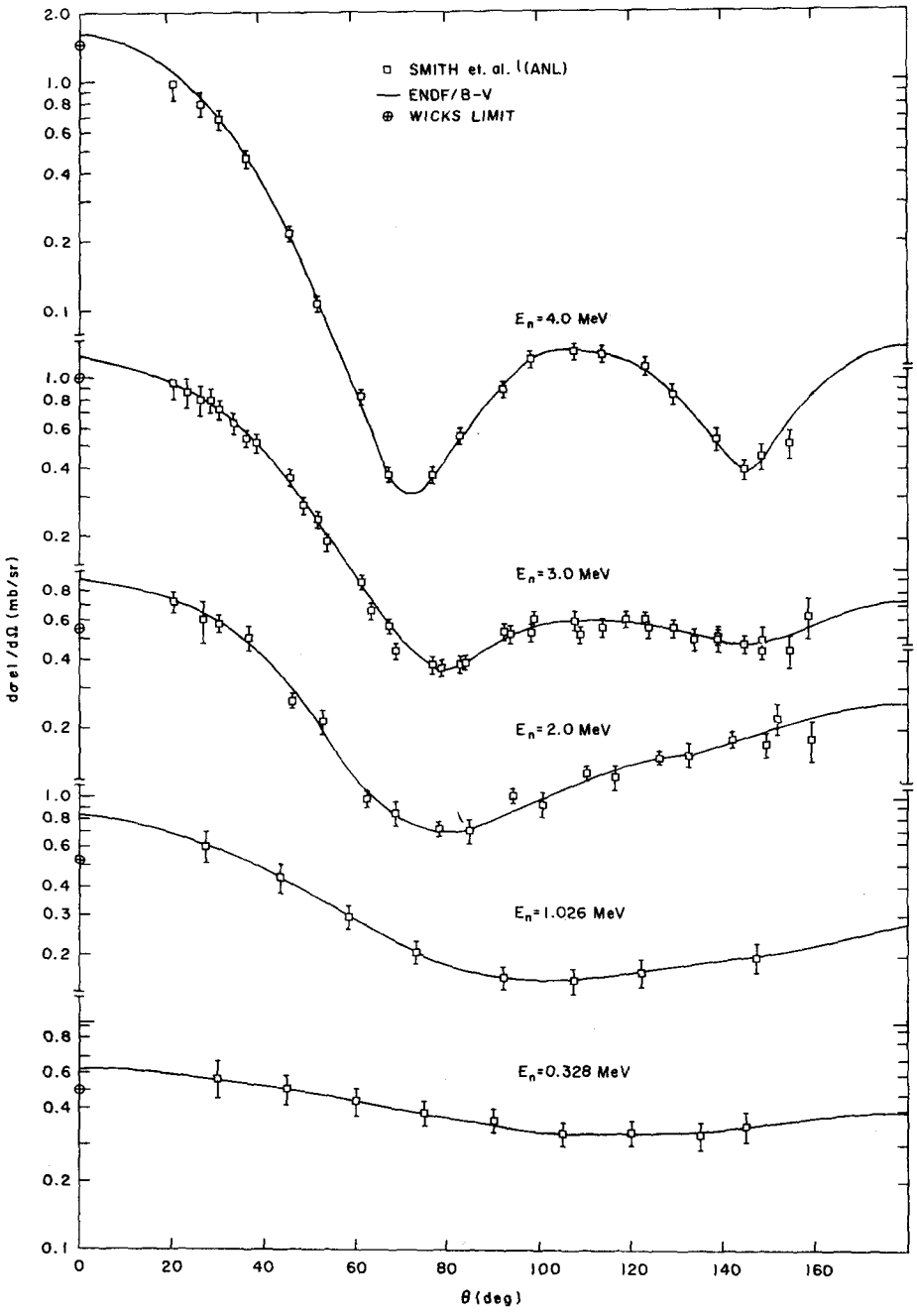

Figure 37. Ni elastic angular distributions 0.328-4.0 MeV.

entered in CSISRS files were beset with some inconsistencies and it was not possible to get a consistent set of analyzed data with the published resonance parameters.

No changes were made in the capture cross section description up to 1 MeV. However, capture cross section in the MeV region was calculated (COMNUC) with the inclusion of the Giant dipole resonance (E_d = 14.8 MeV, Γ_γ = 8 MeV) parameters.[59] The strength function $\langle\Gamma_\gamma\rangle/\langle D\rangle = 2.67 \times 10^{-4}$ was the same that was used for ^{58}Ni by Bhat,[1] in his Ni evaluation. A comparison of ENDF/B-IV and ENDF/B-V capture cross sections is presented in Fig. 38.

Capture resonance cross section profile was generated with the help of RESEND,[123] code which uses resonance parameters part of the ENDF/B file. Group averaged cross sections of the RESEND output with INTEND,[124] is plotted as a histogram (cf. Fig. 39), to compare with experimental (n,γ) data below 1 MeV.

B. Gamma-Ray Production Cross Sections

1. Gamma-Ray Production Due to Neutron Capture. Maerker,[125,126] measured gamma-ray production cross section arising from thermal neutron capture in Ni at the ORNL Tower shielding facility using a calibrated 5 x 5 in NaI(T) detector in good geometry. The resulting reduced spectral intensities in photons per 100 capture were summed over 0.5 MeV bins. The low energy cut-off of their spectrum is 1.0 MeV. To supplement Maerker's data, this part of the spectrum was taken from the measurement of Rasmussen et al,[127] whose γ-ray energies go down to about 250 keV. The Rasmussen spectrum below 1.0 MeV was renormalized and merged with Maerker's spectrum. The normalization factor was determined from the integrated spectra (from 1.0 MeV up) of the two data sets. The combined γ-ray spectrum was normalized to 100% BE by dividing it by 0.945. The resulting γ-ray multiplicity and the corresponding energy distribution are given in files 12-102 and 15-102 respectively.

Energy distribution of gamma-ray production was evaluated by Bhat,[1] from 4.0 keV to 1.0MeV based on the Australian data (Kenny, et al.[128]), which extends from 4 to 9 MeV gamma-ray energy and were measured from 4 to 80 keV neutron energy. In order to fill the gap below 4.0 MeV the thermal spectrum for $E_\gamma = 1.0 \times 10^{-5}$ - 4 keV was used. The spectra were renormalized to conserve energy and given at E_n = 100-250 keV; 250-500 keV, 500-750 keV and 750-1000 keV. Bhat's evaluated energy distribution of gamma-ray production were adopted.

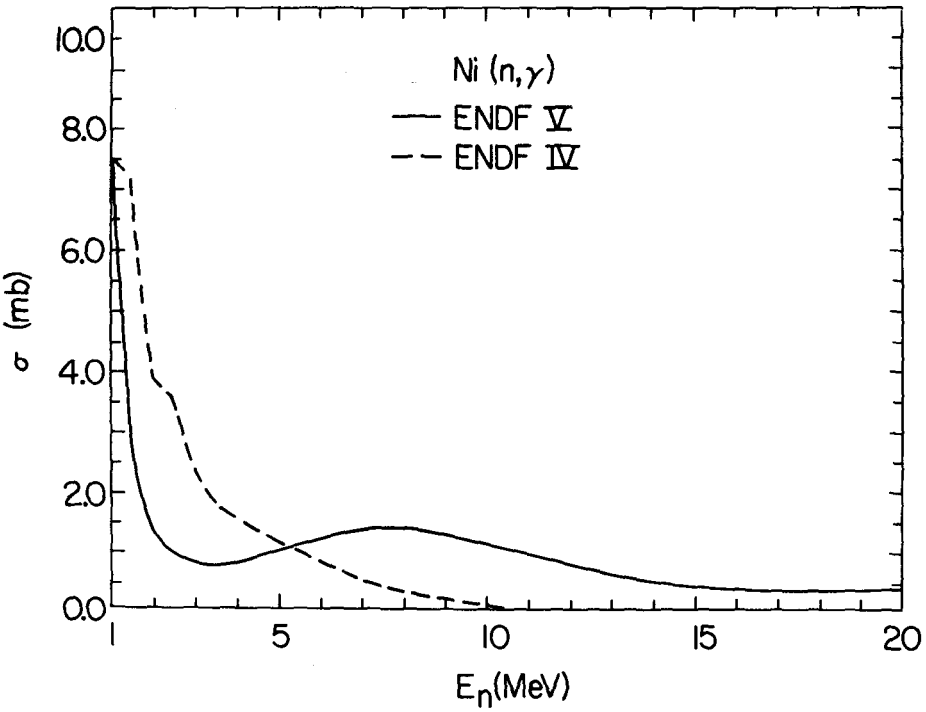

Figure 38. Ni(n,γ) cross section 1.0-20 MeV.

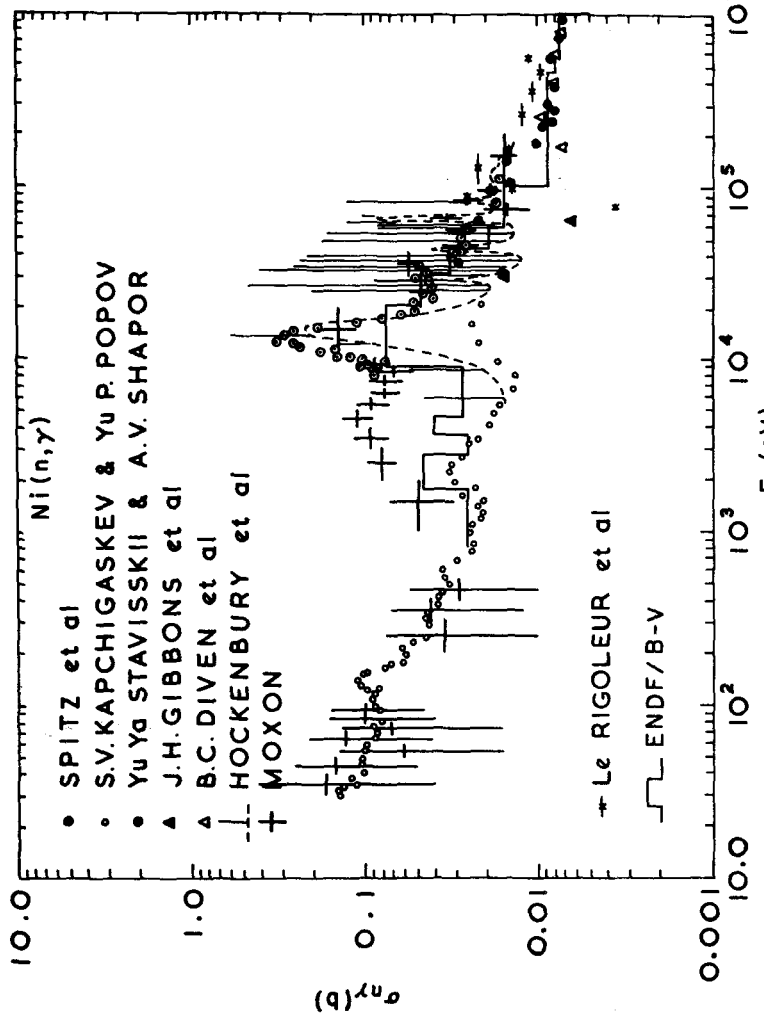

Figure 39. Ni(n,γ) cross section 0.01-1.0 MeV.

2. Gamma-Ray Production Due to (n,xγ) Reactions. Dickens et al.'s data,[129] were used by Bhat in evaluating the gamma ray production cross sections (n,xγ) due to all non-elastic processes for E_n = 1-20 MeV. Dickens et al. measured $d^2\sigma/d\omega dE_\gamma$ at $\theta_r = 125°$ using a NaI(Tℓ) spectrometer. Assuming that the gamma-ray angular distributions are isotropic, the differential cross sections $d^2\sigma/d\omega dE_\gamma$ were multiplied by 4 to obtain the angle-integrated cross sections in the corresponding energy interval. The total production cross sections and the gamma-ray energy distributions are given in 13-3 and 15-3 files respectively. The experimental data have about 10% error from experimental set-up (neutron flux measurements, detector efficiency and beam effective area) and statistical errors of the order of 5% (E_n = 1.5-3 MeV) to 27% (E_n = 17 MeV). Bhat's evaluated gamma-ray production cross section (n,xγ) due to all non-elastic process for E_n = 1-20 MeV were retained without any modification in files 13-3 and 15-3.

X INTEGRAL MEASUREMENTS AND FISSION SPECTRUM AVERAGED QUANTITIES

INTEND,[126] code was used to calculate Fission Spectrum averaged cross sections for (n,p), (n,d), (n,α), (n,2p), (n,2n), (n,α), (n,n'α), and (n,n'p) reactions for two different spectra, Maxwellian (T=1.32 MeV) and Watt. The calculated quantities are compared to the corresponding experimental quantities in Table 5 for ^{58,60,61,62,64}Ni and for Natural Nickel. ENDF V and ENDF IV results are compared for Nickel.

XI COVARIANCE FILES

Error estimates for different reactions are given in Table 6. Covariance files for the following MF-MT were included in the Ni evaluated data file:

33-1
33-2
33-4
33-16
33-22
33-28
33-51 to 76
33-91
33-102
33-103
33-104
33-107
33-111

TABLE 5

Spectrum Averaged Cross Sections (mb)

Reaction	A	ENDF-V Max	ENDF-V Watt	ENDF-IV Max	ENDF-IV Watt	Experiment	
(n,p)	58	102	109			101±5[a]	
	60	2.76	2.80			2.3[b]	2.57±.3[c]
	61	4.01	4.25			1.75[d]	1.13±.15[c]
	62	0.048	0.041				
	64	0.003	0.003				
	Nat	70.43	75.07	70.26	74.86		
(n,d)	58	0.02	0.016				
	60	0.0007	0.0005				
	61	0.003	0.002				
	62	0.001	0.001				
	64	0.00006	0.00004				
	Nat	0.014	0.011	-	-		
(n,α)	58	6.65	6.96			6.06[d]	4.52±.9[c]
	60	1.22	1.28			1.10[d]	2.57±.3[c]
	61	1.30	1.39			1.80[d]	
	62	0.110	0.104			0.097[d]	
	64	0.092	0.075			0.108[d]	
	Nat	4.88	5.11	4.72	4.93	4.76±.54[d]	
(n,2p)	58	0.008	0.005	-	-		
	Nat	0.005	0.004	-	-		
(n,2n)	58	0.005	0.003				
	60	0.086	0.060				
	61	1.100	0.954				
	62	0.239	0.173				
	64	0.622	0.487				
	Nat	0.047	0.034	0.058	0.044		
(n,n'α)	58	0.002	0.001				
	60	0.0009	0.0005				
	61	0.0015	0.0009				
	62	0.0007	0.0004				
	64	0.002	0.001				
	Nat	0.002	0.001	-	-		
(n,n'p)	58	0.150	0.106			0.24±0.35[d]	
	60	0.012	0.008				
	61	0.144	0.113				
	62	0.032	0.019				
	64	0.019	0.012				
	Nat	0.108	0.076	0.054	0.044		

a) *Average of Experimental values*
b) Paulsen, Nucleonics 8, (1966)
c) Wolfe and Qaim, Radio Chemica Acta 27, 65 (1980)
d) H. Farrar (unpublished), private communication, Error ≈ 5%

Since the resonance parameters were taken from the previous evaluated file (ENDF/B-IV), no covariance matrix file for File 2 is given.

Both long range and short (or intermediate) range correlations are given for each MT. Except for the 33-91 file the rest correspond to evaluated errors while the 33-91 file is derived from 33-4 and 33-51...76.

Reliable quality is aimed at generating the MF=3 files in the evaluation, which were constructed both from experimental data and model calculated excitation functions.

The errors used in constructing the covariance files reflect both experimental uncertainties and the uncertainties in the calculated quantities. In the case of the latter the errors reflect only the confidence limit and are not based on any model parameter variation.

TABLE 6

ERRORS (%)

Cross Section/E_n (MeV)	MF	MT	Thermal	Resonance+	.7-1	1-2	2-4	4-6	6-8	8-10	10-12	12-14	14-16	16-18	18-20
Total	3	1	5	5-10	1.5	1.5	2	2	2	3	4	5	6	8	10
Elastic	3	2	3	16-27	20	16	13	6	7	7	7	8	8	8	8
Total (n,n')	3	4	-	-	-	25	25	30	30	30	30	30	30	30	30
Discrete (n,n')	3	55	-	-	-	25	30	35	30	30	30	30	30	30	30
	3	56	-	-	-	25	25	15	30	30	30	30	30	30	30
	3	58	-	-	-	18	18	15	15	30	30	30	30	30	30
	3	60	-	-	-	-	-	20	25	30	30	30	30	30	30
	3	62	-	-	-	-	-	30	30	30	30	30	30	30	30
	3	65	-	-	-	-	-	30	30	30	30	30	30	30	30
	3	66	-	-	-	-	-	20	30	30	30	30	30	30	30
	3	68	-	-	-	-	-	30	30	30	30	30	30	30	30
	3	69	-	-	-	-	-	25	30	30	30	30	30	30	30
Other Discrete (n,n')	3	*	-	-	30	20	30	30	30	30	30	30	30	30	30
Continuum	3	91	-	-	-	30	30	30	30	30	30	30	30	30	30
(n,2n)	3	16	-	-	-	-	-	-	-	-	-	10	10	15	20
(n,αn')+(n,n'α)	3	22	-	-	-	-	-	-	15	15	15	15	15	15	15
(n,pn')+(n,n'p)	3	28	-	-	-	-	-	-	-	15	15	15	15	15	15
(n,γ)	3	102	4	15-25	20	20	20	20	20	20	20	20	20	20	20
(n,p)	3	103	-	-	25	10	10	5	10	10	10	15	15	20	25
(n,d)	3	104	-	-	-	-	-	-	-	-	50	30	30	30	30
(n,α)	3	107	-	-	-	-	-	15	15	15	15	15	15	15	15
(n,2p)	3	111	-	-	-	-	-	-	35	35	35	35	35	35	35
Gamma Prod. (n,γ)	12	102	15	20	20	-	-	-	-	-	-	-	-	-	-
(n,xγ)	13	3	-	-	-	-	11	12	13	14	15	18	23	25	27

+ Resonance region extends up to 690 keV
* The remaining discrete inelastic levels.

Acknowledgments

It is a great pleasure to thank Mulki Bhat whose initial help and sustained confidence was a major impetus in completing the present evaluation. In addition, I would like to thank Sol Pearlstein whose continued interest and patience was of great value.

I would like to express my gratitude to Francis Perey, Harry Farrar and Dick Maerker in connection with their experimental data. I am also thankful to the staff members of the NNDC-BNL who were generous with their time and effort whenever help was needed.

REFERENCES

1. M.R. Bhat, BNL 50435, Brookhaven National Laboratory (1974).

2. P. Guenther, A. Smith, D. Smith, J. Whalen and R. Howerton, ANL/NDM-11, Argonne National Laboratory (1975).

3. N.E. Holden and F.W. Walker, Chart of the Nuclides, 11th Edn, Revised April 1, 1972, Knolls Atomic Power Laboratory.

4. A. Wapstra and N.B. Gove, Nuclear Data Tables, 9, 265 (1971).

5. U. Fanger, D. Heck, W. Michaelis, H. Ottmar, H. Schmidt and R. Gaeta, Nucl. Phys. A146, 549 (1970).

6. S. Cochavi and W.R. Kane, Phys. Rev. C6, 1650 (1972).

7. M. Uhl, Nucl. Phys. A184, 253 (1972). MODNEW: BNL version of Uhl's code.

8. C.L. Dunford, COMNUC, AI-AEC-12931 (1970).

9. E.H. Auerbach, ABACUS II, BNL-6562 (1964).

10. C.M. Perey and F.G. Perey, Atomic Nuclear Data Tables 13, 293 (1974).

11. F.G. Perey, Phys. Rev. 131, 745 (1963).

12. G.R. Satchler et. al, Nucl. Phys. 84, 177 (1966).

13. H.K. Vonach and M. Hille, Nucl. Phys. A127, 289 (1969).

14. W. Dilg, W. Schantl, H. Vonach and M. Uhl, Nucl. Phys., A217, 269 (1973).

15. T. Tamura, ORNL 4152 (1967).

16. M. Blann, Ann. Review of Nucl. Science 25, 123 (1975), Phys. Rev. Letters, 27, 337 (1971); 28, 757 (1972), OVERLAID ALICE, Univ. of Rochester, Report COO3494-29.

17. R.B. Schwartz, R.A. Schrack and H.T. Heaton II, NBS Monograph 138 (1973).

18. S. Cierjacks, P. Forti, D. Kopsch, L. Kropp, J. Nebe and H. Unseld KFK-1000 (1968).

19. F.G. Perey, T.A. Love and W.E. Kinney, private communication to M.R. Bhat (1973).

20. R.W. Bauer, J.D. Anderson, L.H. Christensen, Nucl. Phys. 48, 152 (1963).

21. H.L. Taylor, O. Lonsjo, T.W. Bonner, Phys. Rev. 100, 1974 (1955).

22. V.J. Strizhk, Jour. Nucl. Energy 5, 253 (1957).

23. M.H. MacGreger, W.P. Ball, and R. Booth, Phys. Rev. 108, 726 (1957).

24. M. Walt and H.H. Barshall, Phys. Rev. 93, 1062 (1954).

25. J.R. Beyster, R.L. Henkel, R.A. Nobles and J.M. Kister, Phys. Rev. 98, 1216 (1955).

J.R. Beyster, M. Walt and E.W. Salmi, Phys. Rev. 104, 1319 (1956).

26. M.V. Pasechnik, Proc. Int. National Conf. of Peaceful Uses of Atom. En., Geneva 2, 3 (1955).

27. K.W. Machwe, D.W. Kent, S.C. Snowdon, Phys. Rev. 114, 1563 (1959).

28. B. Holmqvist and T. Wiedling, AE-303 (1967).

29. V.I. Kuktevich, B.J. Sitsin and S.G. Tsipin, Jour. Nucl. Energy 11, 46 (1959).

30. A.I. Abramov, Sovt. Jour. At. Energy 12, 65 (1962).

31. A. Langsdorf Jr., R.O. Lane and J.E. Monohan, Phys. Rev. 107, 1077 (1957).

32. A.B. Smith, private communication, CSISRS-AN-51595 (1976).

33. R.L. Clark and W.G. Cross, Nucl. Phys. A95, 320 (1967).

34. R.W. Bauer, J.D. Anderson and L.H. Christiansen, Nucl. Phys. 48, 152 (1963).

35. B. Holmqvist and T. Wiedling, AE-366 (1969), CSISRS AN-20019.

36. B. Holmqvist, S.G. Johansson, G. Lodin, M. Salama, T. Wiedling, AE-385 (1970), CSISRS AN-20020.

37. G.N. Lovchikova, Sovt. Jour. At. Energy 13, 648 (1963).

38. I.A. Korzh, N.S. Koptin, M.V. Pasehnik, N.M. Provdini, N.T. Skylar and I.A. Trotsky Jour. Nucl. Energy 19, 141 (1965).

39. L. Ya Kaskova, V.E. Kolesov, V.J. Popov, O.A. Salnikov, V.M. Sluchevskaja, V.J. Trikov, Int. Conf. on the Study of Nuclear structure with Neutrons, Antwerp (1965), p 576.

40. I.A. Korz, V.A. Mischenko, M.V. Paschnik, N.M. Pravdivy, I.E. Sauzhur, I.A. Totsky, YFI-4, 36 (1967).

41. I.A. Korz, N. Skylar, UFZ, 8, 1389 (1963).

42. W.E. Kinney and F.G. Perey, ORNL-4807 (1974).

43. J.L. Kammerdiener, UCRL-51232 and L.F. Hansen, private communication.

44. D.L. Broder, A.F. Gamalie, A.J. Lashuk and I.P. Sadokin, Jour. Nucl. Energy 18, 645 (1964).

45. D.L. Broder, A.I. Lashuk and I.P. Sadokin ANL-Trans- 177 (1964).

46. I. Fujita, M. Sonda, A. Kotase, Y. Wakuta, H. Tawara, M. Hyakutake and K. Iwatani, Jour. Nucl. Science and Tech. 9, 301 (1972).

47. O.A. Salnikov, G.N. Lovcikova, G.V. Kotelnikova, N.I. Fetisov and A.M. Trufanav, Second International Conf. on Nucl. Data for Reactors, Helsinki 2, 359 (1970).

48. V.C. Rogers, L.E. Beghian and F.M. Clikemann Nucl. Sc. and Eng. 45, 297 (1971).

49. A.B. Smith et al., Private communication and CSISRS-AN-51596 Library.

50. D.L. Broder, V.E. Kolesov, A.I. Lashuk, I.P. Sadokhin and A.G. Dovbenko, Jour. Nucl. Eng. 18, 645 (1964).

51. W.L. Rodgers, E.F. Shrader and J.T. Lindow COO-1573-33, 2: CSISRS AN-50401.

52. F.G. Perey, C.O. LeRigoleur and W.E. Kinney, ORNL 4523 (1970).

53. P. Boschung, J.L. Lindow and E.F. Shrader, Nucl. Phys. A161, 593 (1971).

54. E.S. Konobeevskii, R.M. Musaelyan, V.I. Popov and I.V. Surkova, IZV. Akd. Nauk. SSSR. Ser. FIZ 35, 2345, 2127 (T) (1971).

55. W.E. Kinney and F.G. Perey, ORNL 4807 (1974).

56. K. Tsukada, S. Tanaka, Y. Tomita and Maruyama, Nucl. Phys. A125, 641 (1969).

57. R.B. Day, Phys. Rev. 102, 767 (1956).

58. H. Beer and R.R. Spencer, Nucl. Phys. A240, 29 (1975).

59. B.L. Berman, Atlas of Photoneutron Cross Sections Obtained With Monoenergetic Photons, UCRL-74622 (1973). ^{58}Ni (γ,x) and ^{60}Ni (γ,x) reactions in the Giant Resonance Region were considered to arrive at the GR parameters.

60. D. Hermsdorf et al., KE. 16, 252 (1973).

61. A. Paulsen and H. Liskien Nuk 7, 117 (1965).

62. M. Bormann, F. Dreyer and V. Zielinski EANDC (E) 66, 42 (1966).

63. R.J. Prestwood and B.P. Bayhurst, Phys. Rev. 121, 1438 (1961).

64. J.M.F. Jeronymo, G.S. Marri, J. Olkowsky, A. Sadeghi and G.F. Williamson, Nucl. Phys. 47, 157 (1963).

65. Wen-deh Lu and R.W. Fink, Phys. Rev. C4, 1173 (1971).

66. W.G. Cross, R.L. Clarke, K. Morin, G. Slinn, N.M. Ahmed and K. Beg, BAPS. Ser. II, 7, 335 (1962).

67. J. Csikai EANDC-50, 2 (1965), Conf. on Study of Nuclear Structure with Neutrons, Antwerp, 102 (1965).

68. M.D. Goldberg, S.F. Mughabghab, B.A. Magurno and V.M. May, BNL-325, Second Ed. Supplement No. 2, II-A, (1966).

69. J.K. Temperley, Nucl. Sci. & Engineering 32, 195 (1968).

70. R.C. Barrall, M. Silbergeld and D.G. Gardner, Nucl. Phys. A138, 387 (1969).

R.C. Barrall, M. Silbergeld and D.G. Gardner SUPH-69-2 (1969)

71. R.C. Barrall, J.A. Holmes and M. Silbergeld AFWL-TR-68-134 (1969) CSISRS AN/SN-10022/14.

72. L.A. Rayburn, Phys. Rev. 122, 168 (1961).

73. I.L. Preiss and R.W. Fink, Nucl. Phys. 15, 326 (1960).

74. E.T. Bramlitt and R.W. Fink, Phys. Rev. 131, 2649 (1963).

75. R.N. Glover and E. Weigold, Nucl. Phys. 29, 309 (1962).

76. B.P. Bayhurst, J.S. Gilmore, R.J. Prestwood, J.B. Wilhelmy, N. Jarmie, B.H. Erkkila and R.A. Hardekopf, Phy. Rev. C12, 451 (1975).

77. M.R. Bhat, in ENDF/B-IV Dosimetry file, Edited by B. Magurno, BNL-NCS-50446 (1975).

78. L. Adamski, M. Herman and A. Marcinkowski, INDC(POL)-8/L, November 1977.

79. S.A. Qaim and G. Stoklin, Proc. 8th Symp. on Fusion Tech. EUR 5182E(1974).

80. S. Pearlstein, Jour. Nucl. Energy, 27, 81 (1973).

81. R. Schenter, in ENDF/B-IV Dosimetry File, Edited by B. Magurno, BNL-NCS-50446 (19 5).

82. D.L. Smith and J.W. Meadows, Trans. Am. Nucl. Soc. 16, 1 (1973), P. Guenther, A. Smith and J. Whalen, Nucl. Sc. and Eng., 59, 106 (1976).

83. D.L. Smith and J.W. Meadows, private communication to M.R. Bhat.

These authors measured $^{58}Ni(n,p)$ reaction cross section by activation method for neutron energies from near threshold to 10 MeV. The cross sections were determined relative to the ^{235}U and ^{238}U fission cross sections.

0.44 - 3.96 MeV	relative to	$^{235}U(n,f)$
4.008 - 5.87 MeV	relative to	$^{238}U(n,f)$
5.398 - 9.87 MeV	relative to	$^{238}U(n,f)$
2.854 - 3.994 MeV	relative to	$^{235}U(n,f)$-high resolution
4.019 MeV	relative to	$^{238}U(n,f)$

Neutrons from the Li(p,n) were used for all the ranges given above except for the 5.398-9.87 MeV range measure- [illegible] (D(d,n) reaction was used as a source for neutron

The 2.854-3.994 MeV range measurements were measured with high resolution. The different data sets were normalized to the corresponding $^{235}U(n,f)$ and $^{238}U(n,f)$ version V standard cross sections.

84. J.W. Meadows and T.F. Whalen, Phys. Rev. 130, (1963).

Meadows and Whalen measured $^{58}Ni(n,p)$ $^{58}Co^{m,g}$ cross section ratios relative to $^{235}U(n,f)$ cross sections. Resolution varied from 100 keV at 1.04 MeV to 75 keV at 2.67 MeV. Overall error is of the order of 8% for all points above 1.14 MeV. All of the data points have been normalized to the ENDF/B-V $^{235}U(n,f)$ cross sections.

85. J.K. Temperley, Nucl. Sci. and Eng. 40, 331 (1970).

Temperley measured $^{58}Ni(n,p)$ cross section by activation method. The neutron flux was determined by associated particle counting. Overall error is of the order of 10%.

86. A. Paulsen and Widera, EANDC(E) 150, 1972

These authors employed the activation technique to measure $^{58}Ni(n,p)$ cross sections in the 1-6 MeV and 12-17 MeV energy regions. Recoil proton telescope was used to determine the neutron fluency. The quoted errors (<7%) reflect the total uncertainties in the cross sections.

87. K. Nakai, H. Grotch and H. Amano, J. Phys. Soc. Japan, 17, 1215 (1962).

Nakai measured σ_{np} from 1.84 - 4.82 MeV neutron energy. No standard information is given in the cited paper. Total uncertainty is 15%. Other data sets in the measured energy region are much more reliable than these are.

88. J.F. Barry, J. Nucl. Energy, Parts A/B, 16, 467 (1962).

The $^{58}Ni(n,p)$ cross sections with respect to the $^{235}U(n,f)$ cross sections were measured. The data set has been renormalized to the version V $^{235}U(n,f)$ cross sections. All errors add up to 10%.

89. J. Konijn and A. Lauber, Nucl. Phys. 48, 191 (1963).

Most of the cross sections are either too high or too low compared to the other data sets in the region of measurements. This data set is not considered in the evaluation.

90. J.J. Van Loeff, Nucl. Phys. 24, 340 (1961).

σ_{np} at 3.3 MeV is very high compared to the rest, hence not used in the evaluation.

91. M. Bormann, Z. Naturforsch, 21A, 988 (1966).

Activation technique was used to measure 13-19 MeV (n,p) cross sections with $^{63}Cu(n,2n)$ and $^{19}F(n,2n)$ reactions as standard cross sections at 14.1 MeV. All errors add up to 10%.

92. R.C. Barrall, Nucl. Phys. A138, 387 (1969). En=14.8 MeV, measured with respect to $^{27}Al(n,\alpha)$. Renormalized to the version IV $^{27}Al(n,\alpha)$ cross section.

93. G.N. Maslov, F. Nasyrov and Paslikin, YK-9-50 (1972).

E_n = 14.6 MeV, $^{65}Cu(n,2n)$ standard. The data point has been renormalized to ENDF IV value.

94. P. Decowski, et al., Nucl. Phys. A112, 513 (1968).

σnp was measured with respect to $^{65}Cu(n,2n)$ in the 12.6 17.8 MeV range. Prestwood and Bayhurst's (Phys. Rev. 121, 1438 (1961)) $^{65}Cu(n,2n)$ cross section at 14.5 MeV was used.

95. R.W. Fink, BAPS 15, 1372 (1975).

E_n = 14.4 MeV, no standard information.

96. W. Cross, R.L. Clark, K. Morin, G. Slinn, N.M. Ahmed and K. Beg, AECL 1542 (1962), and BAPS 7, 335 (1962).

E_n = 14.5 MeV, standard ^{27}Al (n,α), Renormalized.

97. S. Okumura, Nucl. Phys. A93, 74 (1967).

Okumura measured $\sigma_{np}{}^{m}/\sigma_{np}$ for 13.4-15 MeV neutrons.

Associated particle counting was done. Measurements are absolute and the errors <5%.

98. J. Dresler, et al., INR 1464, 12 (1973).

En = 14.6 MeV, with respect to $^{56}Fe(n,p)$. Renormalized.

99. I.L. Preiss and R.W. Fink, BAPS 15, 1372 (19 E_n = 14.8 MeV. Measurements with respect to $^{65}Cu(n,2n)$ and ^{27}Al (n,α). Cross Section renormalized.

100. R.N. Glover and E. Weigold, Nucl. Phys. 29, 309 (1962).

Measurements with respect to $^{63}Cu(n,2n)$ and $^{65}Cu(n,2n)$ in the energy range of 13.8 - 14.9 MeV. Absolute measurements of the $^{63}Cu(n,2n)$ and $^{65}Cu(n,2n)$ were made. Renormalization of $^{58}Ni(n,p)$ to the ENDF/B-IV $^{65}Cu(n,2n)$ and were done.

101. J.D. Hemingway, JNE, 27, 241 (193) E_n = 14.7 MeV. Cross section measured with respect to $^{56}Fe(n,p)$ reaction. $^{58}Ni(n,p)$ cross section was renormalized to version IV $^{56}Fe(n,p)$ cross section.

102. L. Gonzales, et al., Phys. Rev. 120, 1319 (1960).

$^{58}Ni(n,p)$ measured by activation method with respect to $^{31}P(n,p)$ from 2.22 to 3.55 MeV.

103. H. Liskien and A. Paulsen, Nucl. Phys. 63, 393 (1965).

104. H. Liskien and A. Paulsen, Nuk. 8, 315 (1966).

105. A. Paulsen, Nuk. 10, 91 (1967).
A. Paulsen, Z. Phys. 205, 226 (1967).

106. M.R. Bhat, in ENDF/B-IV Dosimetry File, Edited by B. Magurno, BNL-NCS-50446 (1975).

107. W.G. Cross, R.L. Clarke, K. Morin, G. Slinn, N.M. Ahmed and K. Beg, EANDC (Can)-16 (1963).

108. D.L. Allan, Nucl. Phys. 24, 274 (1961).

109. R.S. Storey, W. Jack, and A. Ward, Proc. Phys. Soc. 75, 526, (1960).

110. J.D. Hemingway, Jour. Nucl. Energy 27, 241 (1973).

111. V.N. Levkovskii, G.P. Vinitskaya, G.E. Kovilskaya and V.M. Stepanov, Sovt. Jour. Nucl. Phys. 10, 25 (1969).

112. G.N. Maslov, et al., Yad. Fiz. 9, 50 (1972).

113. R. Ligensa and W. Greiner, Ann. of Phys. 51, 28 (1969).

114. A.K. Valter, V. Yu. Gonchar, I.I. Zalybovskii, G.D. Latyshev and G.P. Chursin, IZV. Akad. Nauk SSSR. Ser. FIZ, 26, 1979 (1962).

115. J.J. Van Loeff, Nucl. Phys. 24, 340 (1961).

116. P.V. March and W.T. Morton, Phil. Mag. 3, 577 (1958).

117. D.L. Allan, Nucl. Phys. 24, 274 (1961)

118. C. Colli, E. Gadioli, S. Micheletti and D. Lucioni, Nucl. Phys. 46, 73 (1963).

119. C. Colli, I. Iori, S. Micheletti, M. Pignelli, CSISRS AN-60551.

120. H. Farrar, private communication to M.R. Bhat (1974) and private communication to M. Divadeenam (1976).

121. P. Cuzzorcrea, E. Perillo, S. Notarrigo, Nuovo Cimento, 4A, 251 (1971).

122. G.P. Dolya, V.P. Bozhko, V. Ya. Golovnya, A.S. Kachan, A.I. Tutubalin, KFTJ 76-50, Karkov Phys. Tech. Inst. (1976) and 3rd Kiev Conf. an Nucl. Phys. Volume 4, 180 (1976).

123. O. Ozer, "RESEND" BNL-17134, Brookhaven National Laboratory (1972).

124. O. Ozer, "INTER", BNL-17408, Brookhaven National Laboratory (1972).

125. R.E. Maerker, Private communication (1978).

126. R.E. Maerker, ORNL-TM-5203 (1976).

127. N.C. Rasmussan, V.J. Orphan, T.L. Harper, J. Cunningham and S.A. Ali, DASA 2570 (GA-10248) (1970).

128. M.J. Kenny, P.W. Martin and J.R. Bird, Private Communication to M.R. Bhat (1973).

129. J.K. Dickens, T.A. Love and G.L. Morgan ORNL-TM-4379 (1973).

U.S. GOVERNMENT PRINTING OFFICE: 614-090-#56